

Self-Consolidating Concrete (SCC) and High-Volume Fly Ash Concrete (HVFAC) for Infrastructure Elements: Implementation

Report A - Bridge A7957 Fabrication, Construction, and Early Age Properties Behavior of HS-SCC, SCC, HVFAC, and Conventional Concrete (CC)



Prepared by
John J. Myers, Ph.D., P.E.
Eli S. Hernandez
Hayder Alghazali
Alexander Griffin
Kaylea Smith



TECHNICAL REPORT DOCUMENTATION PAGE

1. Report No. cmr 16-011A	2. Government Accession No.	3. Recipient's Catalog No.	
4. Title and Subtitle Self-Consolidating Concrete (SCC) and High-Volume Fly Ash Concrete (HVFAC) for Infrastructure Elements: Implementation. Report A, Bridge A7957 Fabrication, Construction, and Early Age Properties Behavior of HS-SCC, SCC, HVFAC, and Conventional Concrete (CC)		5. Report Date March 2016 Published: June 2016	
		6. Performing Organization Code	
7. Author(s) John J. Myers, Ph.D., P.E. http://orcid.org/0000-0001-5269-8218 , Eli S. Hernandez, Hayder Alghazali, Alexander Griffin, Kaylea Smith		8. Performing Organization Report No.	
9. Performing Organization Name and Address Missouri University of Science and Technology Department of Civil, Architectural, and Environmental Engineering 325 Civil Engineering Rolla, MO 65409		10. Work Unit No.	
		11. Contract or Grant No. MoDOT project #TRyy1236 NUTC project # 00040350 USDOT contract # DTRT06-G-0014	
12. Sponsoring Agency Name and Address Missouri Department of Transportation (SPR) http://dx.doi.org/10.13039/100007251 Construction and Materials Division P.O. Box 270 Jefferson City, MO 65102 Center for Transportation Infrastructure and Safety/NUTC program Missouri University of Science and Technology 220 Engineering Research Lab Rolla, MO 65409		13. Type of Report and Period Covered Final report (October 2012-March 2016)	
		14. Sponsoring Agency Code	
15. Supplementary Notes Conducted in cooperation with the U.S. Department of Transportation, Federal Highway Administration. MoDOT research reports are available in the Innovation Library at http://www.modot.org/services/or/byDate.htm . This set of reports is available at https://library.modot.mo.gov/RDT/reports/TR201236/ .			
16. Abstract Because of its unique nature, self-consolidating concrete (SCC) has the potential to significantly reduce costs associated with transportation-related infrastructure, benefiting both MoDOT and the residents of Missouri. SCC is a highly flowable, nonsegregating concrete that can be placed without any mechanical consolidation, and thus has the following advantages over conventional concrete: decreased labor and equipment costs during concrete placement, decreased potential for and costs to repair honeycombing and voids, increased production rates of precast and cast-in-place (CIP) elements, and improved finish and appearance of cast and free concrete surfaces. In addition to SCC, innovative materials, such as high volume fly ash concrete (HVFAC), also provide a significant potential to produce more cost effective mix designs for CIP concrete. Since the 1930's, fly ash – a pozzolanic material – has been used as a partial replacement of portland cement in concrete to improve the material's strength and durability, while also limiting the amount of early heat generation. From an environmental perspective, replacing cement with fly ash reduces the concrete's overall carbon footprint and diverts an industrial by-product from the solid waste stream (currently, about 40 percent of fly ash is reclaimed for beneficial reuse and 60 percent is disposed of in landfills). The objective of this research is to provide an implementation test bed and showcase for the use of sustainable and extended service life concrete. In this implementation study for Missouri Bridge A7957, a level of 50% fly ash to cement proportions was utilized as well as normal strength self-consolidating concrete (NS-SCC) and HS-SCC in the load carrying elements to showcase the use of these innovative materials.			
17. Key Words Cast in place concrete; Cost effectiveness; Durability; High strength concrete; Mix design; Portland cement concrete; Precast concrete; Self compacting concrete		18. Distribution Statement No restrictions. This document is available through the National Technical Information Service, Springfield, VA 22161.	
19. Security Classif. (of this report) Unclassified.	20. Security Classif. (of this page) Unclassified.	21. No. of Pages 217	22. Price

FINAL REPORT A

TRyy1236

Project Title: Self-Consolidating Concrete (SCC) and High-Volume Fly Ash Concrete (HVFAC) for Infrastructure Elements: Implementation

Report A: Bridge A7957 Fabrication, Construction, and Early Age Properties Behavior of HS-SCC, SCC, HVFAC, and Conventional Concrete (CC)

Prepared for
Missouri Department of Transportation
Construction and Materials

By

Dr. John J. Myers (Project Principal Investigator)
Eli S. Hernandez
Hayder Alghazali
Alexander Griffin
Kaylea Smith

Missouri University of Science and Technology, Rolla, Missouri

March 2016

The opinions, findings, and conclusions expressed in this publication are those of the principal investigators. They are not necessarily those of the U.S. Department of Transportation, Federal Highway Administration or the Missouri Department of Transportation. This report does not constitute a standard or regulation.

ABSTRACT

Because of its unique nature, self-consolidating concrete (SCC) has the potential to significantly reduce costs associated with transportation-related infrastructure, benefiting both MoDOT and the residents of Missouri. SCC is a highly flowable, nonsegregating concrete that can be placed without any mechanical consolidation, and thus has the following advantages over conventional concrete: decreased labor and equipment costs during concrete placement, decreased potential for and costs to repair honeycombing and voids, increased production rates of precast and cast-in-place (CIP) elements, and improved finish and appearance of cast and free concrete surfaces.

In addition to SCC, innovative materials, such as high volume fly ash concrete (HVFAC), also provide a significant potential to produce more cost effective mix designs for CIP concrete. Since the 1930's, fly ash – a pozzolanic material – has been used as a partial replacement of portland cement in concrete to improve the material's strength and durability, while also limiting the amount of early heat generation. From an environmental perspective, replacing cement with fly ash reduces the concrete's overall carbon footprint and diverts an industrial by-product from the solid waste stream (currently, about 40 percent of fly ash is reclaimed for beneficial reuse and 60 percent is disposed of in landfills).

The objective of this research was to provide an implementation test bed and showcase for the use of sustainable and extended service life concrete. In this implementation study for Missouri Bridge A7957, a level of 50% fly ash to cement proportions was utilized as well as normal strength self-consolidating concrete (NS-SCC) and HS-SCC in the load carrying elements to showcase the use of these innovative materials.

TABLE OF CONTENTS

	Page
FINAL REPORT A.....	1
ABSTRACT.....	ii
TABLE OF CONTENTS.....	iii
LIST OF ILLUSTRATIONS.....	ix
LIST OF TABLES.....	xiii
NOMENCLATURE	xv
1. INTRODUCTION	1
1.1. BACKGROUND.....	1
1.2. RESEARCH PROGRAM	2
1.2.1. Research Team.....	2
1.2.2. Destructive Testing of Precast-Prestressed NU Girders	3
1.2.2.1. Precast-Prestressed NU Girder.....	6
1.2.2.2. Intermediate Bents.....	8
1.2.2.3. Bridge Elements and Numbering.....	10
1.3. WORK PLAN	10
1.4. SCOPE OF THE REPORT	11
1.5. ORGANIZATION OF THE REPORT	12
2. LITERATURE REVIEW	13
2.1. SELF-CONSOLIDATING CONCRETE (SCC)	13
2.1.1. Definition.....	13
2.1.2. Fresh Material Properties.....	13
2.1.3. Hardened Material Properties	16
2.1.3.1. Compressive strength	16
2.1.3.2. Modulus of elasticity.....	17
2.1.3.3. Tensile strength	17
2.1.3.4. Creep and shrinkage	17
2.2. HS-SCC.....	18
2.2.1. Definition.....	18

2.2.2. Fresh Material Properties	18
2.2.3. Hardened Material Properties	18
2.2.3.1. Compressive strength	18
2.2.3.2. Modulus of elasticity	19
2.2.3.3. Tensile strength	19
2.2.3.4. Creep and shrinkage	20
2.2.4. Hydration Profile	20
2.2.5. Shear Characteristics.....	21
2.2.5.1. Push off test	21
2.2.5.2. Mid-scale and full-scale beam tests.....	22
2.3. PREVIOUS PROJECTS USING SCC AND HS-SCC	24
2.4. HVFAC	25
2.4.1. Definition	25
2.4.2. Fresh Material Properties.....	25
2.4.2.1. Workability.....	25
2.4.2.2. Air content.....	26
2.4.2.3. Setting time.....	26
2.4.3. Hardened Material Properties	26
2.4.3.1. Compressive strength	26
2.4.3.2. Modulus of elasticity	27
2.4.3.3. Hydration profile	27
2.5. CONVENTIONAL CONCRETE	28
2.5.1. Freeze-thaw Resistance.....	28
2.5.2. Abrasion Resistance.....	28
2.6. MODOT STANDARD CONCRETE MIXES	29
3. MATERIAL TESTING PROGRAM	30
3.1. INTRODUCTION.....	30
3.1.1. Member Cast.....	30
3.1.2. Curing Conditions.....	31
3.1.3. Testing Program Overview	31
3.2. COMPRESSIVE STRENGTH.....	32

3.3. MODULUS OF ELASTICITY	32
3.4. SPLITTING TENSILE STRENGTH.....	34
3.5. MODULUS OF RUPTURE	35
3.6. SHRINKAGE AND CREEP	36
3.7. COEFFICIENT OF THERMAL EXPANSION	39
3.8. FREEZE-THAW DURABILITY	40
3.9. CHLORIDE PONDING.....	42
3.10. ABRASION RESISTANCE	45
3.11. NASP BOND TEST	46
3.12. SUMMARY	47
4. MEASUREMENT SYSTEMS	49
4.1. MEASUREMENT TYPES	49
4.1.1. Concrete Temperatures	49
4.1.2. Concrete Strains.....	50
4.1.3. Girder Deflection and Camber.....	50
4.2. MEASUREMENT SYSTEMS.....	51
4.2.1. Load cell.....	51
4.2.2. Thermocouples.....	51
4.2.3. Vibrating Wire Strain Gauges.....	52
4.2.4. Electrical Resistance Strain Gauges.....	53
4.2.5. Demountable Mechanical Strain Gauges.....	54
4.2.6. DEMEC Points.....	55
4.2.7. High Performance Total Station System.....	56
4.2.8. Radio Frequency Identification (RFID) based Corrosion Sensor.....	58
4.3. DATA ACQUISITION	59
4.3.1. Data Acquisition System.....	59
4.3.1.1. Compact RIO.....	59
4.3.1.2. Campbell Scientific CR800.....	60
4.3.2. Programming and Data Collection.....	63
4.3.3. RFID Corrosion Sensor Data Acquisition	64
4.3.3.1. Data acquisition hardware	64

4.3.3.2. Data acquisition software	64
5. RESEARCH PROGRAM PLANS & PROCEDURES	67
5.1. TRIAL MIXES	67
5.1.1. HVFAC	67
5.1.2. HS-SCC.....	68
5.1.3. NS-SCC.....	70
5.2. INSTRUMENTATION PLAN AND FIELD PREPARATION.....	71
5.2.1. Equipment and Gauges	71
5.2.2. Instrumentation Location	72
5.2.3. Gauge Numbering and Identification.....	73
5.2.4. Gauge Locations	75
5.2.5. Embedded Gauges Preparation	76
5.2.6. Field and Plant Installation	77
5.2.6.1. Intermediate bents	77
5.2.6.2. Precast prestressed girders.....	79
5.2.6.3. Precast prestressed panels	81
5.2.6.4. CIP deck	81
5.2.7. RFID Corrosion Sensors	82
5.3. INTERMEDIATE BENT CONSTRUCTION	84
5.3.1. Mix Designs	85
5.3.2. Data Collection	86
5.4. PC/PS GIRDERS AND PANELS FABRICATION.....	87
5.4.1. Mix Designs	89
5.4.2. Data Collection	91
5.5. BRIDGE CONSTRUCTION	92
5.5.1. Girders Erection.....	93
5.5.2. CIP RC Deck.....	95
5.5.2.1. Mix design.....	98
5.5.2.2. Data collection.....	100
5.5.3. Approach Slab Concrete Placement.....	101
5.5.4. Safety Barrier Curbs	101

5.6. PROBLEMS ENCOUNTERED	101
6. RESEARCH PROGRAM RESULTS	103
6.1. MATERIAL TEST RESULTS	103
6.1.1. Trial Mixes.....	103
6.1.1.1. HVFAC	103
6.1.1.1.1. Fresh properties.....	103
6.1.1.1.2. Hardened properties	103
6.1.1.2. HS-SCC	105
6.1.1.2.1. Fresh Properties	105
6.1.1.2.2. Hardened properties	106
6.1.1.3. NS-SCC	109
6.1.1.3.1. Fresh properties.....	109
6.1.1.3.2. Hardened properties	110
6.1.2. Intermediate Bents (HVFAC)	111
6.1.2.1. Fresh properties	112
6.1.2.2. Hardened properties	112
6.1.2.3. Hydration profiles.....	113
6.1.3. Bridge Girders.....	118
6.1.3.1. Fresh properties	118
6.1.3.2. Compressive strength.	118
6.1.3.3. Modulus of elasticity.	120
6.1.3.4. Modulus of rupture.....	122
6.1.3.5. Coefficient of thermal expansion.	124
6.1.3.6. Creep.	125
6.1.3.7. Shrinkage.....	130
6.1.4. NASP Pullout Tests	135
6.1.5. Deck	137
6.1.5.1. Fresh properties	137
6.1.5.2. Compressive strength	137
6.1.5.3. Abrasion resistance.....	138
6.1.5.4. Freeze and Thaw Resistance	139

6.1.5.5. Ponding Test.....	139
6.1.6. Safety Barriers	140
6.1.6.1. Compressive strength.	140
6.2. SUMMARY AND CONCLUSIONS.....	141
6.2.1. Trial Mixes.....	141
6.2.2. Intermediate Bents (HVFAC).....	142
6.2.3. Implementation Program	142
7. PRESTRESS LOSSES	144
7.1. INTRODUCTION.....	144
7.1.1. General.....	144
7.1.2. Measurement of Prestress Losses Using Internal Sensors (VWSGs).....	146
7.2. ELASTIC SHORTENING AT RELEASE	147
7.2.1. Background.....	147
7.2.2. Measurements and Discussion.....	147
7.3. TOTAL LOSSES	153
7.3.1. Background.....	153
7.3.2. Measurements and Discussion.....	153
7.4. SUMMARY AND CONCLUSIONS.....	156
APPENDIX A - DESIGN DRAWINGS	158
APPENDIX B - INSTRUMENTATION PLAN	161
APPENDIX C - INSTRUMENTATION LABELING	179
REFERENCES	189

LIST OF ILLUSTRATIONS

Figure	Page
1.1. Test Girder Cross Section	3
1.2. NU Test Girder Strand Layout.....	4
1.3. Bridge A7957 Location.....	5
1.4. Bridge A7957 Elevation View.....	6
1.5. Bridge A7957 Cross Section Looking East	6
1.6. NU Bridge Girder Cross Section	7
1.7. NU Girder Spans 1 & 3 Strand Layout.....	7
1.8. NU Girder Span 2 Strand Layout.....	8
1.9. Intermediate Bent Elevation View.....	9
1.10. Bridge A7957 Numbering Scheme	10
2.1. HS-SCC vs. HSC Ultimate Shear Stress (Myers et al., 2012).....	23
3.1. QC/QA Specimens Placement at Precast Plant and Jobsite.....	30
3.2. Storage of QC/QA Specimens at Missouri S&T	31
3.3. Compressive Strength Test	34
3.4. MOE Test Set Up.....	34
3.5. Typical Splitting Tensile Test Set Up.....	35
3.6. Modulus of Rupture Test Set Up	36
3.7. Creep & Shrinkage Specimen & DEMEC Point Arrangements.....	37
3.8. Schematic of Creep Loading Frame	38
3.9. Creep Loading Frame & Specimens	39
3.10. Coefficient of Thermal Expansion (CTE) Test at Missouri S&T.....	40
3.11. Freezing and Thawing Specimen Molds.....	41
3.12. Freezing and Thawing Test.....	42
3.13 Ponding Test Specimen Dimensions	43
3.14 Ponding Specimens.....	43
3.15 Ponding Chloride Test	44
3.16. Abrasion Test.....	46
3.17. NASP Bond Test.....	47

4.1. Load cell.....	51
4.2. Thermocouple	52
4.3. Definition of TT-T-20-TWSH	52
4.4. Vibrating Wire Strain Gauge	53
4.5. Electrical Resistive Strain Gauge.....	54
4.6. The DEMEC Gauge and Reference Bar	54
4.7. Gauge Factor Used for Shrinkage and Creep Calculations	55
4.8. Stainless Steel DEMEC points.....	56
4.9. Total Station (Leica TCA2003)	56
4.10. Reflecting Prisms Mounted on PC/PS Girders (Precast Plant).....	57
4.11. RFID Based Corrosion Sensors	58
4.12. Compact RIO System and 90 Watt Solar Panel.....	59
4.13. Campbell Scientific CR800	60
4.14. Components of DAS Box 1	62
4.15. Components of DAS Box 2	62
4.16. Data Acquisition System Installed on Bridge A7957	63
4.17. RFID Data Acquisition Hardware	64
4.18. RFID DAS Software (User’s Interface).....	65
4.19. RFID Sensor’s Output File	65
4.20. Typical RFID Code.....	66
5.1. HVFAC Trial Mix at Osage County Industries	67
5.2. HS-SCC Trial Mix Fresh Property Tests	69
5.3. HS-SCC Trial Mix Specimens.....	69
5.4. NS-SCC Trial Mix Fresh Property Tests	70
5.5. Bridge A7957’s Instrumented Girders and Clusters’ Locations.....	73
5.6. VWSG Installation Detail through the Different Girders’ Sections	75
5.7. Thermocouple Preparation Prior to Field Installation	76
5.8. VWSG Preparation Prior to Field Installation	77
5.9. Thermocouple Sensors Installation Details	78
5.10. Thermocouples Installation on Bent 2’s Web Wall.....	78
5.11. Thermocouples Installed at Specified Bent Sections.....	79

5.12. VWSG Installation within PC Girders at Precast Plant	79
5.13. VWSGs Connected to DAS Box	80
5.14. VWSG Connected to DAS at Precast Plant	80
5.15. VWSG Installed within PC/PS Panels	81
5.16. Instrumented PC/PS Panels	81
5.17. VWSG Installed on CIP RC Deck	82
5.18. Bridge A7957 VWSG Instrumentation	82
5.19. Bridge A7957 RFID Corrosion Sensors Installation (Plan View)	83
5.20. Bridge A7957 RFID Corrosion Sensors Installation (Elevation)	83
5.21. RFID Installed on CIP RC Deck (Before Concrete Placement)	84
5.22. Intermediate Bent QC/QA Specimens	85
5.23. Data Collection at Intermediate Bents	87
5.24. Fresh Property Tests (Concrete Mixtures of Spans 2-3 and 3-4)	89
5.25. PC/PS Girders QC/QA Specimens	91
5.26. Data Collection During the PC/PS Girders Fabrication	91
5.27. Release of PC/PS Girder	92
5.28. Girders Storage at Precast Plant	92
5.29. Shipping of the PC Girders to the Bridge Jobsite	93
5.30. VWSG Sensors Connected to CR800 DAS	93
5.31. Lifting of HS-SCC PC Girder 4 (Span 2-3)	94
5.32. Conventional Concrete and HS-SCC PC Girders Placed on Supports	94
5.33. Lifting and Setting of NS-SCC PC Girders	95
5.34. Diaphragm and PC/PS Panels Erection	95
5.35. Installation of VWSG within CIP Deck and CR800 DAS Boxes	96
5.36. Concrete Placement on Intermediate RC Diaphragm	96
5.37. Concrete Placement on CIP RC Deck	97
5.38. RFID Corrosion Sensor Embedded within CIP Deck	97
5.39. Finished Surface of CIP RC Deck	98
5.40. CIP Deck QC/QA Specimens Collected During Concrete Placement	99
5.41. Detail of RFID Corrosion Sensor Installed in Ponding Test Specimens	100
5.42. Bridge A7957 Completed	101

6.1. HS-SCC Trial Mix Modulus of Elasticity vs. Compressive Strength	107
6.2. HS-SCC Trial Mix Splitting Tensile Strength vs. Compressive Strength	108
6.3. Splitting Tensile Strength Failure Plane	109
6.4. NS-SCC Trial Mix Modulus of Elasticity vs. Compressive Strength	110
6.5. NS-SCC Trial Mix Splitting Tensile Strength vs. Compressive Strength	111
6.6. Intermediate Bents Compressive Strength vs. Age.....	112
6.7. Intermediate Bents Hydration Profiles: Columns and Web Wall.....	115
6.8. Intermediate Bents Hydration Profiles: Pier Cap.....	116
6.9. PC/PS Girders Compressive Strength vs. Age	119
6.10. PC/PS Girders Modulus of Elasticity vs. Compressive Strength	121
6.11. PC/PS Girders Modulus of Rupture vs. Compressive Strength.....	123
6.12. Coefficient of Thermal Expansion.....	124
6.13. Deck Compressive Strength vs. Age	137
6.14. Depth of Wear Results.....	138
6.15. Average Mass Loss Results	138
6.16. Specimen after Abrasion Test.....	139
6.17 Chloride Concentration Profile.....	140
6.18. Deck Compressive Strength vs. Age	141
7.1 Strains at Release	147
7.2 Hydration Temperature Before and After Release	148
7.3 Measured and Predicted Elastic Shortening Losses.....	152
7.4 Measured and Predicted total Prestress Losses for all Instrumented Beams.....	155

LIST OF TABLES

Table	Page
1.1. Test Girder Shear Reinforcement	5
2.1. Suggested Fresh Property Tests (Mix Design and Quality Control)	14
2.2. Workability Values of SCC Used in Precast/Prestressed Applications.....	16
3.1. Summary of Fresh Properties of Material Testing Program.....	32
3.2. Summary of Hardened Properties of Material Testing Program	33
3.3. Specimens for Splitting Tensile Test.....	35
3.4. Creep & Shrinkage Specimens	37
3.5 Ponding Sample Interval.....	44
3.6 Correlation between %Cl by Mass of Concrete and Corrosion Risk.....	45
3.7. Summary of Material Testing Program	48
4.1. Measurement Types	49
4.2. Gauges Needed During Fabrication of PC Girders (Precast Plant).....	60
4.3. Gauges Needed During Construction of Bents.....	61
4.4. Channels Needed During the Long-Term Monitoring of Bridge A7957	61
5.1. HVFAC Trial Mix Design	68
5.2. HS-SCC Trial Mix Design.....	70
5.3. NS-SCC Trial Mix Design.....	71
5.4. Instrumentation Equipment and Gauges	72
5.5. Girders, Panels and Deck's Gauge Identification Designations	74
5.6. Bent's Gauge Identification Designations	75
5.7. RFID Sensors' Coordinates through CIP RC Deck of Bridge A7957.....	84
5.8. Intermediate Bents Construction Schedule.....	85
5.9. Intermediate Bents Mix Designs.....	86
5.10. PC/PS Girders Construction Timeline.....	88
5.11. PC/PS Girders Concrete Mixture Comparison	90
5.12. CIP RC Deck's Concrete Mix Proportions	98
5.13. RFID Sensors' ID Coordinate Locations within Ponding Specimens.....	100
6.1. HVFAC Trial Mix Fresh Properties	103

6.2. HVFAC Trial Mix Compressive Strength	104
6.3. HVFAC Trial Mix Measured and Predicted Modulus of Elasticity	105
6.4. HS-SCC Trial Mix Fresh Properties	105
6.5. HS-SCC Trial Mix Hardened Properties	107
6.6. NS-SCC Trial Mix Fresh Properties	109
6.7. NS-SCC Trial Mix Hardened Properties	110
6.8. Intermediate Bents Fresh Properties	112
6.9. Intermediate Bents Hydration Rates	117
6.10. PC/PS Girders Fresh Properties	118
6.11. Measured Coefficient of Thermal Expansion	124
6.12. Creep Test Summary.....	125
6.13. Creep Results.	126
6.14. Measured & Predicted Creep Coefficient at 120 days.....	130
6.15. CC Shrinkage Strain	134
6.16. HS-SCC Shrinkage Strain.....	134
6.17. NS-SCC Shrinkage Strain.....	134
6.18. Concrete NASP Results	136
6.19. Modified B-2 Concrete Mix Fresh Properties	137
6.20. Freeze and Thaw Results	139
6.21 Average Chloride Content at Specific Depths	140
7.1 Summary of the code equations used in the prediction of total prestress losses by components (Pretensioned Member).....	149
7.2. Measured vs. Predicted Elastic Shortening Losses.....	150
7.3 Measured and Predicted Total Prestress Losses for Instrumented Girders.....	154
7.4. Total Prestress Losses for HSC, HS-SCC, and NS-SCC PC/PS Girders	156

NOMENCLATURE

Symbol	Description
a	Depth of equivalent stress block (in.)
a_g	Maximum aggregate size (in.)
A_c	Area of concrete section (in. ²)
A_{ps}	Area of prestressing steel (in. ²)
A_s	Area of non-prestressing longitudinal steel (in. ²)
A_v	Area of shear reinforcement (in. ²)
b_w	Web thickness (in.)
b_v	Effective web width (in.)
c	Distance from extreme compressive fiber to neutral axis (in.)
d_p	Depth from extreme compression fiber to centroid of prestressing tendons (in.)
d_s	Distance from extreme compression fiber to centroid of non-prestressed tensile reinforcement (in.)
d_v	Effective shear depth, taken as the perpendicular distance between resultants of tensile and compressive forces due to flexure (in.)
E_c	Modulus of elasticity of concrete (psi)
E_{ct}	Modulus of elasticity of concrete at transfer (psi)
E_p	Modulus of elasticity of prestressing steel (ksi)
E_s	Modulus of elasticity of non-prestressing steel (ksi)
f'_c	Specified design concrete compressive strength (ksi)
f'_{ci}	Compressive strength of concrete at release (psi)
f_{cgp}	Concrete stress at centroid of prestressing steel due to prestressing force after elastic losses and member self-weight (ksi)

f_{pc}	Compressive stress at the centroid of the concrete section due to the effective prestress force (psi)
f_{po}	Locked in difference in strain between the prestressing steel and the surrounding concrete multiplied by the modulus of elasticity of the prestressing steel (ksi)
f_{pt}	Stress in prestressing strands immediately after transfer (ksi)
f_r	Modulus of rupture of concrete (psi)
f_y	Specified yield strength of shear reinforcement (ksi)
f_{pe}	Effective stress in the prestressing steel after losses (ksi)
f_{py}	Yield stress of prestressing steel (ksi)
h	Total depth of member (in.)
H	Relative humidity (%)
h_c	Total depth of composite member (in.)
I_c	Gross moment of inertia of composite section (in. ⁴)
I_g	Gross moment of inertia of girder (in. ⁴)
k_f	Factor for strength of concrete at release
K_{df}	Transformed section coefficient that accounts for time dependent interaction between concrete and bonded steel for time period between deck placement and final time
k_{hc}	Humidity factor for creep
k_{hs}	Humidity factor for shrinkage
K_{id}	Transformed section coefficient that accounts for time dependent interaction between concrete and bonded steel for time period between transfer and deck placement
K_L	Factor for type of prestressing steel
k_s	Factor accounting for V/S of concrete section
k_{td}	Time development factor

MAS	Maximum aggregate size
M_{cr}	Flexural cracking moment (k-ft)
M_{cr}	Flexural cracking moment due to applied loads (k-ft)
M_{fl}	Nominal moment capacity as noted in Kani (1967) (k-ft)
M_{max}	Maximum applied moment at section due to externally applied loads (k-ft)
M_u	Factored moment at section (k-ft)
N_u	Factored axial force at section (kips)
P_e	Effective prestress force (ksi)
P_{Δ}	Prestress force lost due to long term prestress losses before deck placement (kips)
r_u	Relative strength of member
s	Center to center spacing of shear reinforcement (in.)
s_x	Cracking spacing parameter (in.)
s_{xe}	Equivalent value of s_x taking into account the MAS
t	Age of specimen (days)
t_d	Age of concrete at deck placement (days)
t_f	Age of concrete at final time (days)
t_i	Age of concrete at transfer (days)
V/S	Volume to surface ratio (in.)
V_c	Nominal concrete shear resistance (kips)
V_{ci}	Nominal shear resistance when diagonal cracking results from applied shear and moment (kips)
V_{cw}	Nominal shear resistance when diagonal cracking results from high principle stresses in the web (kips)
V_d	Applied shear force at section due to unfactored dead load (kips)

V_i	Factored shear force at section due to externally applied loads (kips)
V_n	Nominal shear resistance (kips)
V_p	Component of prestressing force in the direction of shear force (kips)
V_s	Nominal shear reinforcement resistance (kips)
V_u	Factored shear force at section (kips)
w	AASHTO unit weight of concrete (k/ft^3)
w/cm	Water to cement ratio
w_c	ACI unit weight of concrete (lb/ft^3)
α	Angle of inclination of shear reinforcement to longitudinal reinforcement (degree)
β	Factor indicating ability of diagonally cracked concrete to transmit tension
ϵ_{bdf}	Concrete shrinkage strain of girder between time of deck placement and final time
ϵ_{bid}	Concrete shrinkage strain of girder between time of transfer and deck placement
ϵ_{ddf}	Concrete shrinkage strain of deck between placement and final time
ϵ_s	Net longitudinal strain at centroid of longitudinal reinforcement
Δf_{cd}	Change in concrete stress at centroid of prestressing strands due to shrinkage of deck concrete (ksi)
Δf_{cdf}	Change in concrete stress at centroid of prestressing strands due to long term losses between transfer and deck placement combined with deck weight and superimposed loads (ksi)
Δf_{pCD}	Prestress losses due to creep of CIP deck concrete (ksi)
Δf_{pCR}	Prestress losses due to creep of girder concrete (ksi)
Δf_{pES}	Elastic shortening prestress losses (ksi)
Δf_{pR1}	Prestress losses due to relaxation of tendons before placement of CIP deck (ksi)

Δf_{pR2}	Prestress losses due to relaxation of tendons after placement of CIP deck (ksi)
Δf_{pSD}	Prestress losses due to shrinkage of concrete after placement of CIP deck (ksi)
Δf_{pSR}	Prestress losses due to shrinkage of concrete before placement of CIP deck (ksi)
Δf_{pSR}	Prestress gain due to shrinkage of CIP deck (ksi)
θ	Angle of inclination of diagonal compressive stress (degrees)
λ	Reduction factor for lightweight concrete
ϕ	Shear resistance factor
$\psi(t_2, t_1)$	Creep coefficient at time t_1 due to loads applied at time t_2
AASHTO	American Association of State Highway and Transportation Officials
ACI	American Concrete Institute
ASTM	American Society for Testing and Materials
CA	Coarse aggregate
CC	Conventional concrete
CIP	Cast in place
CR	Creep
DOT	Department of Transportation
EPG 751	Engineering Policy Guide section 751 from the Missouri Department of Transportation
FA	Fine aggregate
FEA	Finite element analysis
FEM	Finite element model
HS-SCC	High strength self-consolidating concrete

HSC	High strength concrete
HRWR	High range water reducer
HRWRA	High range water reducing admixture
LRFD	Load and resistance factored design
MoDOT	Missouri Department of Transportation
MOE	Modulus of elasticity
MOR	Modulus of rupture
MS	Mild steel shear reinforcement
NCHRP	National Cooperative Highway Research Program
NU	Nebraska University
PC/PS	Precast prestressed concrete
QC/QA	Quality control/quality assurance
R2K	Response 2000
RC	Reinforced concrete
SCC	Self-consolidating concrete
SERL	Structural Engineering Research Laboratory
SH	Shrinkage
T1	First test conducted on each girder, with shear reinforcement
T2	Second test conducted on each girder, without shear reinforcement
TG1	Test girder 1, consisting of WWR shear reinforcement
TG2	Test girder 2, consisting of MS shear reinforcement
WWR	Welded wire mesh shear reinforcement.

1. INTRODUCTION

1.1. BACKGROUND

Due to recent catastrophes in our nation's aging infrastructure, there is a need to develop resilient concrete mix designs for precast prestressed (PC/PS) bridges that will extend beyond the current 50-year service life.

To accomplish this goal, innovative concrete mix designs have been developed. Self-consolidating concrete (SCC) has been implemented in bridge infrastructure most notably in Japan and Europe. However, its implementation for PC/PS concrete bridges in the United States has been limited due to insufficient test bed applications. Additionally, high volume fly ash concrete (HVFAC) has been implemented at 30% replacement levels; there is little evidence of replacement levels on the order of 50% as investigated in this study.

SCC has been documented to reduce both costs associated with fabrication and long-term maintenance as well as expedite the construction process. Without a need for mechanical vibration, there is a reduction in labor cost and a reduced risk for employee injuries. However, the modifications required of the mix design to produce a flowable, nonsegregating concrete provide reluctance in the full scale application of this concrete. Reductions in both the size and proportions of coarse aggregate and an increase in the paste content hinder some mechanical properties: namely the modulus of elasticity, creep, and shrinkage with respect to conventional concrete. This in turn can lead to increased deflections and prestress losses. These material modifications, coupled with lower water to cementitious materials (w/cm) ratio, can create problems regarding the post-cracking shear behavior of high strength self-consolidating concrete (HS-SCC).

In addition to the environmental benefits of using replacement levels of fly ash in concrete, the fly ash can also reduce the heat generation during curing. The long-term strength gaining characteristics of HVFAC also correlate to a tighter concrete matrix, leading to improved durability properties.

In recent years, the use of high strength concrete (HSC), noted as a design strength equal to or greater than 8,000 psi (55 MPa), has created a demand for more

economical and efficient cross sections for PC/PS concrete bridge elements. This resulted in the development of the Nebraska University (NU) cross section at the University of Nebraska-Lincoln in Omaha, Nebraska in the early 1990's. Not only is the cross section more suitable for high strength concretes, but also easily enables the transformation of a traditional simple-span PC/PS concrete bridge to a continuous structure. As of 2006, the MoDOT began implementing the NU Series into their new bridge construction.

Following the laboratory findings at Missouri University of Science and Technology (Missouri S&T) with regards to SCC and HVFAC (Reports TRyy1103 and TRyy1110, respectively), the MoDOT proceeded to move forward with a full scale implementation of these innovative materials.

This study combines the efforts of previous work at Missouri S&T regarding normal strength self-consolidating concrete (NS-SCC), HS-SCC, and HVFAC with the NU girder series into a three span, PC/PS continuous concrete bridge along Highway 50 in Osage County, Missouri. In addition to the construction of the bridge, the shear resistance of the HS-SCC was examined in a full-scale laboratory testing using the NU girder cross section.

1.2. RESEARCH PROGRAM

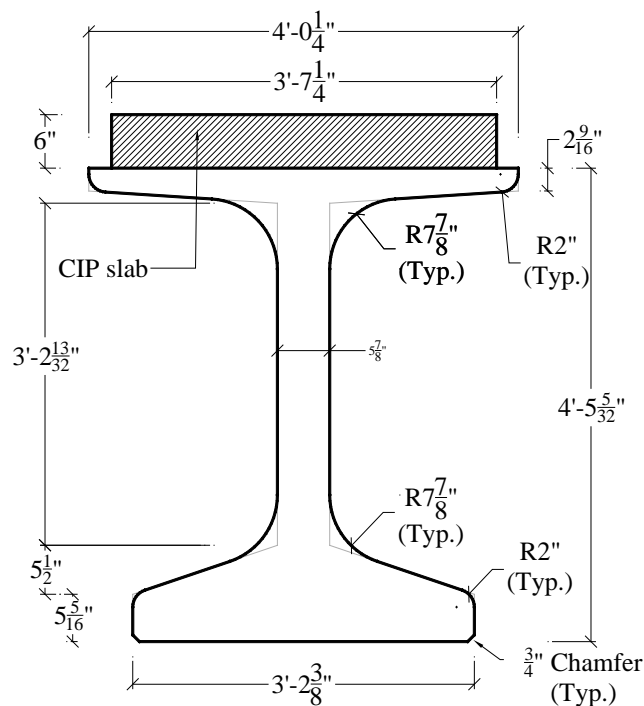
1.2.1. Research Team

Dr. John Myers, professor at Missouri S&T, served as the principal investigator (PI) for the project. Dr. Jeffrey Volz, former assistant professor at Missouri S&T, served as a co-principal investigator before leaving the university in the summer of 2013. Eli Hernandez served as the lead graduate assistant, with assistance from Alex Griffin and Hayder Alghazali. Graduate student Benjamin Gliha also helped with the instrumentation during the fabrication process of the bridge girders. Reed Norphy and Michael Janke, undergraduate students at Missouri S&T, helped with material testing and preparation. Jason Cox (Senior Research Specialist) and John Bullock (Research Laboratory Technician) at the Center for Infrastructure Engineering Studies (CIES) at Missouri S&T, helped with instrumentation and preparation of the NU girders for destructive testing. Technical help with data programming and collection and destructive girder testing was

done by Brian Swift (Electronic Research Engineer) and Gary Abbott (Senior Research Electronic Technician) from the Department of Civil, Architectural, and Environmental Engineering (CArEE) at Missouri S&T. The research was completed through careful coordination between the Missouri Department of Transportation (MoDOT), Fred Weber, Inc. of Maryland Heights, MO, and County Materials Corporation of Bonne Terre, MO. The program was funded by the MoDOT and the National University Transportation Center (NUTC) at Missouri S&T.

1.2.2. Destructive Testing of Precast-Prestressed NU Girders

Two precast, prestressed full scale NU girders were fabricated at County Materials Corporation and tested for shear capacity at the Butler Carlton Civil Engineering Hall Structural Engineering Research Laboratory (SERL).

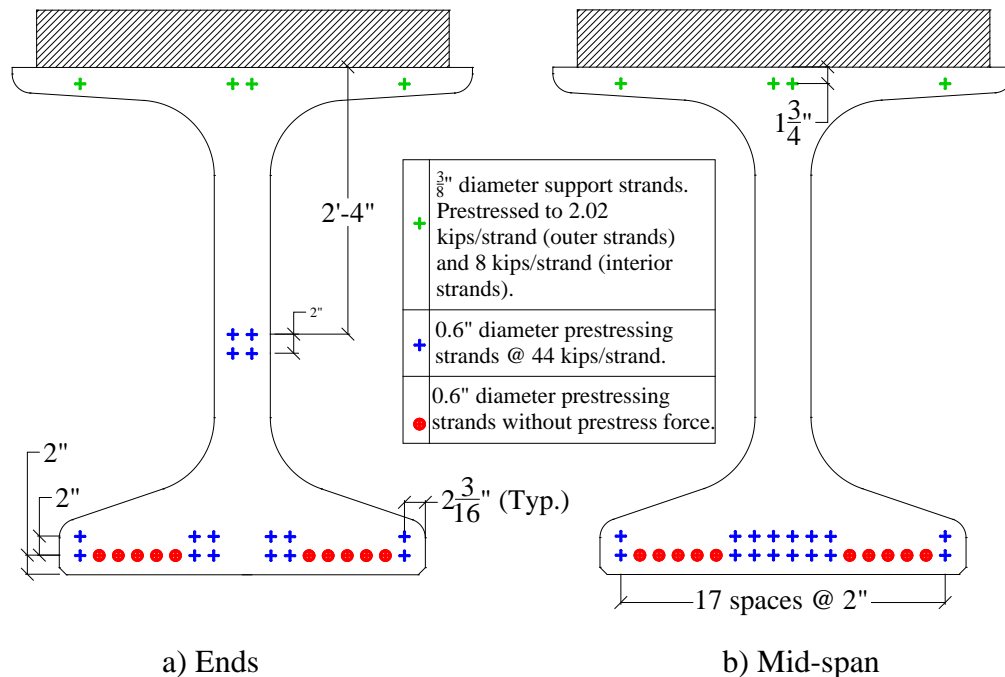


Conversion: 1 in. = 25.4 mm

Figure 1.1. Test Girder Cross Section

The girders were constructed with the same cross section as was used in construction of the bridge on Highway 50 in Osage County. A 6 in. (152 mm) thick CIP concrete deck was fabricated on top of each girder to simulate the road deck on the

bridge. The cross section is illustrated in Figure 1.1. Both girders were 40 ft.-10 in. (12.4 m) long, with a total of 16 Grade 270 (1,862 MPa) prestressed low-relaxation prestressed tendons, 4 of which were harped.



Conversion 1 in. = 25.4 mm

Figure 1.2. NU Test Girder Strand Layout

Figure 1.2 illustrates the locations of the prestressed tendons at the end of the girder and at mid-span. Each girder had three distinct sections of shear reinforcement described in Table 1.1: a middle 10 ft. (3.05 m) region and two 15 ft. (4.57 m) end regions. Both Grade 70 ksi (483 MPa) welded wire reinforcement and Grade 60 ksi (414 MPa) mild steel bars were investigated. Each end region was tested in shear, and external strengthening was provided in the non-tested region during each test. The girders had a target design strength of 10,000 psi (68.9 MPa) and a release strength of 8,000 psi (55.2 MPa). Design drawings provided by MoDOT are located in Appendix A.

Bridge Details.

Bridge A7957 is located along Highway 50 in Osage County shown in Figure 1.3. Latitude and longitude coordinates of the site are 38 29 39.11 N, 91 59 14.00 W. The bridge was constructed adjacent to bridge A3425 as part of a two lane expansion of

Highway 50. The bridge consists of three continuous precast-prestressed concrete spans, two exterior 100 ft. (30.5 m) spans and one interior 120 ft. (36.6 m) span. Precast-prestressed concrete panels extend between spans in the transverse direction below a CIP concrete deck. Two intermediate bents and two abutments support the superstructure. The bridge has a superelevation of 2.0%. An elevation view and cross section of the bridge are shown in Figure 1.4 and Figure 1.5

Table 1.1. Test Girder Shear Reinforcement

Test Girder	Shear Regions		
	Region 1	Region 2	Region 3
1	D20 spaced at 12 in.	D20 spaced at 4 in.	No Shear Reinforcement
2	#5 spaced at 24 in.	#5 spaced at 12 in.	No Shear Reinforcement

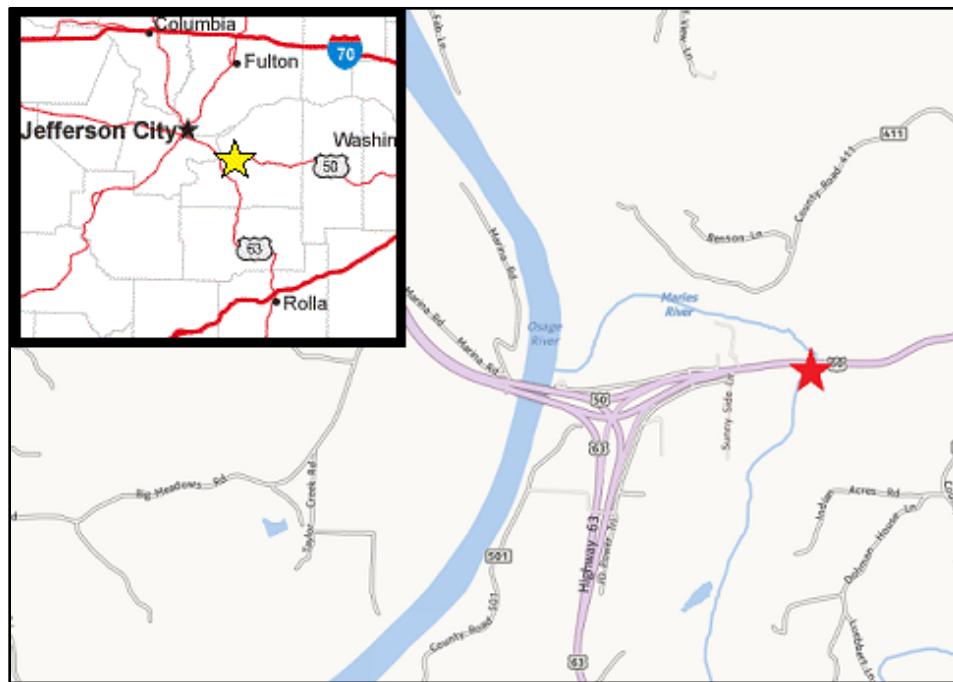
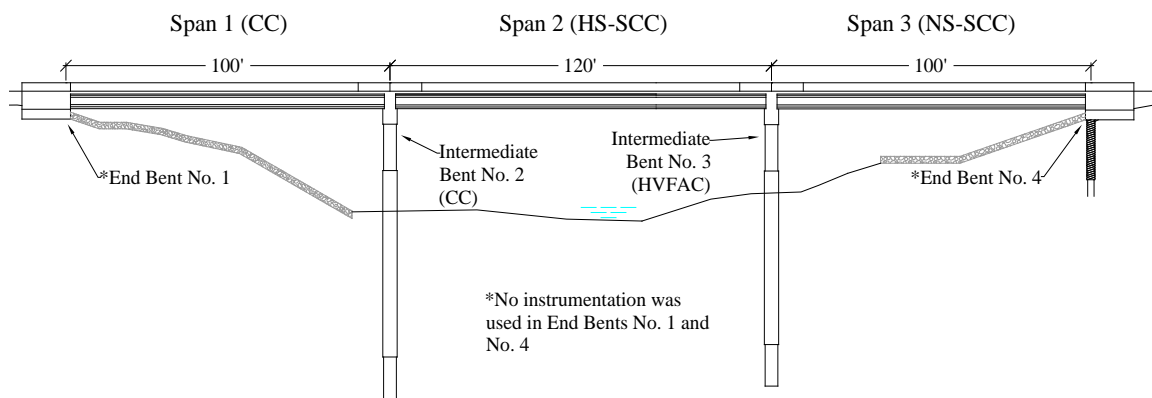
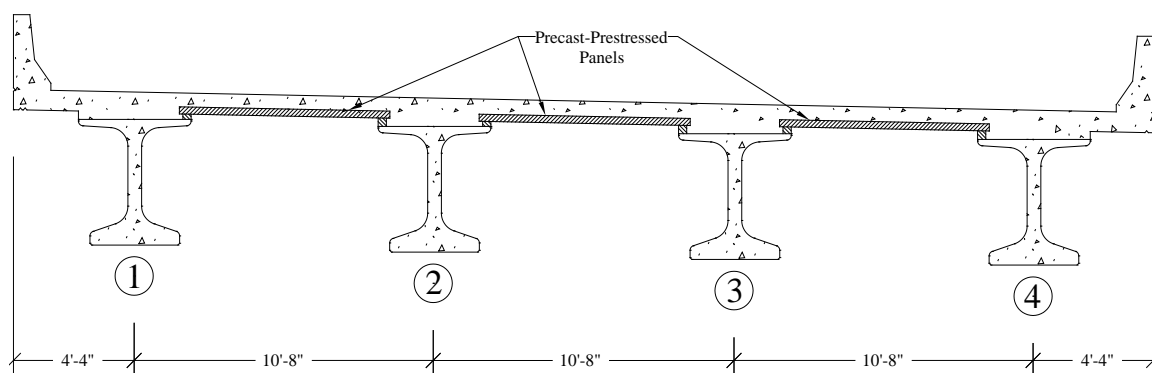


Figure 1.3. Bridge A7957 Location



Conversion: 1 ft. = 0.3048 m

Figure 1.4. Bridge A7957 Elevation View



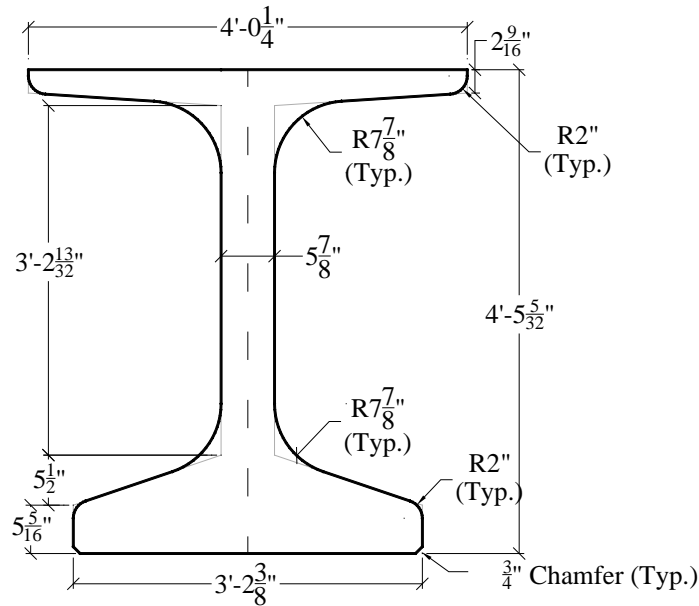
Conversion: 1 in. = 25.4 mm

Figure 1.5. Bridge A7957 Cross Section Looking East

1.2.2.1. Precast-Prestressed NU Girder.

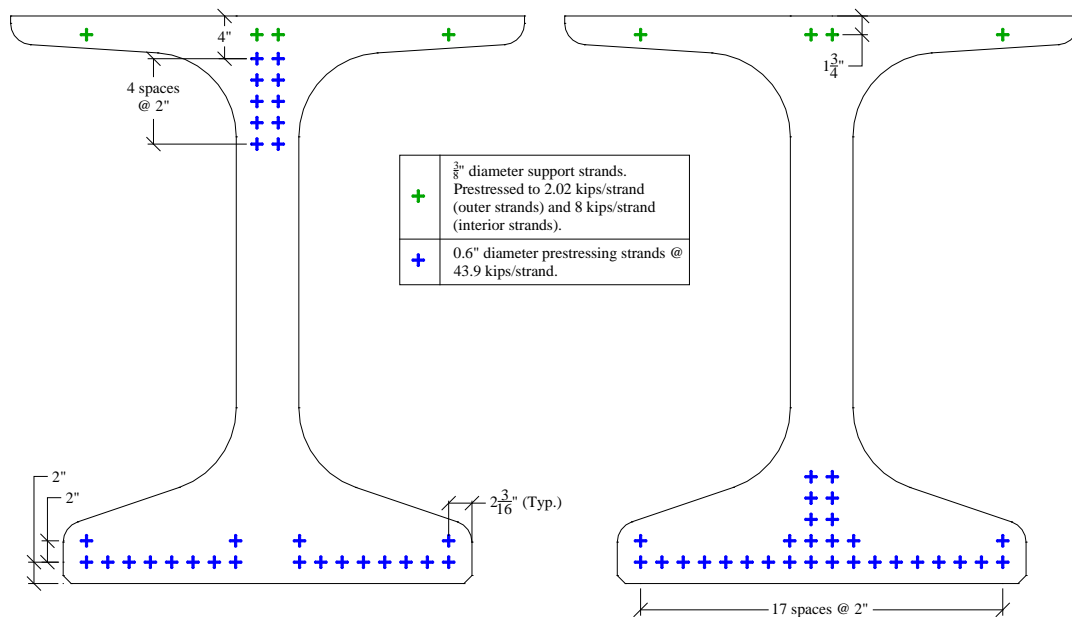
Each span consisted of four precast-prestressed NU 53 girders. Girders in Span 1 and 3 each had 30 Grade 270 ksi (1,862 MPa) low-relaxation prestressing strands, 10 of which were harped, while span 2 consisted of 38 Grade 270 (1,862 MPa) low-relaxation prestressing strands. Cross sectional dimensions are illustrated in Figure 1.6. The strand arrangement for each span at the ends and at mid-span is displayed in Figure 1.7 and Figure 1.8. D20 welded wire reinforcement was provided for shear resistance at spacing intervals of 4 in., 8 in., and 12 in. (101.6, 203.2, and 304.8 mm, respectively) along the length of the girder. The design strength of spans 1 and 3 was 8,000 psi (55.2 MPa) with a release strength of 6,500 psi (44.8 MPa). Span 2 had a design strength of 10,000 psi

(68.9 MPa) with a release strength of 8,000 psi (55.2 MPa). Design drawings provided by MoDOT can be found in Appendix A.



Conversion: 1 in. = 25.4 mm

Figure 1.6. NU Bridge Girder Cross Section



Conversion: 1 in. = 25.4 mm

a) Ends

b) Mid-span

Figure 1.7. NU Girder Spans 1 & 3 Strand Layout

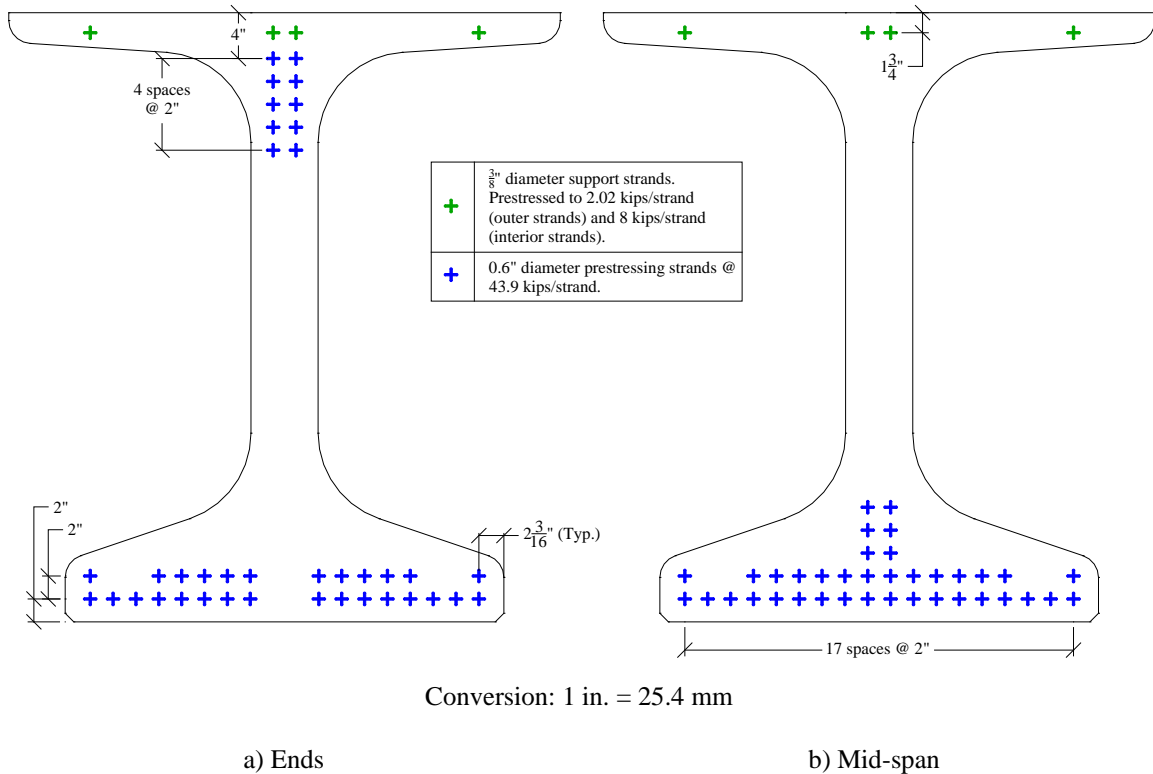
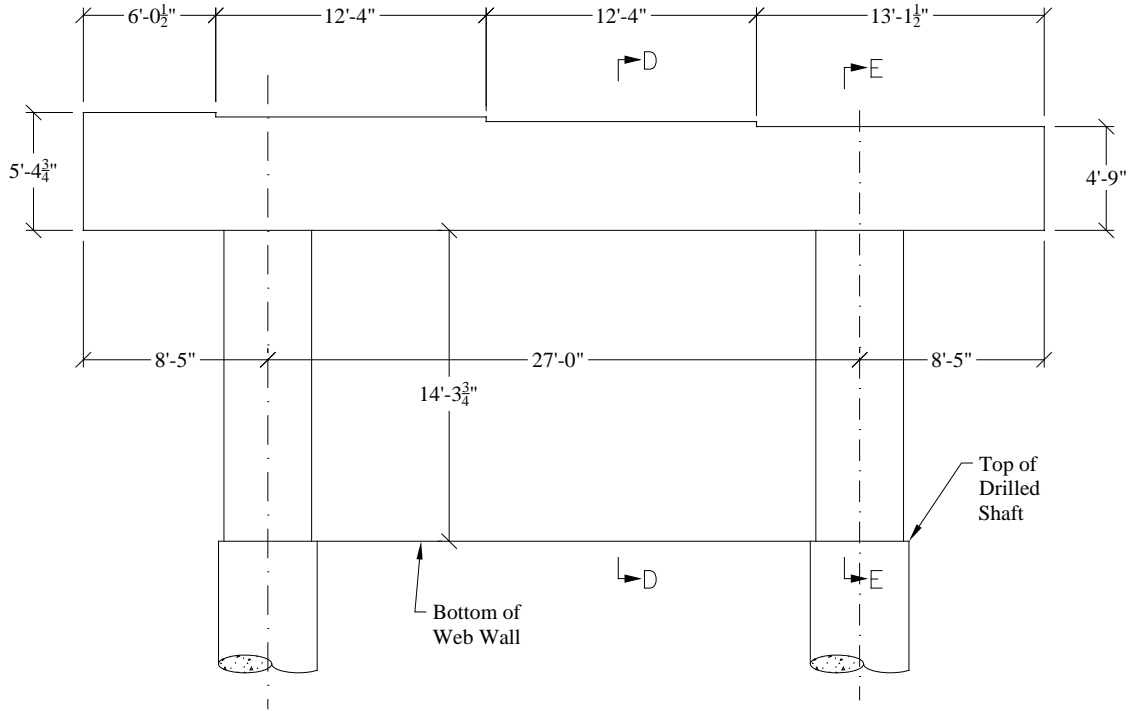


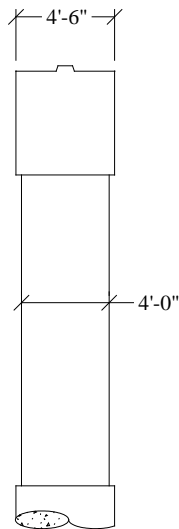
Figure 1.8. NU Girder Span 2 Strand Layout

1.2.2.2. Intermediate Bents.

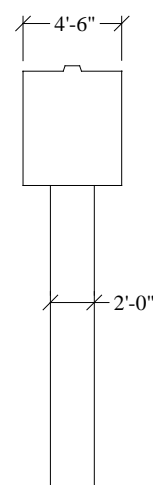
Two intermediate bents identified previously in Figure 1.4 were investigated in the study. Both bents were identical with the exception of the material properties of the concrete. Intermediate bent no. 3 used HVFAC while intermediate bent no. 2 consisted of MoDOT's standard conventional concrete 'B' mix. Each intermediate bent consisted of two columns, an integral web wall and the pier cap. The columns and web wall were cast as one unit while the pier cap was cast as a second unit. The target design strength of bent 3 (HVFAC) and bent 2 was 3,000 psi (20.7 MPa). An elevation view is provided below in Figure 1.9.



(a) East Elevation



(b) Section E-E



(c) Section D-D

Conversion: 1 in. = 25.4 mm

Figure 1.9. Intermediate Bent Elevation View

1.2.2.3. Bridge Elements and Numbering.

The superstructure and substructure elements of Bridge A7957 were labeled for consistency during the course of the research program. The bents were numbered 1 through 4 from west to east. Spans were labeled S1 through S3 from west to east, and girders were labeled G1 through G4 from north to south. Each girder had a unique abbreviation identifying the span number and girder number, i.e., S1-G3 for span 1-2, girder 3. Only girder lines 3 and 4 included instrumentation within the member. The numbering sequence is shown below in Figure 1.10.

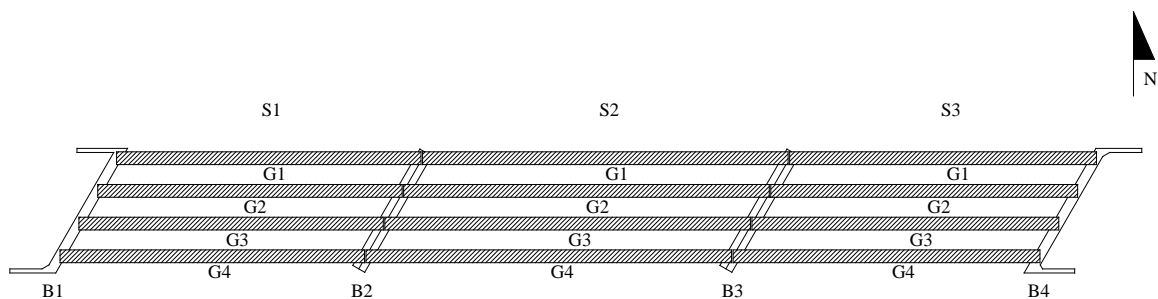


Figure 1.10. Bridge A7957 Numbering Scheme

1.3. WORK PLAN

A work plan was drafted for this research program to outline the major tasks involved in the project. Ten major tasks were identified in the work plan for *MoDOT FRP Proposal Number: TRyy1236*. The tasks are listed here with the original instrumentation plan in Appendix B.

1. Pre-Construction Planning and Coordination
2. Development of Bridge Instrumentation Plan and Load Testing Plan (Bridge A7957)
 - Addressed in Report D (Sections 3 and 4)
3. Mix Design and Quality Control Procedures/Quality Assurance – Trial Mixes
 - Addressed in Section 5.1 with results located in Section 6.1.1
4. Shear Testing and Evaluation of HS-SCC Precast NU Girders
 - Addressed in Report B with results
5. Precast-Prestressed Plant Specimen Instrumentation and Fabrication
 - Addressed in Sections 5.2.6, 5.4 and in Section 3.6 of Report D

6. Field Cast-In-Place Elements and Instrumentation
 - Addressed in Section 5.2.6
7. Hardened Properties of Plant and Field Produced Concrete
 - Results located in Section 6.1
8. Bridge Load Testing and Monitoring/Evaluation of Experimental Load Testing Results
 - Addressed in Report D
9. Reporting/Technology Transfer
 - Presented in Summary Report
10. Value to MoDOT and Stakeholders to Implementing SCC/HVFAC
 - Presented in Summary Report

1.4. SCOPE OF THE REPORT

This report includes the instrumentation, fabrication, and construction of Bridge A7957 in Osage County Missouri. First, three trial mixes of HVFAC, NS-SCC, and HS-SCC were batched and collected for quality assurance of the following mechanical properties: compressive strength, modulus of elasticity, and splitting tensile strength. After the trial mix specimens were collected and tested, two precast-prestressed HS-SCC. For Bridge A7957, HVFAC and CC (MoDOT's class B mixture) were used in the substructure (columns, web walls, and pier caps) to compare the strength gaining characteristics and hydration profiles via thermocouple wire. Each of the three spans of the bridge was unique: the first span (span 1-2) utilized CC (MoDOT's class A-1 mixture), the second span (span 2-3) HS-SCC, and the third span (span 3-4) NS-SCC. Furthermore, material properties were collected from the three concretes and compared including: compressive strength, modulus of elasticity, modulus of rupture, shrinkage, creep, and coefficient of thermal expansion. Freeze-thaw, chloride penetration, and abrasion resistance tests were also performed on the concrete of the CIP deck (MoDOT modified class B-2 mixture). More details about the MoDOT's standard concrete mixtures are given in Section 2.6. During the course of this research, the MoDOT's mixes class A-1 and class B were referred to as conventional concrete (CC) mixes when they were compared to their counterpart mixes: NS-SCC, HS-SCC and HVFAC.

1.5. ORGANIZATION OF THE REPORT

The report is organized into seven sections. Section 1 contains an overview of the research program and general bridge details and numbering sequence. The instrumentation plan is also described as referenced from Appendix B of the MoDOT RFP Proposal Number: TRyy1236.

A literature review of SCC, HS-SCC, and HVFAC, and MoDOT's mix designs used in the study is addressed in section 2.

Section 3 contains the material testing program. A plethora of tests were conducted on the different concretes investigated during the program from compressive strength to creep and shrinkage to abrasion resistance.

The measurement types and systems are listed in section 4. Concrete temperatures and strains and member deflections were recorded. Among others, vibrating wire strain gauges (VWSG) were the primary instrumentation used during the program. The data collection system is also included in section 4.

Section 5 describes the chronological progression of events in the research program. The trial mixes were first conducted, followed by the member instrumentation and fabrication. The construction of the bridge is documented regarding girder erection, the CIP deck, approach slabs, and safety barriers followed by problems that were encountered in the study.

The results of the study are documented in Section 6. All material test results for the various concretes are documented. Conclusions are drawn and presented.

2. LITERATURE REVIEW

2.1. SELF-CONSOLIDATING CONCRETE (SCC)

2.1.1. Definition

According to ACI 237R-07, self-consolidating concrete (SCC) is a highly flowable, non-segregating concrete that can spread into place, fill the formwork and encapsulate the reinforcement without any mechanical vibration. SCC has numerous advantages over conventional concrete (CC) which includes:

- Reduce equipment, labor, and associated cost;
- Less need for screeding operations to ensure flat surface (self-leveling characteristics);
- Is cast with desired mechanical properties which is independent of the skill of the vibrating crew;
- Accelerated construction;
- Facilitates filling complex formwork or members with congested reinforcement;
- Decrease employee injuries;
- Permits more flexible reinforcement detailing and design; and
- Creates smooth, aesthetically appealing surfaces free of honeycombing and signs of bleeding and discoloration.
- All of these benefits can be obtained through the use of conventional concrete materials and admixtures and, in some cases, with high viscosity-modifying admixture (VMA).

2.1.2. Fresh Material Properties

The definition of SCC includes properties that are related to the fresh state of the concrete. Terms as flowable, nonsegregating, and fill refer to standardized tests that have been developed with definable quantitative measurements and suggested ranges.

Table 2.1, taken from NCHRP Report 628 (also ACI 237R 2007), summarizes the fresh properties of interest that were utilized for this implementation project. In addition,

the associated test methods (standard and non-standard), suggested test result targets, and recommendations related to whether these tests should be conducted for routine quality control or as part of an SCC mix design program are presented.

Table 2.1. Suggested Fresh Property Tests (Mix Design and Quality Control)

Property	Test Method	Target Values	Design	QC
Filling ability	Slump flow T-50 (ASTM C1611)	23.5-29 in (600-735 mm) 1.5-6 s (upright cone position)	√	√
Passing ability	J-Ring flow (ASTM C1621)	21.5-26 in (545-660 mm) 0-3 in. (0-75 mm)	√	√
Filling capacity	Slump flow and J-Ring flow tests			√
Static stability	Column segregation (ASTM C 1610)	Column segregation index (C.O.V.) ≤ 5%. Percent static segregation (S) ≤ 15%	√	
Air volume	AAHTO T 152	4% - 7% depending on exposure conditions, MSA, and type of HRWRA.	√	√

MSA: Maximum size of coarse aggregate

An important aspect of the suggested SCC fresh concrete quality control tests is that these can be satisfied by a combination of ASTM standardized tests, namely the slump flow, J-ring flow and the air content tests. The slump flow and J-ring tests are simple and have demonstrated repeatability. In addition, both tests have to be conducted within 6 minutes to be in conformance with the standard (ASTM C1621 2009).

The slump flow test is a measure of mixture filling ability, and it is performed similarly to the conventional slump test using the standard ASTM C143/C 143M slump cone. Instead of measuring the slumping distance vertically, the mean spread of the resulting concrete patty is measured horizontally. The value obtained is recorded as the slump flow (ACI 237R 2007).

The J-ring comprises a ring of reinforcing bars that will fit around the base of a standard ASTM C 143/C 143M slump cone. The slump cone is filled with concrete and then lifted in the same way a slump flow test is conducted. The final spread of the

concrete is measured, and the difference between the conventional slump flow and the J-ring slump flow values is calculated (ACI 237R 2007).

The column segregation test, as prescribed in ASTM C1610, evaluates the static stability of a concrete mixture by quantifying aggregate segregation. A 26 in. (610 mm) high column is filled with concrete. The concrete is allowed to sit for 15 minutes after placement. The column has three parts that are removed individually. The concrete from the top and bottom sections is washed over a No. 4 (4.75 mm) sieve, and the retained aggregate is weighed. A nonsegregating mixture will have consistent aggregate mass distribution between the top and bottom sections. A segregating mixture will have a higher concentration of aggregate in the lower section (ACI 237R 2007).

SCC mixtures used in PC/PS concrete girders should displayed a slump flow value of 23.5 to 29 in. (600-735 mm). In addition, a J-Ring flow value within a range of 21.5 to 26.0 in. (545 to 660 mm), and a difference in slump flow and J-Ring flow values lower than 4 in. (100 mm) should be displayed. Regardless of the MSA, stable SCC should develop a column segregation index (C.O.V.) less than 5% and percent static segregation lower than 15% (Khayat and Mitchell 2009).

Viscosity modifying admixtures (VMA) can be used to reduce the impact of material variability and improve the robustness of the designed SCC. However, it is important to prevent using VMA as a substitute of a well-formulated mix design or poor quality constituents. In addition, a careful selection of constituent materials, and a continuous quality assurance program (EFNARC 2006) are necessary.

Table 2.2 presents some slump flow test values as well as slump flow minus J-ring flow test values recommended by NCHRP that are based on the intended application of SCC (Khayat and Mitchell 2009). The fresh characteristics of SCC are described in terms of the two simple tests described early, namely the slump flow and J-ring tests. In 2006, Hwang concluded that the filling capacity is best described by a combination of passing ability and non-restricted deformability test (Hwang et al. 2006) such as the two shown in Table 2.2.

Table 2.2. Workability Values of SCC Used in Precast/Prestressed Applications

Relative Values		Slump flow, in			Slump flow – J-ring flow, in		
		23.5-25	25-27.5	27.5-29	3-4	2-3	≤2
Low	Reinforcement density	■				■	
Medium			■				
High				■			■
Small	Shape intricacy	■				■	
Moderate			■				
Congested				■			■
Shallow	Depth	■			■		
Moderate			■			■	
Deep							■
Short	Length	■				■	
Moderate			■				
Long							■
Thin	Thickness		■				
Moderate			■			■	
Thick		■				■	
Low	Coarse Aggregate			■			■
Medium						■	
High		■			■		

2.1.3. Hardened Material Properties

The mixture proportions may be adjusted to obtain a SCC concrete with similar or better hardened properties than those of a conventional concrete mixture. The following sections give an insight of the most important aspects that influence key mechanical properties when the SCC mixture is being developed.

2.1.3.1. Compressive strength

The strength of SCC mixtures is highly affected by the water to cementitious material (w/cm) ratio, age, powder content (cement and supplementary cementitious materials), curing conditions, admixtures used, aggregate gradation and surface texture (Mindess et al. 2003). SCC mixtures usually require a high flowable concrete with enough cohesion to improve the stability of the mixture. This requires SCC concrete mixtures to have a lower w/cm when compared to traditional concrete mixtures. As a result of using a lower w/cm (typically between 0.32 and 0.40), higher compressive

strengths are attained. The enhanced compressive strength is the result of the lack of vibration and reduction of bleeding and segregation that promotes a more uniform microstructure and less porous interface zone between the aggregate, paste and embedded reinforcement (ACI 237R 2007).

2.1.3.2. Modulus of elasticity

The modulus of elasticity (MOE) in concrete is affected by the compressive strength, aggregate type and content, and unit weight of concrete. SCC concrete mixtures typically have a decrease in the MOE because of the lower coarse aggregate and higher paste proportions utilized in their production. Various researchers have reported that for equal compressive strength, the elastic modulus of SCC can be as much as 10 to 15% lower than that of conventional concrete with similar compressive strength (ACI 237R 2007). Because MOE controls the response of RC and PC elements to load as well as the camber, creep and shrinkage, it is mandatory to quantify and understand the reduction in MOE for the mixtures in use.

2.1.3.3. Tensile strength

The tensile strength of concrete is determined by two separate tests: modulus of rupture (MOR) test (determined in accordance to ASTM C 78 or C 293), and splitting tensile strength (STS) test (determined in accordance to ASTM C 496). The tensile strength of SCC also depends on the w/cm, coarse aggregate volume, and the quality of the interface between aggregate and cement paste. Some researchers have reported that SCC may exhibit higher tensile strength than conventional concrete with similar batch proportions (ACI 237R 2007).

2.1.3.4. Creep and shrinkage

Creep and shrinkage are mostly influenced by the coarse aggregate volume and stiffness, rigidity of the cement paste and concrete, curing time, curing method, temperature, relative humidity, and concrete age at time of load application. Creep and shrinkage of SCC is affected by the mixture composition, paste volume and aggregate content. The high paste volumes and reduction in the aggregate content used in SCC mixtures results in a greater potential for shrinkage and creep. Shrinkage has been

reported to be similar to or lower than that of CC with similar compressive strength. Creep is expected to be similar for SCC and CC with similar mixture proportions. When SCC is proportioned with a greater paste volume, a higher creep is exhibited than it is for a CC with similar compressive strength. In addition, Persson (1999), reported that for mature SCC and CC with similar properties, the creep coefficient was compatible when the strength at load application was similar and held constant (ACI 237R 2007).

2.2. HS-SCC

2.2.1. Definition

High strength self-consolidating concrete uses the benefits of SCC with the added strength gain of HSC. ACI 363 defines high strength concrete as concrete with a specified concrete compressive strength for design of 8,000 psi (55 MPa) or greater (ACI 363 2010). Additionally, consideration must be taken when applying design equations in the ACI 318 code and AASHTO LRFD Bridge Design Specifications as many empirical relations were developed from data with compressive strengths less than 8,000 psi (ACI 318 2011, AASHTO 2012). A review of the mechanical and shear properties of this innovative material is presented.

2.2.2. Fresh Material Properties

The plastic state of HS-SCC is expected to be similar to that of NS-SCC. The reduced w/cm ratio in HS-SCC can lead to greater static stability (ACI 237 2007).

2.2.3. Hardened Material Properties

2.2.3.1. Compressive strength

The use of high-range water reducing admixtures (HRWRA) in HS-SCC mixes increases the compressive strength of equivalent HSC mixes (Myers et al. 2012). The HRWRA disperses the cement particles, which increases the proportion of cement particles available for hydration. Myers et al. (2012) also noted that the effect of the HRWRA increases as the compressive strength increases. This can be attributed to the lower w/cm ratio in high strength concrete mixes. Aforementioned results consisted of

dolomitic limestone coarse aggregate and a CA content of 48%, matching that used in this study. ACI 237R-07 also notes that, for a given w/cm ratio, SCC can achieve greater compressive strength than CC due to the reduction in bleeding and segregation resulting from mechanical vibration. Without vibration, SCC can achieve a more uniform microstructure with a less porous interfacial bond zone between the paste and aggregate (ACI 237R 2007).

2.2.3.2. Modulus of elasticity

An understanding of the elastic modulus of HS-SCC is necessary to more accurately predict camber, deflections, shrinkage, creep, and prestress losses. The MOE of HS-SCC has typically been found to be less than that of conventional high-strength concrete. The reduction in stiffness can be attributed to the smaller percentage and size of the coarse aggregate. Additionally, the larger paste content in HS-SCC theoretically leads to a reduction in the MOE. In 2007, Domone discovered that the reduction in MOE for SCC can vary from 40% to 5% for low and high strength concretes, respectively (Domone 2007). The reduction diminishes with compressive strength since high strength concretes already rely on the strength of the paste for stiffness. Various studies indicate that the AASHTO model more accurately predicts the MOE for SCC with crushed aggregate over ACI 363 and ACI 318 models (Khayat and Mitchell 2009; Long et al. 2013). Both ACI 363 and ACI 318 tend to underestimate the MOE (Long et al. 2013).

2.2.3.3. Tensile strength

The tensile strength of concrete is measured in two ways: splitting tensile strength (STS) test and modulus of rupture (MOR) test following ASTMs C496 and C78, respectively (ASTM C 496 2011, ASTM C 78 2010). The flexural strength depends on the w/cm ratio, coarse aggregate volume and the quality of the interface between the aggregate and cement paste. ACI 237 states that for a given set of mixture proportions, the flexural strength of SCC may be higher. However, Myers et al. (2012) found comparable results between HSC and HS-SCC in terms of MOR and STS tests.

2.2.3.4. Creep and shrinkage

The creep and shrinkage of HS-SCC is expected to be greater than that of its high-strength concrete (HSC) counterpart for similar compressive strength, a result of the smaller percentage and size of coarse aggregate as well as increased binder content of HS-SCC (Khayat and Mitchell 2009). Khayat and Mitchell found that for a given w/cm ratio, SCC exhibited 10-20% higher creep and 30% higher shrinkage than the HSC control mix. Additionally, for a given w/cm ratio, an increase in the binder content leads to an increase in drying shrinkage; this supports the trend that SCC mixes exhibit increased drying shrinkage than HSC. ACI 209 and AASHTO 2007 models underestimated both the drying shrinkage and creep for SCC mixes with Type I Portland cement (Khayat and Mitchell 2009).

In contrast, Myers et al. (2012) discovered that at a given w/cm ratio, HS-SCC exhibited less shrinkage and creep compared to HSC. This trend is confirmed at the University of Texas at Austin where the creep of HS-SCC was approximately 30% less than that of HSC when limestone was used. However, there was no difference in creep between the two mixes when river gravel aggregate was incorporated. The stiffness of the aggregate also contributes to the extent of creep in both conventional and SCC mixes. It was also noted that the AASHTO 2006 model best predicted the creep of the SCC mixtures containing limestone aggregate (Trejo et al. 2008). A more extensive parametric study should be undertaken to evaluate the effects of aggregate type, content and size in addition to the w/cm ratio and binder content.

2.2.4. Hydration Profile

Due to the increased paste content in HS-SCC, these mixes experience greater temperature gradients during curing. ACI 363 states that a temperature rise of 11 to 15°F per 100 lb/yd³ (10 to 14°C per 100 kg/m³) cement is expected in HSC depending on the geometry of the structural element (ACI 363 2010). Myers and Carrasquillo discovered that hydration temperatures above 170°F (76.7°C) can lead to microcracking within the concrete, hindering strength and durability properties (Myers and Carrasquillo 1998).

2.2.5. Shear Characteristics

A principal reason for hesitation in the implementation of HS-SCC lies in its reduced shear performance. The mechanisms which contribute to the shear strength of conventional prestressed concrete are listed as follows (Frosch and Wolf 2003):

- Uncracked concrete and the flexural compression zone. Shear is transferred through inclined principle tensile and compressive stresses.
- Aggregate interlock. As a crack forms around the aggregate, the protruded section creates a friction force that prevents slippage of the crack.
- Dowel action of longitudinal reinforcement. The reinforcement provides a vertical tension force that prevents slippage of the concrete.
- Residual tensile stresses across cracks. For hairline cracks, less than 0.006 in. (0.15 mm), the concrete can still bridge tensile stresses. However, this contribution is limited.

In the case of HS-SCC, modifications on material proportions, namely the reduced content and size of coarse aggregate, hinder the ability of the concrete to transmit shear stresses through aggregate interlock. Furthermore, when limestone aggregates are used in a HSC application, the failure plane can propagate through the aggregate particles, rather than at the paste-aggregate interface zone.

2.2.5.1. Push off test

A collection of researchers has studied the shear response of HS-SCC in push off tests. This is a widely recognized test, used and refined by Mattock (1969 and 1972), Reinhardt (1981), Walraven (1981 and 1994), and (Sells 2012).

Sells discovered that the coarse aggregate fraction and concrete type (HS-SCC vs. HSC) showed little impact on the shear resistance of the specimens. There was a slight trend that showed reduced shear stress for a given crack opening for higher strength concretes. The smoother failure plane in the high strength specimens explains the results. However, there was no distinguishable difference in shear stress at a given crack opening between the HS-SCC and HSC mixes for a given aggregate type.

The most distinguishable findings related to the aggregate type. The limestone aggregate carried significantly less shear stress across a crack opening than the river gravel. Thus, the river gravel exhibited greater aggregate interlock (Sells 2012).

Kim et al observed similar trends regarding push off tests of high and low strength SCC and CC mixes. Push off tests revealed a decreasing contribution of aggregate interlock at high compressive strength level, and an increased contribution of river gravel over limestone aggregates. There was also statistically significant data which showed the volume of coarse aggregate influences the contribution of aggregate interlock.

Additionally, the researchers noted a lower fraction reduction factor, c , and friction coefficient, μ , for HS-SCC than HSC at maximum shear stress. The fraction reduction factor accounts for the reduced contact area at a crack due to particle fracturing. The smaller volume of coarse aggregate in HS-SCC explains this trend (Kim et al. 2010).

2.2.5.2. Mid-scale and full-scale beam tests

There is limited evidence regarding beam shear testing on HS-SCC. In the case of SCC, there are mixed results concerning the ultimate shear capacity with respect to CC. Hassan et al. (2010) reported that SCC beams showed reduced shear resistance and ductility compared to their CC counterparts. Their results supported theory in which the ultimate shear stress decreases with an increase in the effective beam depth. Lin and Chen found that for an equivalent CA content, SCC beams had increased shear resistance; however, for typical SCC beams in which the CA content is lower than a CC mix for a given compressive strength, the shear resistance was found to be less than the CC beam (Lin and Chen 2012).

Sells conducted shear tests on mid-size precast-prestressed rectangular beams. His tests included high and low strength SCC and CC beams. The SCC and HS-SCC beams experienced increased deflections over the CC beams. This could be attributed to the lower MOE reported in the SCC mixtures. The failure loads for the HS-SCC beams exceeded the predicted failure from ACI 318, AASHTO 2007, and modified compression field theory (MCFT) estimates. The normalized shear stress for the HS-SCC beams slightly outperformed that of the HSC mix shown in Figure 2.1. The HS-SCC mix is

denoted by S10-48L and the HSC mix by C10-5L. The two HS-SCC beams exhibited less variation at ultimate failure loads than the HSC beams (Sells 2012). This could be attributed to the robustness of the SCC mixtures.

Full scale structural performance testing on AASHTO Type II girders was completed by Khayat and Mitchell. Four girders were fabricated from 8,000 and 10,000 psi (55 and 69 MPa, respectively) SCC as well as CC. The researchers noted the following in terms of shear performance (Khayat and Mitchell 2009):

- All four girders exceeded the nominal shear resistance according AASHTO 2007 specifications. However, the HS-SCC maximal shear load was 6.5% less than that of the 10,000 psi (69 MPa) CC girder
- Both the HSC and HS-SCC girders experienced initial shear cracking at similar loads
- The HS-SCC girders exhibited less ductility prior to shear failure
- The reduced ductility and shear resistance associated with the SCC mixtures could be attributed to the reduction in coarse aggregate volume, thereby reducing the energy absorbing characteristic of aggregate interlock

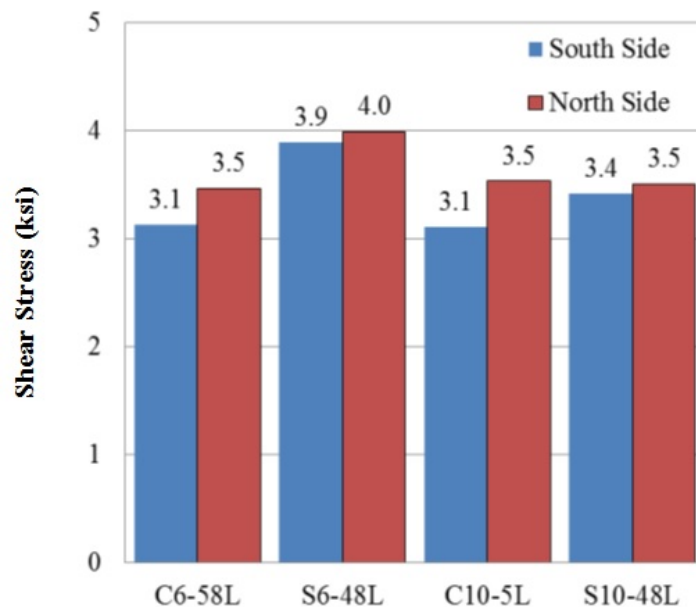


Figure 2.1. HS-SCC vs. HSC Ultimate Shear Stress (Myers et al., 2012)

2.3. PREVIOUS PROJECTS USING SCC AND HS-SCC

Self-consolidating concrete has been widely implemented across Japan, Europe and the United States. ACI 237 cites sixteen references linked to the use of SCC in both the precast and cast-in-place industry. The production in the precast industry in the United States raised from 17,000 yd³ in 2000 to 2.3 million yd³ in 2003 and continues to climb to this day (ACI 237 2007). The use of SCC has been widespread; however, the implementation of HS-SCC in structural applications is extremely limited. Examples of the implementation of SCC include:

Shin-kiba Ohashi Bridge, Japan. SCC was used in the production of the cable stay bridge towers (Okamura and Ouchi 2003).

Ritto Bridge, Japan. Due to congested steel reinforcement and the need for high earthquake resistance, SCC was chosen for the pier construction. The specified compressive strength of the SCC mixture was 7,250 psi (50 MPa) (Ouchi et al. 2003).

Higashi-Oozu Viaduct, Japan. SCC was chosen to produce the precast-prestressed T-girders to alleviate noise complaints from vibration of the concrete and to create a smoother finished surface. The specified compressive strength used in the T-girders was 7,250 psi (50 MPa) (Ouchi et al. 2003).

Soda Lanken Project, Sweden. Difficulties in compaction of conventional concrete in rock lining, wall sections and arch sections in the tunnel led to project managers choosing SCC. The decision also provided an increased aesthetic appearance. The 28-day cube compressive strength ranged from 10,000 to 11,600 psi (70-80 MPa) (Ouchi et al. 2003).

Pedestrian Bridges, Rolla, Missouri. An implementation project comparing the use of HSC and HS-SCC concrete was conducted on two pedestrian bridges in Rolla, MO. Both the hardened properties and time-dependent deformations were studied via load tests. This was the only discovered project implementing HS-SCC in a bridge application (Myers and Bloch 2011).

Tauranga Harbour Link, Tauranga, New Zealand. Self-consolidating concrete was chosen to expand the multi-span existing bridge at the Port of Tauranga. The

expansion was completed in the fall of 2010. SCC was chosen to achieve the goal 100-year design life in a harsh marine environment. Durability models predicted a useful design life ranging from 103 to 156 years depending on the structural element and level of clear cover. The design strength of the pretensioned beams was 8700 psi (60 MPa); however, to achieve the desired durability properties, the two SCC mix designs developed for the project had 28-day design cylindrical compressive strengths of 10,400 psi and 12,600 psi (71.5 and 87.0 MPa), respectively. By incorporating HS-SCC, the cost advantage for the design build team was 20% of the bid price, or \$20 million dollars. This project provides a prime example of the cost savings associated with SCC (McSaveney et al. 2011).

2.4. HVFAC

2.4.1. Definition

High volume fly ash (HVFA) concrete has been typically defined as concrete mixtures that contain more than 30% fly ash by mass of cementitious material (Volz et al. 2012; Naik et al. 1995). Other authors have defined HVFA concrete mixtures as having more than 50% fly ash by mass of cementitious material with a low water content of $w/cm < 0.40$ (Reiner and Rens 2006).

2.4.2. Fresh Material Properties

2.4.2.1. Workability

Bouzoubaa et al. (2010) evaluated the effects of varying the fly ash contents and the required dosage of HRWRA on the concrete mixtures' slump. The results indicated that the mixtures prepared with unground fly ash required less HRWRA to obtain a target slump than the mix that had been interground with the cement. An increment in the required HRWRA was primarily due to the larger fineness of the interground fly ash.

Bouzoubaa et al. (2007) studied the variation of the mass replacement of cement (30%, 40%, and 50%) by fly ash. Three different concrete mixes with compressive strength of: 2.9, 5.8 and 8.7 ksi (20, 40, and 60 MPa, respectively) were obtained by

varying the cement content. By increasing the fly ash content, the water requirement to attain a given slump decreased, and consequently the w/cm decreased.

2.4.2.2. Air content

Bouzoubaa et al. (2001) also investigated the effect of varying the fly ash content on the concrete mix's air content. In the case of fly ash interground with cement, the results indicated that a higher dosage of air entraining agent was required than when the mix was prepared with unground fly ash. The reason was due to the increase of the fineness of the interground fly ash.

Bilodeau et al. (1994) reported that the amount of air entraining agent required to attain the desired air content was greatly influenced by both the fly ash and the cement used in the mix. Different dosages were necessary due to the carbon, alkali contents, and fineness of the fly ash as well as the alkali content of the cement used.

2.4.2.3. Setting time

It has been observed that the initial and final setting times are arbitrarily defined in test methods, and they do not mark a specific physical or chemical change in the cement paste (Mehta and Montiero 1993). However, the initial setting time defines the limit of handling, and the final setting time marks the beginning of development of mechanical strength.

In addition, Bouzoubaa et al. (2001) reported that the setting times for HVFA concrete mixtures were 30 minutes to 3½ hours longer than those of the baseline mixes. The fly ash mixes used in this study consisted of 45% by mass of cement, and 55% by mass of a Class F fly ash.

2.4.3. Hardened Material Properties

2.4.3.1. Compressive strength

The compressive strength of HVFA concrete typically suffers in the short term as highly reactive cement is replaced with less reactive fly ash. Bouzoubaa et al. (2001) reported that 55% Class F fly ash mixtures achieved around half the strength of

conventional concrete mixes at one day. The fly ash mixtures began to match or exceeded the strength of the control mixes between 14 and 28 days. In addition, substantial strength gains occurred at one year.

Galeota et al. (1995) conducted a maturity study to determine the difference in strength gains by using Class F fly ash to obtain mixes at 30%, 40%, and 50% replacement by mass of cement with fly ash. The results showed a strength development delay behind their control mix counterpart. This difference between the HVFA mixtures and the control mix diminished as the specimens age, and at one year of age, the 40% fly ash mix has exceeded the control mix in compressive strength.

In terms of the long-term effects of high volumes of both Class C and Class F fly ash on concrete mixtures, it was observed that increasing volumes of both types of fly ash resulted in a similar decrease in early strengths. However, Class F fly ashes show a better long-term strength gain correlation with increased fly ash volume. Due to the pozzolanic activity given by the higher calcium content in Class C fly ashes, Class C fly ashes performed better at early age strength gains than Class F fly ashes (Naik et al. 2003).

2.4.3.2. **Modulus of elasticity**

Rivest et al. (2004) reported that the MOE for HVFA concrete mixes was generally higher than for control concretes made with Type I and Type II cement. This was related to the content of unreacted glassy fly ash particles acting as a very fine aggregate rather than hydration products, thereby, increasing the rigidity of the concrete. Additionally, the filler effect of the fly ash contributes to a stronger transition zone that contributes to increase the rigidity of the concrete.

2.4.3.3. **Hydration profile**

An important aspect to be considered when large volumes of cement are replaced with fly ash is the effect produced on the hydration curve of the cementitious system. Some researchers have investigated this effect when Type I and II cement was replaced with 20% of Class C and Class F fly ash (Wang et al. 2006). Class C fly ash helped reduce the heat release and delay the peak of the hydration curve which effectively retarded the set of the concrete mixture. Additionally, Class F fly ash only provoked a

reduction of the heat release. When a substitution of fly ash was coupled with an addition of a water reducer (WR) and a retarding admixture, the Class C mixes were significantly affected compared to any other combination. The addition of these two admixtures caused a delay of the hydration for an extended time (Wang 2006a).

2.5. CONVENTIONAL CONCRETE

A brief review of the durability properties that were investigated for the CIP deck of Bridge A7957 is presented.

2.5.1. Freeze-thaw Resistance

An exposure to cycles of freezing and thawing is considered a severe exposure condition on the concrete. Air entrainment has been used since the 1930s to improve the resistance to freezing and thawing. Stark (1989) found that long freeze-thaw cycles more severe than freeze-thaw cycles for same number of cycles, even where air void spacing factors were no greater than 0.008 in (0.2 mm). Sun et al. (2002) showed that there is a large difference in the freeze-thaw effects of a specimen in water and one in NaCl solution. Also, concrete in chloride loses weight faster and reaches the failure threshold earlier than concrete in water. The loss of weight is mainly due to surface scaling which was found to be twice as fast in NaCl solution as it was in water, Sun et al. (2002).

2.5.2. Abrasion Resistance

Abrasion is wearing due to repeated rubbing or frictional processes. For pavements, abrasion results from traffic wear. Laplante et al. (1991) indicated that concrete resistance to abrasion is strongly influenced by the relative abrasion resistance of its constituent materials such as coarse aggregates and mortar. Where concretes with trap rock or granite as aggregates exhibit higher abrasion resistance compared to the "softer" limestone aggregate concretes. On other hand, Nanni (1989) showed that compressive strength is a poor parameter to evaluate abrasion because of the influence of surface finishing and curing conditions. In general, proper finishing and curing practices are known to enhance the abrasion resistance of concrete considerably.

2.6. MODOT STANDARD CONCRETE MIXES

The Missouri Department of Transportation (MoDOT) specifies four concrete class mix designs for use in new bridge construction. The four mixes according to section 751.4.1 of MoDOT's Engineering Policy Guide (EPG) are as follows (MoDOT 2011):

- A-1. Used for prestressed concrete girders including precast panels.
- B. Typically used for the above-ground substructure elements.
- B-1. Used for barrier curbs and substructure elements needing additional compressive strength.
- B-2. Used for slabs, and subsurface structural elements.

All four of the above mixes were used during the course of this research program in addition to a NS-SCC mix with a design compressive strength of 8,000 psi (55.2 MPa), a HS-SCC mix with a design strength of 10,000 psi (68.9MPa), and a HVFAC with a specified design strength of 3,000 psi. Mix designs for the bridge elements investigated are discussed in Section 5.

3. MATERIAL TESTING PROGRAM

3.1. INTRODUCTION

To provide more accurate results and get a comparison of CC, HVFAC, NS-SCC, and HS-SCC, material and mechanical tests were conducted. In this section, the compressive strength, MOE, modulus of rupture, splitting tensile strength, shrinkage, creep, freeze-thaw, ponding chloride concentration, and coefficient of thermal expansion tests were determined.

3.1.1. Member Cast

The precast girders and deck panels were fabricated at County Materials Corporation, located in Bonne Terre, MO. The bents and deck slab were cast-in-place (CIP). The deck slab was cast from the east to the west side of the deck after erection of PC/PS girders at the site.

To ensure concrete quality control/quality assurance (QC/QA) compliance, all girders and panels specimens were cast next to the precast members (PC/PS girders and deck panels). This exposed the specimens to similar curing conditions as the precast members fabricated within the precast concrete plant. The specimens of the bents, deck slab, and safety barriers were fabricated at the jobsite. The specimens that were collected during this stage are shown in Figure 3.1.



a) Precast Girder QC/QA Specimens



b) Deck Slab QC/QA Specimens

Figure 3.1. QC/QA Specimens Placement at Precast Plant and Jobsite

3.1.2. Curing Conditions

For the first days the girders, deck panels, and CIP member specimens were field cured where they were left close to the members to have same member condition. After releasing the prestressing strands for the precast member, the QC/QA specimens were taken to Rolla, MO. The Compressive strength, MOE, splitting tensile, and modulus of rupture were stored outside a storage area on campus which had similar environmental conditions as the member in the precast concrete plant yard. The shrinkage, creep, and coefficient of thermal expansion specimens were placed within an enclosed temperature controlled environment. The chloride ponding and abrasion resistance specimens were kept in a 70°F (21.1 °C) room. This room is called ASTM moist curing room which had a temperature of 70 F (21.1 °C) and a humidity of 100%. Figure 3.2 displays the location of the material specimens during storage.



a) Summer Storage



b) Winter Storage

Figure 3.2. Storage of QC/QA Specimens at Missouri S&T

3.1.3. Testing Program Overview

Table 3.1 and Table 3.2 summarize the material testing program for the testing of fresh properties and collection of QC/QA specimens.

Table 3.1. Summary of Fresh Properties of Material Testing Program

Test	ASTM Standard	Mix Type
Slump	C143	CC, HVFAC
Cylinders	C31	CC, SCC, HVFAC
Air content	C231	CC, SCC, HVFAC
MOR beams	C31	CC, SCC
Creep molds	C470	CC, SCC
Segregation column	C1610	SCC
Slump flow	C1611	SCC
Passing ability (J-ring)	C1621	SCC

3.2. COMPRESSIVE STRENGTH

The compressive strength test was measured according to ASTM C39-12 “Standard Test Method for Compressive Strength of Cylindrical Concrete Specimens.” This standard requires a cylinder with 4 x 8 in. (100 x 200 mm) dimensions. Each specimen was capped using a high-strength, sulfur-based capping compound before being placed into a compressive testing machine. The specimens were tested by using the Tinius-Olsen testing machine at the Construction Materials Load Frame Laboratory located in the Butler-Carlton Civil Engineering Hall of the Missouri S&T, Rolla, MO. Figure 3.3 shows the testing machine and specimens after the test.

3.3. MODULUS OF ELASTICITY

The MOE of the concrete is considered as a function of the MOE of aggregates and cement matrix and their relative proportions. The MOE is one of the important mechanical properties of concrete. So, to determine serviceability and performance of the HVFAC, NS- SCC, and HS-SCC, the MOE is required. ASTM C469 -10 “Standard Test Method for Static Modulus of Elasticity and Poisson’s Ratio of Concrete in Compression” was used to determine MOE using 4 x 8 in. (100 x 200 mm) cylinders. All specimens were tested with the Tinius-Olsen testing Machine at the Construction

Materials Load Frame Laboratory located in the Butler-Carlton Civil Engineering Hall at Missouri S&T, Rolla, MO.

Table 3.2. Summary of Hardened Properties of Material Testing Program

Tests	Test Method	Specimens	Material
Compressive Strength	ASTM C39 -12	4 x 8 in. (100 x 200 mm) cylinders	A, B, C, D, E, F, G, H, I
Modulus of Elasticity	ASTM C469 -10		A, B, C, D, E, H, I
Splitting Tensile Strength	ASTM C496 -11		B, C
Modulus of Rupture	ASTM C78 -10e1	6 x 6 x 21/24 in. (150 x 150 x 500/600 mm) beams	D, E
Creep	ASTM C512 -10	4 x 24 in. (100 x 600 mm) cylinders	E
Shrinkage	ASTM C157 -08		
Freeze-Thaw Durability	AASHTO T161-12	3.5 x 4.5 x 16 in. (90 x 115 x 400 mm) beams	H
Chloride Ponding	ASTM C1543-10	18 x 18 x 4 in. (460 x 460 x 100 mm) square specimen	H
A: HVFAC Trial Mix D: HS-SCC Test Girders G: Precast Panels B: HS-SCC Trial Mix E: Bridge Girders H: CIP Bridge Deck C: NS-SCC Trial Mix F: Intermediate Bents I: Safety Barriers			

To determine the MOE, the compressive stress, f_{ct} , that is produced when the strain reaches 0.00005 in/in and the strain, ϵ_{ct} , at 40% of the ultimate stress, f'_c , are required. The MOE was calculated by $(0.4f'_c - f_{ct})/(\epsilon_{ct} - 0.00005)$. The testing apparatus is displayed in Figure 3.4.



a) Tinius-Olsen Testing Machine

b) Compressive Specimens after Test

Figure 3.3. Compressive Strength Test



Figure 3.4. MOE Test Set Up

3.4. SPLITTING TENSILE STRENGTH

ASTM C496-11 “Standard Test Method for Splitting Tensile Strength of Cylindrical Concrete Specimens” was used to determine the splitting tensile strength. Cylindrical specimens, 4 x 8 in. (100 x 200 mm), were used for splitting tensile tests. The specimens were steam cured. The tests were done with the Tinius-Olsen testing machine at the Construction Materials Load Frame Laboratory located in the Butler-Carlton Civil Engineering Hall at Missouri S&T, Rolla, MO. In order to run this test, wooden strips were utilized to induce the stress locations required in the ASTM. The test setup is shown

in Figure 3.5. The specimens were loaded at a continuous rate of 100 to 200 psi per minute (0.7 to 1.4 MPa per minute) until failure. Table 3.3 shows the testing apparatus and set up.



Figure 3.5. Typical Splitting Tensile Test Set Up

Table 3.3. Specimens for Splitting Tensile Test

NS-SCC Trial Mix	HS-SCC Trial Mix
1 day (3 Cylinders)	3 day (3 Cylinders)
7 days (3 Cylinders)	7 days (3 Cylinders)
28 days (3 Cylinders)	28 days (3 Cylinders)
Pour Date: 1/30/2013	Pour Date: 3/8/2013
Total Cylinders: 18	

3.5. MODULUS OF RUPTURE

The flexural strength of concrete is determined by calculating the concrete's modulus of rupture. ASTM C78 -10e1 "Standard Test Method for Flexural Strength of Concrete (Using Simple Beam with Third- Point loading)" was used to perform modulus of rupture test. The specimen tested was a 6 x 6 x 24 in. (150 x 150 x 600 mm) beam. The test was completed at Butler-Carlton Hall at the Missouri S&T in Rolla, MO, using a Tinius-Olsen testing machine. The specimens were loaded continuously at a rate of 125 and 175 psi per minute (0.86 and 1.21 MPa per minute). Test set up can be seen in Figure 3.6.



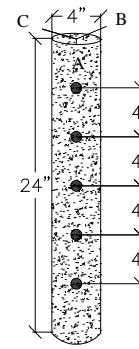
Figure 3.6. Modulus of Rupture Test Set Up

3.6. SHRINKAGE AND CREEP

Creep and shrinkage can be critical factors for design of structural members due to the length change by time dependent deformation. A modified version of the ASTM C512 (2010) “Standard Test Method for Creep of Concrete in Compression” was performed to determine the creep of 4 x 24 in. (100 x 600 mm) concrete cylinders. The cylinders were loaded to 40 percent of the design strength of 10,000 psi and 8000 psi (68.9 MPa and 55.2 MPa). In addition, the same cylinders were used to determine the shrinkage of the specimens using a modified version of ASTM C157 (2008) “Standard Test Method for Length Change of Hardened Hydraulic-Cement Mortar and Concrete.” The concrete specimens are similar to the cylinders used by Myers’ research on high performance concrete (Myers 1998). The molds preparation and test of creep and shrinkage followed the same procedure that was done in Myers’s research on HSC and HS-SCC (Myers and Bloch 2010). Figure 3.7 displays the cylindrical specimens and the location of the various DEMEC points used to determine the strain of the specimens. Each specimen was placed in 4 x 24 in. (100 x 600 mm) polyvinyl chloride (PVC) pipes.



a) Creep and Shrinkage Specimens



b) DEMEC Points Installation

Conversion: 1 in = 24.5 mm

Figure 3.7. Creep & Shrinkage Specimen & DEMEC Point Arrangements

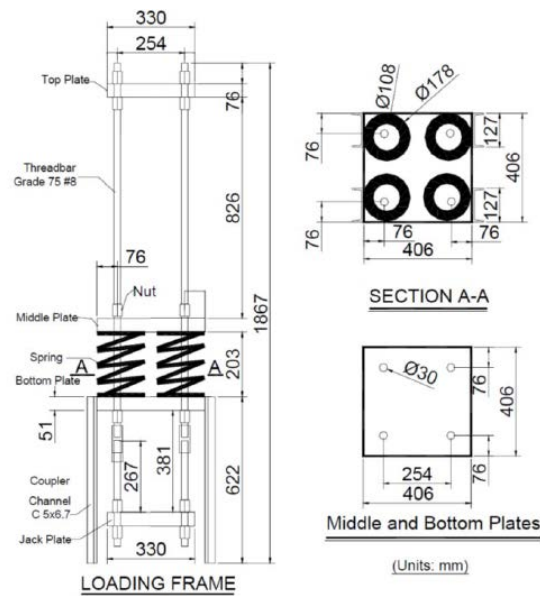
Within 24 hours of placement, the specimens were de-molded and DEMEC points were outfitted with five-minute quick set epoxy on the specimens and preliminary readings were taken. Nine locations on each cylinder could be read to determine the change in strain over that length. The average of all of the readings was computed to be the total strain of the specimen. Table 3.4 lists the specimens made to determine the creep and shrinkage of CC, NS-SCC, and HS-SCC.

Table 3.4. Creep & Shrinkage Specimens

Material	CC	NS-SCC	HS-SCC
Placed	7/29/2013	8/6/2013	8/13/2013
Shrinkage	1,2,3	1,2,3	1,2,3
Creep	1,2,3	1,2,3	1,2,3
CC: 6 cylinders NS-SCC: 6 cylinders HS-SCC: 6 cylinders		Total: 18 cylinders	

Specimens were read every day for the first two weeks, every two days for the next week, once a week for the first month, and then every month for a full year, thereafter. The specimens were stored and monitored in the Engineering Research Lab (ERL) Structural Engineering Laboratory to keep the specimens within an area that would maintain an average relative humidity of 50% and a temperature around 70 °F (21.1°C). However, fluctuations in humidity and temperature did occur on days when the

loading dock door was opened and closed for large scale specimen delivery and removal. The creep specimens were loaded after the bridge erection when the bridge experienced loading applied by the deck panels. While waiting for the bridges to be erected, the specimens were sulfur capped to provide a smooth surface that would be in uniform contact with the load frame. In addition, the load frames were assembled. The frames loaded the specimens at 40% of the target load, and the springs had an average radius of 7.7 in. (195 mm) and an approximate stiffness of 10.25 k/in (1.795 kN/mm). After the CIP deck was placed (October 21, 2013), the creep specimens were loaded in the creep frames (October 23, 2013). In order to load the specimens, a jack and load cell were required to be positioned under the load frame on a jack plate. After the creep specimen was centered within the frame, the jack increased the load to the required stress level of 4,000 psi (27.6 MPa) in the case of the 10,000 psi (68.9 MPa) concrete specimens. In the case of the 8,000 psi (55.2 MPa) concrete specimens, the jack load applied was 3,200 psi (22 MPa). Once the required axial load was obtained, the bolts were tightened and the jack was removed. In Figure 3.8, a representative schematic is provided for the creep load frame utilized for the 4,000 psi (27.6 MPa) stress level.



(Myers and Yang, 2005)

Conversion: 1 in. = 25.4 mm

Figure 3.8. Schematic of Creep Loading Frame



(a) Creep Frames in High Bay Laboratory



(b) Creep Cylinder Loaded in Creep Frame

Figure 3.9. Creep Loading Frame & Specimens

This schematic was provided by Myers and Yang in their research on HPC girders and used in the creep load frame assembly since the same creep frames were implemented in their research (Myers and Yang 2005). Readings were taken in the same interval as those of the shrinkage specimens. Figure 3.9 displays images of the apparatuses used to apply the required sustained load to the creep specimens.

3.7. COEFFICIENT OF THERMAL EXPANSION

The coefficient of thermal expansion (CTE) in concrete is the measure of how concrete changes in volume in response to changes in temperature. The CTE of concrete is defined as the rate at which concrete contracts or expands as temperature changes. The following method was used to determine the CTE (Myers and Bloch 2011). A shrinkage specimen was taken from each concrete mixture. The test was completed 6 months after curing to ensure that shrinkage strain was not contributing to the change in length of the specimen. Initial strain and temperature readings were taken on each specimen utilizing the DEMEC gauge and a laser surface thermometer. The temperature was taken at the top, middle, and bottom of each specimen. Each specimen was placed into a freezer set at -25°C (-13°F). The freezer is shown in Figure 3.10. After 24 hours, each specimen was taken out and strain and temperature readings were immediately taken.



(a) CTE Specimen



(b) Specimen Inside the Refrigerator

Figure 3.10. Coefficient of Thermal Expansion (CTE) Test at Missouri S&T

Due to the rapid temperature change of the specimens while taking the strain readings, an average temperature was determined using the temperature immediately after the specimens were removed from the freezer and after strain readings were taken. Calculation of the CTE is provided in Equation (6.45), where $\alpha_{concrete}$ is the CTE of the concrete mixture, $\Delta \epsilon_{temp}$ is the change in strain measured, and ΔT is the difference in measured temperatures.

$$\alpha_{concrete} = \frac{\Delta \epsilon_{temp}}{\Delta T} \quad (3.1)$$

3.8. FREEZE-THAW DURABILITY

The resistance to freezing and thawing of the concrete was performed in accordance with AASHTO T161 “Standard Method of Test for Resistance of Concrete to Rapid Freezing and Thawing.” Procedure B was used. Stainless steel molds 3.5 in. (89 mm) in width, 4.5 in. (114 mm) in height, and 16 in. (406 mm) in length were used to fabricate specimens as shown in Figure 3.11. A specialized bolt was installed at the ends of each mold through a threaded hold in the end of each mold. After the specimens were de-molded, the end of this bolt protruded from both ends of the prism. The embedded bolt gives a mechanism to measure the length change of the concrete prism as it is subjected to freezing and thawing cycles. The beams were wet cured for 35 days in lime

water. All rapid freezing and thawing tests were performed by MoDOT employees of the Construction & Materials Division in Jefferson City, Missouri. The F-T test process can be seen in Figure 3.12.



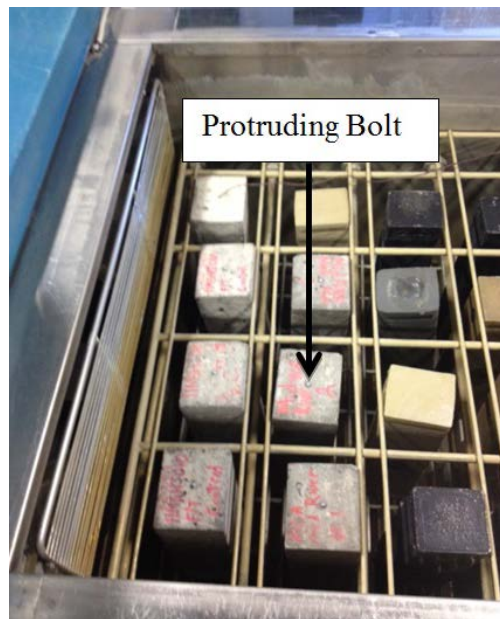
Figure 3.11. Freezing and Thawing Specimen Molds



(a) Preparing F-T Specimens



(b) Specimens during Curing



(c) Freezing and Thawing Test Machine

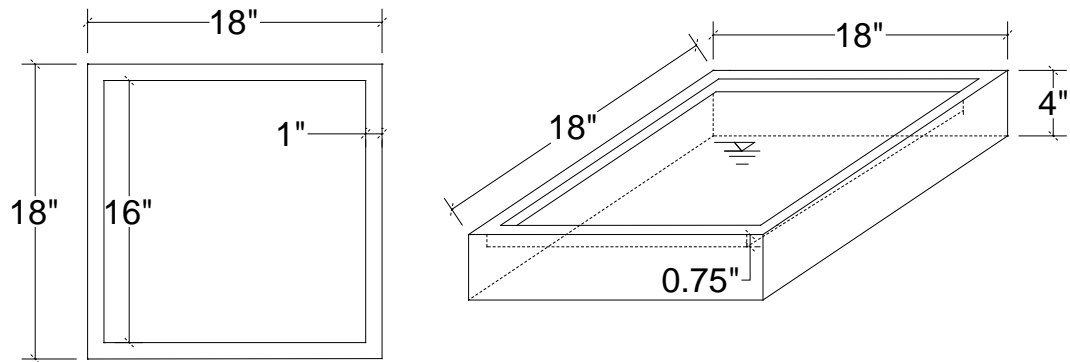


(d) Inside the MoDOT Construction & Materials Laboratory

Figure 3.12. Freezing and Thawing Test

3.9. CHLORIDE PONDING

In reinforced concrete bridges, one of the major forms of environmental attack is chloride ingress, which leads to corrosion of the reinforcement steel and a subsequent reduction in the strength and serviceability of structure. Also, during winter season, de-icing salts are used to dissolve snow and ice from bridge deck. The chloride in the de-icing penetrates to the concrete caused problems. The ability of chloride ions to penetrate the concrete must then be known for design as well as quality control purpose. Therefore, in order to assess chloride penetration, Ponding test was conducted. ASTM C1543-10 “Standard Test Method for Determining the Penetration of Chloride ion into Concrete by Ponding” was used to fabricate the concrete specimens for Ponding test. Three specimens were made as shown in Figure 3.13. After 24 hours from placed the concrete into formwork, the specimens were de-molded and placed in a moist curing room at 100% relative humidity. After 14 days of moist curing, the specimens were transported to a temperature and humidity controlled environment where they would cure at 75 °F (23.8°C) and 65% relative humidity for another 14 days.



Conversion: 1 in. = 25.4 mm

Figure 3.13 Ponding Test Specimen Dimensions

After 28 days of curing, the specimens would then begin the ponding test. A 5% by weight chloride solution was placed into the ponding specimens and covered with plastic sheeting and the sheets were secured with plastic bands to prevent evaporation of solution. Figure 3.14 shows the specimens after the chloride solution was added and the specimens were covered with plastic sheet.



Figure 3.14 Ponding Specimens

The specimens were periodically monitored to ensure that the depth of chloride solution was maintained. After 60 days of ponding, the solution was replaced with a fresh one and the plastic sheet was changed. After 120 days of ponding, the solution was

removed and the specimen's surface was allowed to dry. After drying was completed, salt crystals were removed from the surface by brushing with wire brush.

Table 3.5 Ponding Sample Interval

Sampling Intervals (in)	
ASTM Range	Sample Range
0.39-0.79	3/8-3/4
0.98-1.38	1.0-1.4
1.57-1.97	1.6-2.0
2.17-2.56	2.2-2.5

Conversion: 1in=25.4mm

Concrete powder samples were collected using a hammer drill as shown in Figure 3.15. At least 3.3×10^{-3} lb. (1.5g) samples were taken at the intervals within those listed in ASTM C1543-10 (Table 3.5). The chloride analysis of water soluble chlorides was performed using the Rapid Chloride Testing (RCT) equipment made by Germann Instruments, Inc. The equipment was calibrated before each use and the calibration results were used to find the chloride content once the mV was found using the RCT meter. Findings were classified using the ranking proposed by Broomfield (2007) (Table 3.6).



Figure 3.15 Ponding Chloride Test

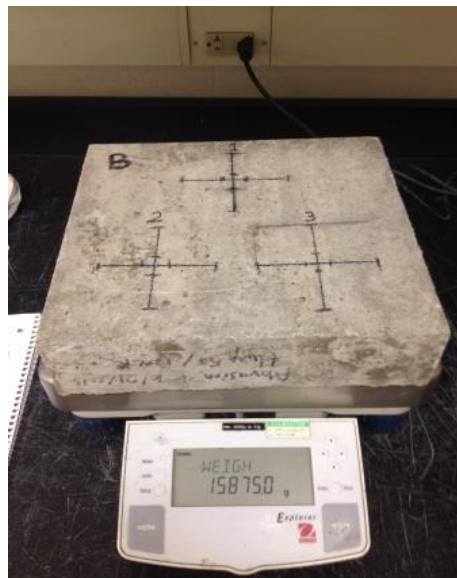
Table 3.6 Correlation between %Cl by Mass of Concrete and Corrosion Risk

% Chloride by mass of concrete	Corrosion Risk
<0.03	Negligible
0.03-0.06	Low
0.06-0.14	Moderate
>0.14	High

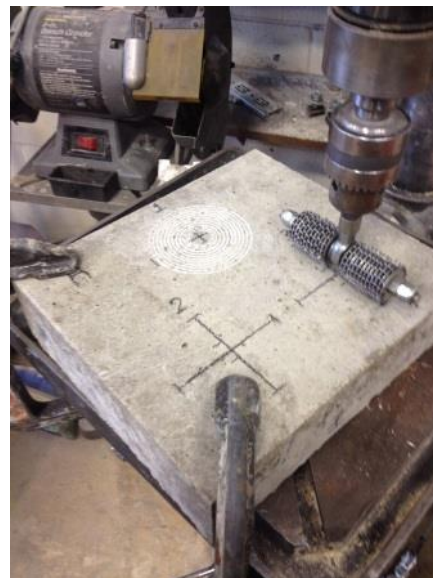
Note: Adapted from Broomfield, 2007

3.10. ABRASION RESISTANCE

ASTM C944 “Standard Test Method for Abrasion Resistance of Concrete or Mortar Surfaces by the Rotating Cutter Method” was used to determine abrasion resistance. Three 12 x 12 x 3 in. (305 x 305 x 75 mm) specimens were cast from the deck slab concrete in a 2 x 3 in. (50 x 75 mm) mold made of wooden sections and attached to a plywood base. Concrete was placed and external vibration was used. Specimens were moist cured until testing at 28-day age. The test was conducted at the Butler-Carlton Civil Engineering Hall in the High Bay Laboratory at Missouri S&T. Figure 3.16 shows the specimens during and after completion the abrasion test.



(a) Specimen before the Test



(b) Specimen during the Test

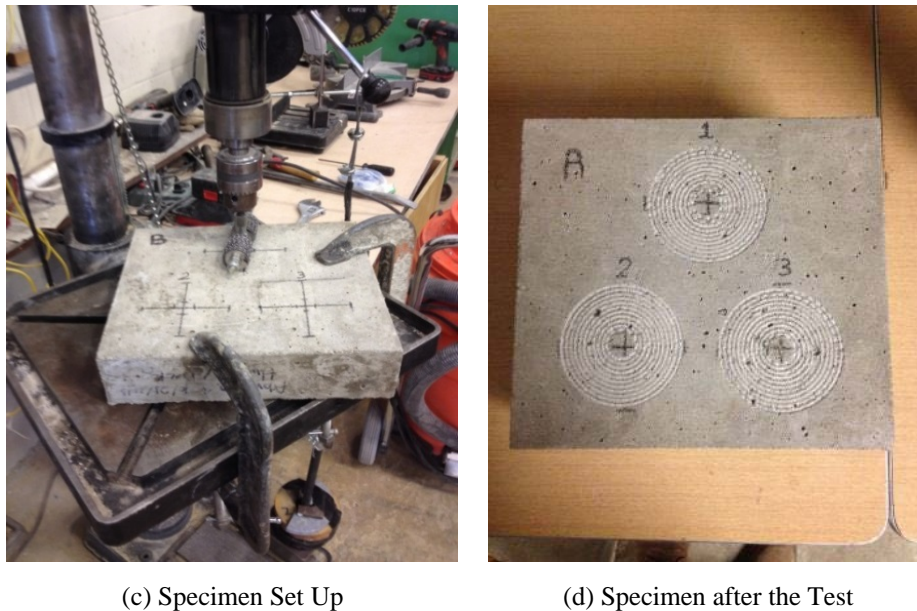


Figure 3.16. Abrasion Test

3.11. NASP BOND TEST

The NASP bond test was conducted following a procedure that was developed by Russell at Oklahoma State University in 2006. The test aims to assess the bonding abilities of seven wire prestressing strand with concrete. Strand with 0.6 in diameter was used and cut to 32 in lengths. The molds were constructed with 18-in (457 mm) long sections of 5 in. (127 mm) outside diameter, 1/8-in thick (3 mm) steel tubing. The sections of tube were welded to 6 x 6 x 0.25 in. (152 x 152 x 6 mm) steel plates with a 5/8 in. (16 mm) diameter hole in the center. A 1.75 in. (45 mm) section of inverted 2 x 2 in. (51 x 51 mm) angle was welded onto the side of the tube at the open end to allow for the attachment of an LVDT during testing. Figure 3.17(a) shows the NASP specimens. Three specimens for NS-SCC and three for CC were tested. The test was completed at the Butler-Carlton Civil Engineering Hall in the High Bay Laboratory using the MTS-880 testing machine. The free end slip of the specimen was monitored by an LVDT mounted on the specimen. The specimens were loaded at a rate of 0.1 in/minute until the test was completed. The NASP result value is the load that is required to displace the free end by 0.1 in. Figure 3.17(b) shows the NASP test.

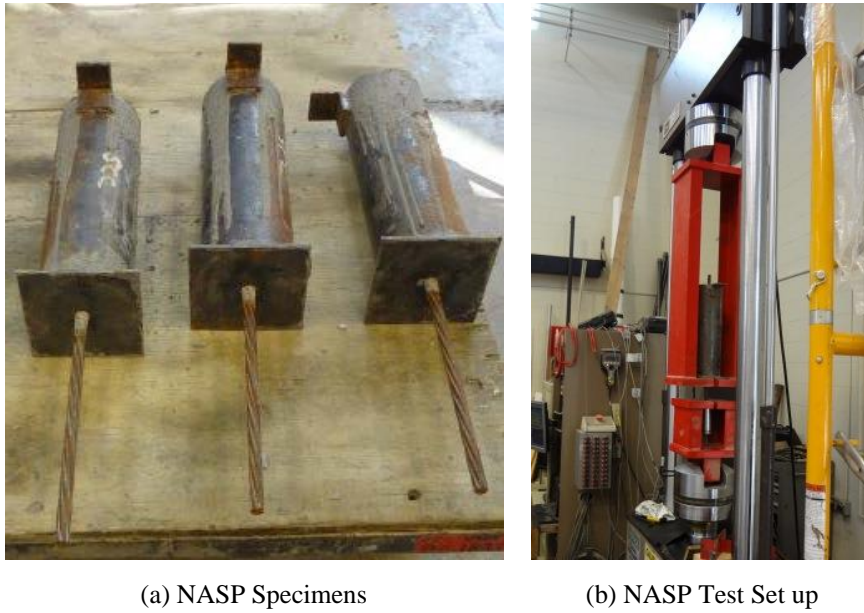


Figure 3.17. NASP Bond Test

3.12. SUMMARY

In this section, a material testing program for the concrete types investigated was developed. Tested hardened properties included compressive strength, MOE, splitting strength, rapid chloride ponding, freeze- thaw, creep, shrinkage, and coefficient of thermal expansion. Table 3.7 below summarizes the test program for Bridge A7957

Table 3.7. Summary of Material Testing Program

Time	Bents		Girders			Panels**	Deck*	Barriers*
	HVFAC*	CC*	Span1	Span2	Span3			
			CC**	HS-SCC**	NS-SCC**			
Release	C	C	C, E	C, E	C, E	C		
3 days	C	C	C, E	C, E	C, E	C	C,E	
7 days	C	C	C, E	C, E	C, E	C	C,E	C,E
14 days	C	C	C, E	C, E	C, E			
28 days	C	C	C, E, R	C, E, R	C, E, R	C	C,E	C,E
56 days	C	C	C, E	C, E	C, E	C	C,E	C,E
1 st Load Test			C, E, R	C, E, R	C, E, R	C	C,E	C,E
2 nd Load Test			C, E, R	C, E, R	C, E, R	C	C,E	C,E
1 year	C	C	C, E	C, E	C, E	C	C,E	C,E
Additional			CTE	CTE	CTE		AB***, P***, FT***	
Continuous			CR, SH	CR, SH	CR, SH			

*Field curing

C - compressive strength

FT - freeze-thaw

SH - shrinkage

**Member curing

E - modulus of elasticity

CTE - coefficient of thermal expansion

AB - abrasion resistance

***ASTM specified curing

R - modulus of rupture

CR - creep

P - ponding

4. MEASUREMENT SYSTEMS

4.1. MEASUREMENT TYPES

Three central measurement types were collected throughout the research program including concrete strains, concrete temperatures, and girder camber and deflection. Prestressing tendon strains as well as the concrete corrosion process were also investigated. Table 4.1 lists the gauges used and the data obtained for each measurement type.

Table 4.1. Measurement Types

Measurement Type	Measurement System	Data Collected
Concrete Strains	<ul style="list-style-type: none"> • Vibrating Wire Strain Gauges • Demountable Mechanical Strain Gauges 	<ul style="list-style-type: none"> • Stress-strain response • Development length of prestress force • Prestress losses
Concrete Temperatures	<ul style="list-style-type: none"> • Thermocouples • Thermistors 	<ul style="list-style-type: none"> • Hydration profiles • Strain corrections due to thermal effects • Deflection corrections due to thermal effects • Seasonal temperature variations
Girder Response Properties	<ul style="list-style-type: none"> • Precise Surveying System 	<ul style="list-style-type: none"> • Camber • Time dependent deflections (creep) • Service life deflections
Prestressed Tendon Strains	<ul style="list-style-type: none"> • Electrical Resistance Strain Gauges • Load cell 	<ul style="list-style-type: none"> • Tendon stresses • Verification of initial prestress force
Corrosion	<ul style="list-style-type: none"> • RFID Corrosion Sensor 	<ul style="list-style-type: none"> • Onset of corrosion

4.1.1. Concrete Temperatures

Concrete temperatures were collected in both the intermediate bents and bridge girders. Thermocouples were embedded in the pier cap, columns and web wall of the intermediate bents to measure the hydration profile within the first 48 hours of concrete

curing. A thermocouple wire was attached outside of the formwork during data collection to measure the ambient temperature through the curing process. Within the bridge girders, each vibrating wire strain gauge (VWSG) included a built in thermistor to correct the measured strain and to record hydration temperatures. The hydration temperature measurements were of value during the casting and early service life of the bridge girders. In span 2, girders 3 & 4 were instrumented with VWSG at mid-span and at both ends. Girders 3 & 4 in spans 1 and 3 were instrumented with VWSG at mid-span and at the end closest to the intermediate bent.

4.1.2. Concrete Strains

Concrete strains were measured in selected prestressed girders and panels and the cast-in-place (CIP) deck. A combination of VWSGs and a Demountable Mechanical Strain Gauge with exterior fixed discs referred to as “DEMEC points” were used with the NU girders, and VWSGs were embedded in two of the precast panels and across the CIP deck. By embedding up to five VWSG in the girder and two VWSG in the CIP deck at a given section, the strain profile could be accurately determined. This was accomplished at the mid-span location of each instrumented girder and at sections above the intermediate bent supports. Strains in the transverse direction of the bridge were also measured in the precast panels and CIP deck. Long-term creep and shrinkage effects could also be measured using the VWSGs. Furthermore, an attempt was made to measure the transfer of force from the prestressing tendons to the girder by using the DEMEC system at the precast plant, but it was unsuccessful.

4.1.3. Girder Deflection and Camber

The camber and time-dependent deflection of each instrumented girder was obtained at the pre-cast plant shortly after fabrication. At the plant, deflection measurements were made at the ends, mid-span and quarter points of each member. In-service deflections were also measured during the live load test at five equidistant locations (including mid-span) along the bottom of each girder along line 3.

Additionally, mid-span deflections were also recorded for girder lines 1, 2 and 4 of each span. The measured camber and deflections were used to assess the in-situ serviceability performance of the girders from fabrication through in-service conditions.

4.2. MEASUREMENT SYSTEMS

4.2.1. Load cell

A 100 kip (44.8 kN) load cell was attached to one prestressing strand during the fabrication of girder S2-G4 as shown in Figure 4.1. The load cell was used to check the applied load to each prestressing tendon.



Figure 4.1. Load cell

4.2.2. Thermocouples

A thermocouple is a temperature sensing device that produces a voltage that is transmitted as a measure of temperature. Thermocouples are junctions of specific metals (wires) which have a predictable and repeated relation between voltage and temperature. These wires are coupled simply by tightly twisting thermocouple wire. Figure 4.2 shows these wires.



Figure 4.2. Thermocouple

Thermocouple model TT-T-20-TWSH from OMEGA In. was used in this project. Figure 4.3 shows the meaning of this term. The temperature range is reported to be -450 to 500 °F (-267 to 260 °C) by the manufacturer. The accuracy of measurements was stated to be ± 1.8 °F (± 1.0 °C) for the thermocouple used.

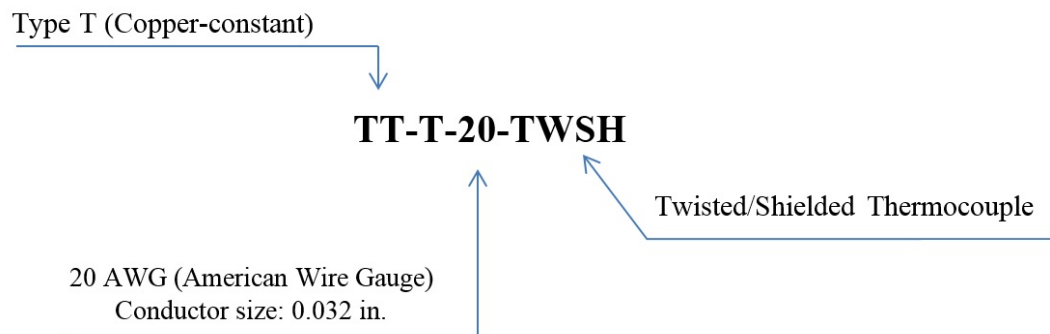


Figure 4.3. Definition of TT-T-20-TWSH

4.2.3. Vibrating Wire Strain Gauges

A vibrating wire strain gauge is used for monitoring strain in concrete caused by stress variations. The sensor is installed by placing the gauge at a location in the structure (normally tied to rebar with soft iron or plastic wire) suitable to accurately pass loads from the cured concrete into the gauge. Each strain gauge consists of two end blocks with a tensioned steel wire between them. As the concrete surface that encompasses the strain gauge undergoes strain, the end blocks will move relative to each other. The tension in

the wire between the blocks will change accordingly, thus altering the resonant frequency of the wire. Vibrating wire readout is utilized to generate voltage pulses in the magnet/coil assembly located at the center of the strain gauge. The magnet/coil assembly plucks the wire and measures the resulting resonant frequency of vibration. The VWSGs used in this project were EM-5 series manufactured by Roctest, Inc. shown in Figure 4.4.

The EM-5 has an adjustable 3000 microstrain range with an accuracy of 1 microstrain. This is the usable microstrain limit of the EM-5 VWSG. The gauge has a built in thermistor to record concrete temperatures ranging from -122 °F to 140 °F (-50 °C to 60 °C). Embedded VWSGs were selected for this project because of their durability and have been found to be reliable for several years in field conditions (Myers and Yang, 2005). 86 VWSGs were used at specific points of interest.



Figure 4.4. Vibrating Wire Strain Gauge

4.2.4. Electrical Resistance Strain Gauges

A linear strain gauge, model EA-06-125BT-120-LE by Micro Measurements, was used in the test girders. The gauge has a constantan foil with a tough, flexible, polyimide backing (EA), with pre-attached leads and encapsulation (LE). The gauge has a resistance of $120 \pm 0.15\%$ ohms and an usable temperature range of -100° to +350°F (-75° to +175°C). The gauge has an overall length of 0.37 in. (9.4 mm) and an overall width of 0.16 in. (4.1 mm). Two gauges were applied to each girder at mid-span: one in each of the two bottom rows of prestressed tendons. The gauges were used to monitor the stress in the prestressing tendons during the course of the shear testing. The gauge is shown in Figure 4.5 prior to installation.



Figure 4.5. Electrical Resistive Strain Gauge

4.2.5. Demountable Mechanical Strain Gauges

The demountable mechanical strain gauge (DEMEC) is used for determining the linear deformation caused on two reference points fixed on a loading member. The system utilizes a standard digital gauge that is attached and supported by a bar. One end is fixed, the other can move on a pivot.



Figure 4.6. The DEMEC Gauge and Reference Bar

The digital gauge measures the movement of the pivot. A reference bar is used to position pre-drilled stainless steel discs which are attached to the locations with a five-minute quick set epoxy. After the discs set to the location, initial readings are taken. The conical points of the gauge are inserted into the holes in the discs and the reading on the dial gauge noted. In this way, strain changes in the structure are converted into a change in the reading on the dial gauge. The gauge has been designed so that only minor temperature corrections are required for changes in ambient temperature, and an Invar reference bar is provided for this purpose. Figure 4.6 shows the DEMEC gauge and the reference bar.

Equation (4.1) was used to determine the change in strain, $\Delta\varepsilon$ (microstrain), from one reading to the next.

$$\Delta\varepsilon = G((R_i - R_0) - (D_i - D_0)) \quad (4.1)$$

Terms used in this equation are defined as followed: G is the gauge factor as shown in Figure 4.7, 0.400×10^{-5} strain per division (4 macrostrains), D_0 is the datum reading on the reference bar, D_i is the subsequent reading on the reference bar, R_0 is the datum reading on the tested material, and R_i is the subsequent reading on the tested material.



Figure 4.7. Gauge Factor Used for Shrinkage and Creep Calculations

4.2.6. DEMEC Points

Small predrilled stainless steel disks as shown in Figure 4.8 were adhered to the surface of specimens with five-minute quick set epoxy. They were arranged in three vertical lines of five points, 120° apart and from this arrangement nine readings can be taken per specimen by inserting the DEMEC gauge in the DEMEC point and then the

reading is taken. The average of all readings can be used to obtain the shrinkage strain in the specimen.



Figure 4.8. Stainless Steel DEMEC points

4.2.7. High Performance Total Station System

At the precast plant, a laser-based High Performance Automated Total Station (ATS) system was used to obtain vertical deflection data before and after the release of the prestressing force acting on the PC girders. The ATS employed to monitor the camber deflection of the PC/PS girders was a Leica TCA2003 (Figure 4.9).



Figure 4.9. Total Station (Leica TCA2003)

The ATS equipment was set atop a secure tripod with an unobstructed view of the prisms (targets) that were placed on the top flange of the girders. Additionally, two prisms were set atop secure tripods located between the PC/PS girder and the ATS. These additional prisms were used as reference targets that help verify if ATS had not

experienced any additional relative movement before and after the strands release. Five prisms were set on steel plates installed atop the flange of the girders at 5 different locations: 1.0 ft. (0.30 m) from the ends and at sections located at L/4 and L/2 from each end.



Figure 4.10. Reflecting Prisms Mounted on PC/PS Girders (Precast Plant)

The ATS, also called Robotic Tacheometry System (RTS), (Hernandez et al. 2006), obtains three-dimensional coordinates of every target by measuring the horizontal and vertical angle as well as the distance between the ATS and prisms. The instrument was configured to take three readings per point measured. This was internally done by four diodes that optically read a fine bar code set on a glass ring inside the Leica TCA2003. During monitoring, the equipment continuously read the bar codes on the horizontal and vertical planes by sending a laser ray that reflected on the targets mounted on the structure (Figure 4.10) that was being monitored. By means of triangulation with the fixed reference points placed aside the PC/PS girders, the ATS determines how much the element has moved in a three-dimensional array with an accuracy of 0.5 arc-seconds on angular measurements and 1mm+1ppm on distance measurements (1 in = 25.4 mm).

The Leica TCA2003 is very accurate through the use of robotics, and this feature allows the instrument to rotate on the horizontal and vertical axes by itself. The system automatically recognized and locked onto targets that were manually entered by the user at the beginning of the test. The Leica TCA2003 automatically relocated the targets and obtained their coordinates. Because of the high sensitivity of the equipment to movement

and vibration, its robotic capability helps eliminate any human error through less physical contact during operation.

The Leica TCA2003 was also used to obtain the vertical deflections of the bridge at different sections located along the longitudinal axis of the PC/PS girders. The first part of the first series of non-destructive load tests was conducted in April 2014 to evaluate the live-load response of the bridge during serviceability loading. The second part of the first series of load tests has been scheduled to be conducted in August 2014. The results obtained during this first series of load test are presented in the final report D.

4.2.8. Radio Frequency Identification (RFID) based Corrosion Sensor

A RFID based corrosion sensor was employed to detect the chloride salt concentration that initiates the onset of corrosion within the reinforcing steel of the CIP RC deck. Figure 4.11 shows the sensor employed in this implementation project. The body of the sensor is about the size of a quarter (Myers and Hernandez 2014). The sensor houses an internal circuit board that registers voltage variations of the wire links shown in Figure 4.11. This sensor does not rate the mass loss or corrosion rate of reinforcing steel. Instead, each external iron wire acts as a trigger mechanism that fails when the content of chloride ingress reaches a critical value in the sensor's surrounding concrete.

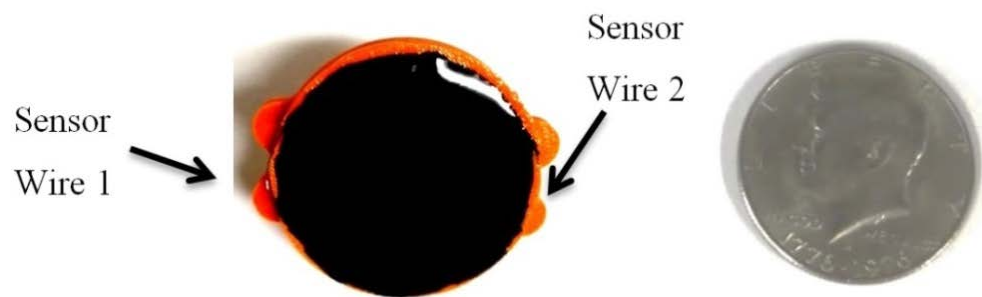


Figure 4.11. RFID Based Corrosion Sensors

The wires' diameters are 0.065 mm (thinner link) and 0.100 mm (thicker link), respectively. This second generation of the sensor allows detecting two critical chloride concentration values. The thinner wire detects the chloride content that initiates the corrosion, and the second detects a chloride concentration that produces an important loss of the reinforcing steel area within the CIP RC deck. Additional information about the

RFID corrosion sensor and its implementation on this project can be found in Myers and Hernandez (2014).

4.3. DATA ACQUISITION

4.3.1. Data Acquisition System

Three data acquisition systems (DAS) were used for strain and temperature data collection during the fabrication and construction of Bridge A7957. These DAS were custom-built by the researchers at Missouri S&T. The first built DAS was a compact RIO system, and the two remaining DAS were Campbell Scientific CR800 boxes that work wirelessly.

4.3.1.1. Compact RIO

The compact RIO system (Figure 4.12) with a NI9214 High Accuracy Thermocouple module was used for temperature data collection during the construction of the bents along with a 90 Watt solar panel. Four thermocouples were connected to the Compact RIO DAS during concrete placement of the web wall and pier cap of each bent. The thermocouples collected data for at least 23 hours during and after concrete placement. These sensors provided a temperature profile development for each part of the bents.



Figure 4.12. Compact RIO System and 90 Watt Solar Panel

4.3.1.2. Campbell Scientific CR800

During the girders fabrication, erection and construction, the VWSG were connected to either of two Campbell Scientific CR800 DAS that have AVW200 and AVW206 VWSG reading modules. Following the erection of the girders, these two CR800 DAS were anchored to the interior side of the intermediate bent pier caps for long-term monitoring. A cellular antenna, also anchored to the interior side of the bent 2 pier cap, was used to send the data from the CR800s in real time back to the researchers at Missouri S&T during fabrication of the precast PC girders and the different stages of the bridge construction. Figure 4.13 through Figure 4.15 show the data acquisition systems and their components. The number of channels employed during the fabrication of each instrumented girder is presented in Table 4.2.



CR800 DAS



CR800 Modules

Figure 4.13. Campbell Scientific CR800

Table 4.2. Gauges Needed During Fabrication of PC Girders (Precast Plant)

Span	Member	Gauges		DAS Type	Total of Channels
1-2 (CC)	Girder 3	VWSG +	9	CR800	9
	Girder 4	Thermistor			
2-3 (HS-SCC)	Girder 3	VWSG +	13	CR800	13
	Girder 4	Thermistor			
3-4 (NS-SCC)	Girder 3	VWSG +	9	CR800	9
	Girder 4	Thermistor			

Table 4.3 lists the number of channels used to monitor the bents during their construction.

Table 4.3. Gauges Needed During Construction of Bents

Bent	Member	Gauges		DAS Type	Total No. of Channels
2 (CC)	Web Wall	Thermocouple	4	Compact RIO	8
	Pier Cap		4		
3 (HVFAC)	Web Wall	Thermocouple	4	Compact RIO	8
	Pier Cap		4		

The number of channels employed during the different construction stages and long-term monitoring of Bridge A7957 is presented in Table 4.4.

Table 4.4. Channels Needed During the Long-Term Monitoring of Bridge A7957

Part	Gauges		DAS Type	Total of Channels
PC/PS Girders (Longitudinal VWSG)	VWSG + Thermistor	62	CR800	62
CIP Deck (Longitudinal VWSG)	VWSG + Thermistor	20	CR800	20
CIP Deck (Transverse VWSG)	VWSG + Thermistor	2	CR800	2
PC/PS Panels (Transverse VWSG)	VWSG + Thermistor	2	CR800	2
Total channels for long-term monitoring:				86

The components of the two DAS boxes are shown in the diagrams of Figure 4.14 and Figure 4.15.

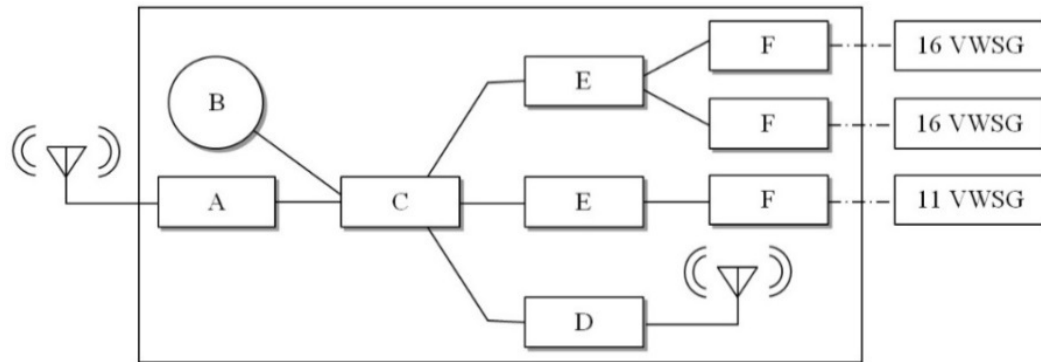


Figure 4.14. Components of DAS Box 1

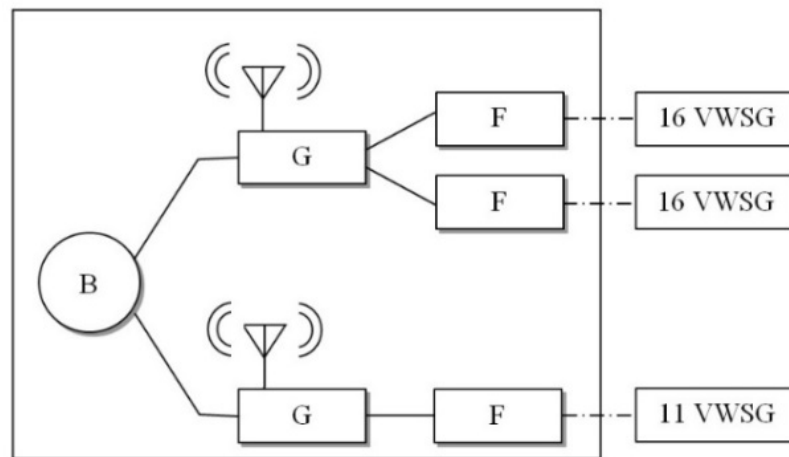


Figure 4.15. Components of DAS Box 2

Where:

A: Sierra Raven XT (wireless modem with high boost antenna)

B: 12V solar panel with backup battery

C: CR800 (logger)

D: RF401 radio transceiver (send/receive)

E: AVW200 (2-port VW reader, serial connection)

F: AM16/32 B (16/32 channel multiplexer)

G: AVW206 (2 port VW reader, wireless)

Within each CR800 DAS box, the first two multiplexer modules host 16 VWSGs, and the third module hosts 11 VWSG. A total of 43 VWSG can be connected to each CR800 DAS.

4.3.2. Programming and Data Collection

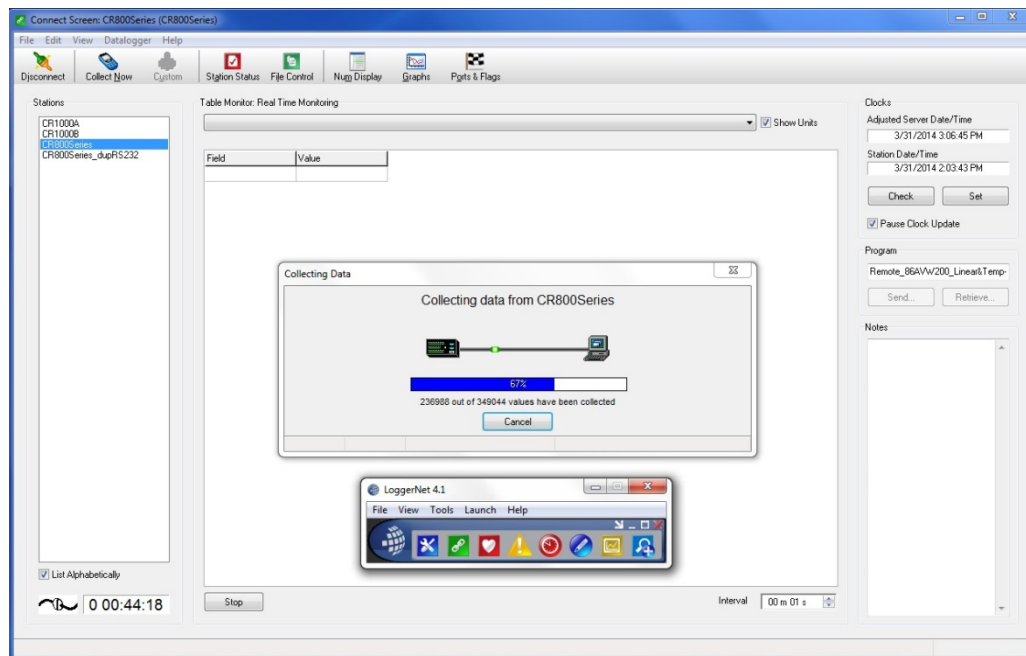
A portable personal computer (Dell Latitude E6520 Laptop) and the CR800Series software package supplied with LoggerNet 4.1 by Campbell Scientific were used for programming and collecting stored data. The data, obtained at the different construction stages and during the long-term monitoring of Bridge A7957, can also be downloaded wirelessly to this portable personal computer that is installed in the research laboratory (Figure 4.16).



a) CR800 DAS Box Installed on Bent 3



b) CR800 Modules and VWSGs



c) CR800 DAS Software with LoggerNet 4.1

Figure 4.16. Data Acquisition System Installed on Bridge A7957

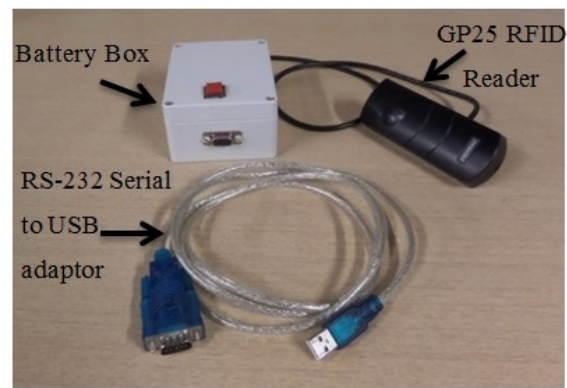
4.3.3. RFID Corrosion Sensor Data Acquisition

4.3.3.1. Data acquisition hardware

The data acquisition hardware consists of a Dell Latitude E6520 Laptop, with an Intel® Core™ i7-2620M CPU, 2.7 GHz Processor, and a 15-in HD Monitor [Figure 4.17(a)], and an RFID scanning system [Figure 4.17(b)]. The RFID scanning system has three main components: an RS-232 Serial to USB adaptor cable, a GP25 proximity RFID reader (model EM4200/4102), and a battery box (Myers and Hernandez 2014).



(a) Dell Laptop



(b) RFID Scanning System

Figure 4.17. RFID Data Acquisition Hardware

The GP25 RFID reader is a low frequency component, high-performance, proximity reader featuring a long range data acquisition that can be used within a distance of 4 in (100 mm) from the corrosion sensor. In addition, this unit was configured to the interface format Clock/Data and RS-232 serial ASCII output. The battery box houses eight 1.5-volt AA batteries that supply power to the RFID reader.

4.3.3.2. Data acquisition software

The data acquisition software is the user's interface that controls and orders the RFID reader what information to read and how to collect it from the RFID sensor tag. LabVIEW™ (2013) was the graphical programming language used to write and compile the software "Serial Reader.vi" that controls the DAS equipment. Figure 4.18 shows the

user's interface of "Serial Reader.vi" that is utilized to control the RFID reader and to receive the output data from the sensor tag in the form of RFID code IDs.

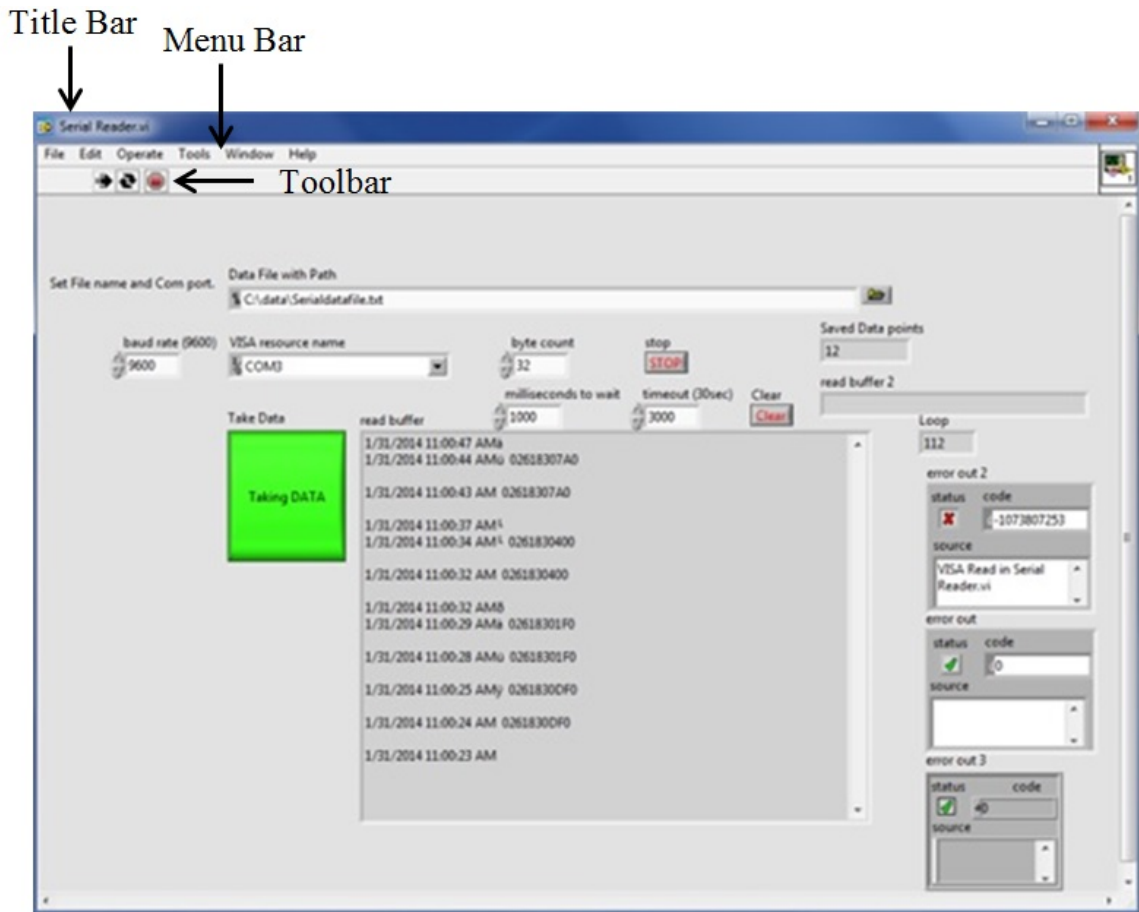


Figure 4.18. RFID DAS Software (User's Interface)

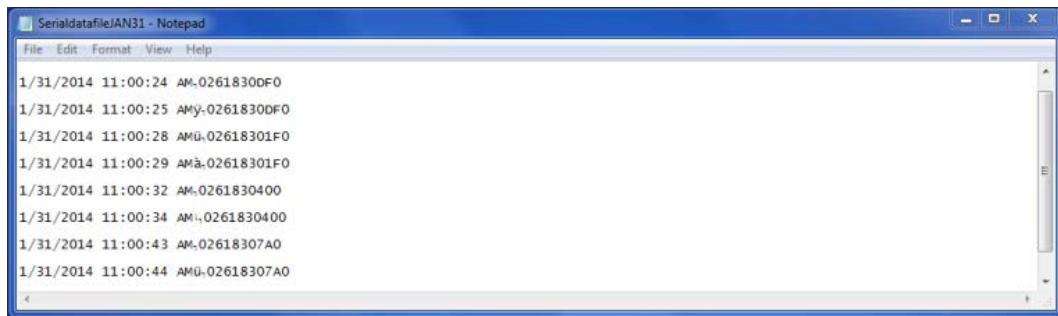


Figure 4.19. RFID Sensor's Output File

Figure 4.19 shows an output file written by the data acquisition software "Serial Reader.vi". The RFID reader collects an RFID code each time the sensor is scanned and

sends the reading to “Serial Reader.vi” and is written into an output file (.txt format). The file can be edited by any commercial word processor (Myers and Hernandez 2014).

The first, second and third columns of the data file represent the date, time, and RFID codes obtained by the RFID data acquisition system. Figure 4.20 displays a typical RFID code.

Digit Value	→	<u>0</u>	<u>2</u>	<u>6</u>	<u>1</u>	<u>8</u>	<u>3</u>	<u>0</u>	<u>D</u>	<u>F</u>	<u>0</u>
Digit Position	→	1	2	3	4	5	6	7	8	9	10

Figure 4.20. Typical RFID Code

From the RFID ID code of Figure 4.20, the following information is extracted:

Digits 1 and 2 represent the revision number of the RFID tag. For this case, the “02” indicates the RFID sensor belongs to the second prototype generation

Digits 3 through 9 contain a fixed tag’s ID, in other words, this is the sensor’s serial or identification. For this reading, the tag’s ID is: **61830DF**

Digit 10 is the decoded response that the RFID tag sends through the reader to the data acquisition software. It indicates the status of the sensors’ wire links. This digit can take four different values. A value equal to zero (0) means that both iron wires are intact; therefore, no critical chloride content is surrounding the sensor. A value of one (1) or two (2) means that the thinner or thicker iron wire has failed, respectively (i.e. the resistance measured by the sensor is greater or equal than about 500 ohm). A value of 4 means that both sensors’ link wires have failed.

5. RESEARCH PROGRAM PLANS & PROCEDURES

5.1. TRIAL MIXES

Before the fabrication of the bridge elements or test girders could begin, trial mixes had to be developed to validate the fresh and hardened properties of the various concretes used in the research program. The three mixes investigated during this phase of the project were high-volume fly-ash concrete (HVFAC), high strength self-consolidating concrete (HS-SCC), and normal strength self-consolidating concrete (NS-SCC). All three mixes were developed by MoDOT based on previous research at Missouri S&T (Myers et al. 2012; Volz et al. 2012).

5.1.1. HVFAC

The mix design was based off of MoDOT's B mix with 50% fly ash replacement. The official mix ID is 13CDHVFA003. The mix had a specified water-to-cementitious material ratio (w/cm) of 0.33 and a design air content of 6.0%. The target compressive strength was 3,000 psi (20.7 MPa). The mix design proportions are listed in Table 5.1.



(a) Batching



(b) Sampling

Figure 5.1. HVFAC Trial Mix at Osage County Industries

The high volume fly-ash concrete was batched on January 8, 2013 at Osage County Industries in Linn, Missouri (Figure 5.1a) with MoDOT representatives present. Concrete slump and air content were measured before specimen collection. Nine 4 x 8 in. (100 x 200 mm) cylinders were collected for compressive strength testing at 7 and 28

days. Osage County Industries collected cylinders for compressive strength testing at 1, 2, 3, 4, 7, and 28 days. Figure 5.1(b) shows the test cylinders collected by the Osage County Industries and Missouri S&T teams.

Table 5.1. HVFAC Trial Mix Design

Type	Material	Design Weight (lb./yd ³)	Batched Weight (lb./yd ³)
Coarse Aggregate	Choteau-Burlington-Cedar Valley – Gradation D Ledges 1A, 1B, 1, 2, 3	1750	1780
Fine Aggregate	Missouri River/Class A	1242	1269
Cementitious Material	Portland Cement – Type I/II	325	325
	Fly Ash – Class C	325	325
Water	--	213	213
Chemical Admixtures	Air Entraining Agent	0.2-2.0 oz./yd ³	5.0 oz./yd ³
	Water Reducer	2.0-6.0 oz./cwt	2.0 oz./cwt
	Accelerator	0-32.0 oz./cwt	16.0 oz./cwt
w/cm	--	0.33	0.33

Conversions: 1 lb./yd³ = 0.5933 kg/m³, 1.0 oz./yd³ = 0.03708 kg/m³, 1.0 oz./cwt = 6.5 oz./yd³

5.1.2. HS-SCC

The high strength self-consolidating concrete (HS-SCC) mix was batched on January 30, 2013 at County Materials Corporation in Bonne Terre, Missouri. The mix ID is 13SECSPE001, with the mix design shown in Table 5.2. The w/cm ratio was 0.329 with a target air content of 5.0%. The percentage of coarse aggregate in the mix was 48%; significant reductions in the coarse aggregate content would compromise the stiffness and shear behavior of the mix. The mix's fresh properties were tested following ASTM standards and included: air content, slump flow, passing ability (J-Ring), and static segregation. Figure 5.2 exhibits these tests. Eighteen 4 x 8 in. (100 x 200 mm) cylinders were cast for testing of compressive strength, modulus of elasticity, and splitting tensile strength as illustrated in Figure 5.3. The cylinders were stream cured at 120°F (49°C) for approximately 24 hours to simulate the curing conditions during the precast-prestressed girder fabrication process.



(a) Segregation Column



(b) Air Content



(c) J-Ring (Passing Ability)



(d) Slump Flow

Figure 5.2. HS-SCC Trial Mix Fresh Property Tests



Figure 5.3. HS-SCC Trial Mix Specimens

Table 5.2. HS-SCC Trial Mix Design

Type	Material	Weight (lb./yd ³)
Coarse Aggregate	Leadbelt 1/2" Dolomite	1340
Fine Aggregate	Mississippi River Sand	1433
Cementitious Material	Portland Cement Type I	850
Water	--	280
Chemical Admixtures	Air Entraining Agent	17 oz./yd ³
	High Range Water Reducer	76.5 oz./yd ³
	Retarder	25.5 oz./yd ³
w/cm	--	0.329

Conversions: 1 lb./yd³ = 0.5933 kg/m³, 1.0 oz./yd³ = 0.03708 kg/m³

5.1.3. NS-SCC

The normal strength self-consolidating concrete (NS-SCC) mix was batched on March 8, 2013 at County Materials Corporation in Bonne Terre, Missouri. The mix ID is 13SECSPE002, with the mix design shown in Table 5.3. The w/cm ratio, target air content, and coarse aggregate content were 0.346, 5.0%, and 51%, respectively.



(a) Slump Flow



(b) J-Ring (Passing Ability)

Figure 5.4. NS-SCC Trial Mix Fresh Property Tests

The mix had a target compressive strength at 28 days of 8,000 psi (55.2 MPa) and a specified release strength of 6,500 psi (44.8 MPa). The mix's fresh properties were tested following ASTM standards and included: air content, slump flow, passing ability (J-Ring), and static segregation.

Table 5.3. NS-SCC Trial Mix Design

Type	Material	Weight (lb./yd ³)
Coarse Aggregate	Leadbelt 1/2" Dolomite	1476
Fine Aggregate	Mississippi River Sand	1433
Cementitious Material	Portland Cement Type I	750
Water	--	260
Chemical Admixtures	Air Entraining Agent	17 oz./yd ³
	High Range Water Reducer	67.5 oz./yd ³
	Retarder	25.5 oz./yd ³
w/cm	--	0.346

Conversions: 1 lb./yd³ = 0.5933 kg/m³, 1.0 oz./yd³ = 0.03708 kg/m³

Figure 5.4 exhibits two of these tests. Eighteen 4 x 8 in. (100 x 200 mm) cylinders were cast for testing of compressive strength, modulus of elasticity, and splitting tensile strength. The cylinders were steam cured at 120⁰F (49⁰C) for approximately 72 hours to simulate the curing conditions during the precast-prestressed girder fabrication process.

5.2. INSTRUMENTATION PLAN AND FIELD PREPARATION

5.2.1. Equipment and Gauges

The instrumentation equipment and gauges employed on this implementation project are summarized in Table 5.4. Two data acquisition systems were assembled for the girders' data collection. The VWSG can provide a strain profile through the cross

section of the PC girders as well as temperature profiles. A total of 86 VWSG with thermistors were embedded in the PC/PS girders, PC/PS panels and CIP deck of Bridge A7957.

Table 4.4 presents the number of VWSG installed within the different components of Bridge A7957. A compact RIO acquisition system was assembled for temperature data collection during and after the bents' concrete placement. A total of 16 thermocouples were connected to the compact RIO acquisition system. Two electrical resistance strain gauges were used for each girder tested in the laboratory. At the precast plant, a TS equipment was used to obtain the camber deflections of the PC/PS girders as described in sections 4.1.3 and 4.2.7.

Table 5.4. Instrumentation Equipment and Gauges

EQUIPMENT & GAUGES	QUANTITY	DESCRIPTION
CR800 DAS	2	Collecting data from VWSG
Compact Rio	1	Collecting data from thermocouples
Thermocouples	16	Monitoring temperature
Vibrating wire strain gauges (VWSG)	86	Monitoring strain and temperature
Electrical resistance strain gauges (ERSG)	4	Monitoring strain
Total Station (TS)	1	Monitoring deflection

5.2.2. Instrumentation Location

In the precast plant, six out of twelve PC/PS girders were instrumented at the cluster locations displayed in Figure 5.5. A total of 86 VWSG with built-in thermistors, type EM-5, manufactured by Roctest Inc., were employed to monitor the stress variation as well as temperature changes in the girders, panels and CIP deck from fabrication through service life. The VWSG were installed prior to casting of the PC girders and were limited to girder lines 3 and 4 of the bridge (Figure 5.5). The CIP deck was instrumented at 16 different locations before concrete placement.

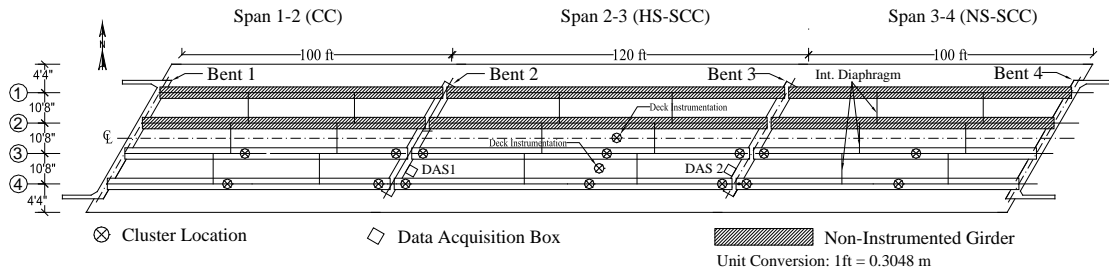


Figure 5.5. Bridge A7957's Instrumented Girders and Clusters' Locations

5.2.3. Gauge Numbering and Identification

A complete identification of each gauge was performed to minimize confusion when installing and analyzing the data. The gauge identification designations are listed in Table 5.5 and Table 5.6.

Table 5.5. Girders, Panels and Deck's Gauge Identification Designations

ITEMS	IDENTIFICATION		
	Type	Range	Named
Embedded Gauge Number	Deck VW	See Appendix C	(1-2)
	Girder VW	See Appendix C	(1-7)
	Girder ER	N/A	(1-2)
Girders and Decks Designation	Sm	S=Span; m=Span #	
	Gn	G= Girder; n= Girder #	
	Dmn	D= Deck; m, n= Girder line #	
Embedded Gauge Depth (Mid-span and Near Support Sections)	TD*: M7, W5, E5	Top Deck [#] (6 in. Above Bottom Fiber)	
	BD*: M6	Bottom Deck (2 in. Above Bottom Fiber)	
	TF*: M5, W4, E4	Top Flange (2 in. Below Top Fiber)	
	CGC*: M4, W3, E3	Center of Gravity of Composite Beam Section	
	CGU/CGI*: M3	Center Gravity of Non-Composite Beam Section	
	CGS*: M2, W2, E2	Center of Gravity of Pretensioned Strands	
	BF*: M1, W1, E1	Bottom Flange (2 in. Above Bottom Fiber)	
Embedded Gauge Depth (Deck's Mid-span)	M2	Top Deck [#] (4½ in. above Bottom Fiber)	
	M1	Mid Height of PC Panel	
Embedded Gauge Depth (Lab Test Girders)	TF*: M2	Top Flange (2 in. Below Top Fiber)	
	BF*: M1	Bottom Flange (2 in. Above Bottom Fiber)	
Longitudinal Location of Gauges	W	Near Girder's West Support	
	M	Girder's Mid-span	
	E	Near Girder's East Support	
Gauge Type	Embedded Gauges	VW	Vibrating Wire Strain Gauge, VWSG
		TR	Thermistor (Integral with VWSG)
		ER	Electrical Resistance Strain Gauge
	Other Sensor	TS	Total Station
DAS	CR800	DAS BOX 1	DAS BOX 2

*: VWSG depth according to instrumentation plan (Appendix B).

#: The original depth locations proposed in the instrumentation plan (Appendix B) were adjusted to precast plant conditions.

Table 5.6. Bent's Gauge Identification Designations

ITEMS	IDENTIFICATION		
	Type	Range	Named
Embedded Gauge Number	Bent TC	N/A	2-3
	Bent Designation	Bm	B=Bent; m=Bent #
Web Wall Designation	NC	NC= North Column's Center Line	
	SC	SC= South Column's Center Line	
	NW	NW= Web Wall 's North Side	
	SW	SW= Web Wall 's South Side	
Pier Cap Designation	PC	Pier Cap	
	B	Bottom	
	M	Mid Height	
	T	Top	
	MT	Ambient Temperature	
Gauge Type	TC	Thermocouple	
DAS	Compact RIO		

5.2.4. Gauge Locations

Within each girder of span (1-2) and span (3-4), the instrumentation clusters were located at two cross-sections. The first cross-section was located at mid-span, and the second was at 2ft (610 mm) from the centerline of bents 2 and 3, respectively. For span (2-3), the instrumentation clusters were located at three different locations: one at mid-span, and the remaining two at approximately 2 ft. (610 mm) from each support centerline.

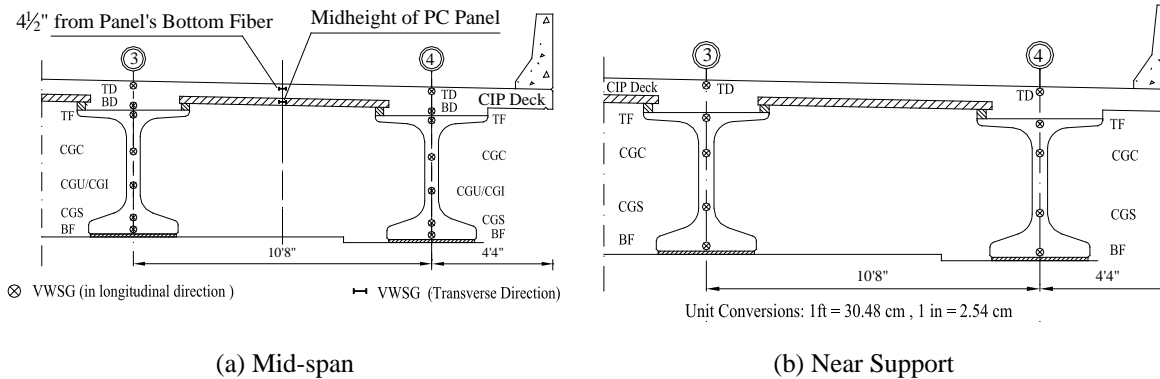


Figure 5.6. VWSG Installation Detail through the Different Girders' Sections

The locations at which the VWSG were installed are specified in Table 5.5. Figure 5.6 shows the cluster locations and layers at which the sensors were installed (mid-span and near the supports). More details about the instrumentation are presented in Appendices B and C.

5.2.5. Embedded Gauges Preparation

All sensors were prepared in the Structural Engineering Research Laboratory at Missouri S&T prior to installation in the field. The first step consisted in cutting the thermocouples to the specified length of the different sections of the interior bents (web wall and pier cap).



Figure 5.7. Thermocouple Preparation Prior to Field Installation

To prepare the thermocouple sensors, the two wires at one end were twisted and welded. Afterwards, the same end was coated with a rubber coating (Performix Plasti Dip®) for protection. Additionally, the sensors were labeled according to information specified in Table 5.6. Additional details about the locations where the thermocouples were installed and the corresponding label used for each of them are given in Table 5.6 and Figure 5.9. The VWSG did not require a significant work preparation. To prevent any damage on the VWSG's body, a zip tie was fastened around its body as shown in Figure 5.8a. Afterwards, all the wires were numbered and labeled (Figure 5.8b) according

to the information listed in Table 5.5. Finally, the VWSG were grouped depending on the section they were going to be installed within the PC girders and CIP deck.



(a) VWSG Secured with Zip Tie



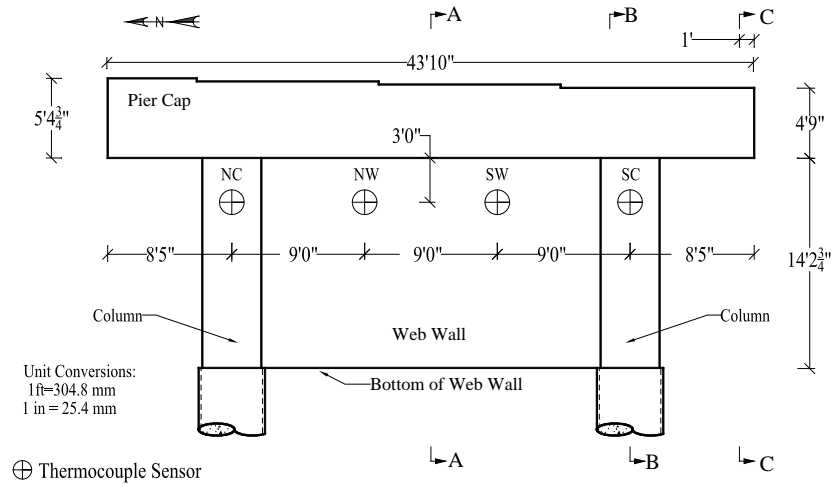
(b) VWSG Labeled for Field Installation

Figure 5.8. VWSG Preparation Prior to Field Installation

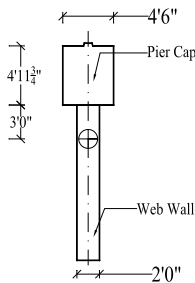
5.2.6. Field and Plant Installation

5.2.6.1. Intermediate bents

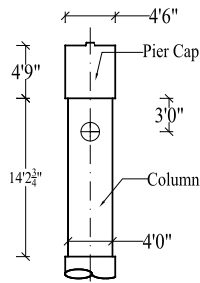
Thermocouple sensors were installed within bents 2 and 3 to read temperature data during and after casting. Additionally, the ambient temperature was recorded to adjust for any differences between the materials used in both bents when they were subjected to similar environmental conditions. For each bent, a thermocouple was installed at the center line of each column 3 ft. (0.91 m) from the bottom edge of the pier cap [Figure 5.9(a) and Figure 5.9(c)]. A second set of thermocouples were placed in the web wall 9 ft. (2.74 m) from the center line of each column [Figure 5.9(a) and Figure 5.9(b)] in the same horizontal plane. At section C [Figure 5.9(a)], located 1 ft. (0.30 m) from the south end of the pier cap, one exterior and three interior thermocouples were installed according to the detail shown in Figure 5.9(d).



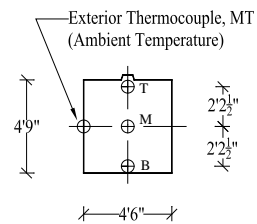
(a) Bent Elevation



(b) Section A-A



(c) Section B-B



(d) Section C-C

Figure 5.9. Thermocouple Sensors Installation Details

Figure 5.10 shows the installation procedure of the thermocouple sensors within the bents' web wall. The thermocouples were strapped around the reinforcing steel by zip ties to avoid any possible damage of the sensors during concrete placement.



Figure 5.10. Thermocouples Installation on Bent 2's Web Wall

Figure 5.11 shows some of the thermocouples installed at specified bent sections.



(a) Column (B3-NC)

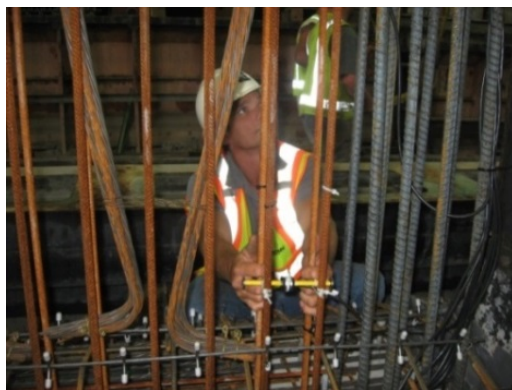


(b) Web Wall (B3-SW)

Figure 5.11. Thermocouples Installed at Specified Bent Sections

5.2.6.2. Precast prestressed girders

After all the strands were tensioned, usually about one or two days prior to casting, placement of the shear reinforcement was conducted by the fabricator. The placement of embedded VWSG within the prestressed girders was performed after this procedure because the steel reinforcement was used as a framework for the gauges. Figure 5.12(a) shows the process of placing a VWSG within a section located near the end of a girder. Gauges located at a mid-span section are shown in Figure 5.12(b). After the installation was completed, the gauges were connected to one of the DAS boxes as shown in Figure 5.13.



(a) VWSG Installation at Specified Depth



(b) VWSG Installed at Specified Sections

Figure 5.12. VWSG Installation within PC Girders at Precast Plant



(a) DAS Box 1



(b) Antenna Installation to DAS Box 1

Figure 5.13. VWSGs Connected to DAS Box

DAS box 1 was employed as the main acquisition system while DAS box 2 worked as the auxiliary acquisition system (Figure 5.13 and Figure 5.14). When the secondary box was used, it was always necessary to employ the main box to allow remote communication of the data to the lab. In such a case, the DAS box 1 was installed aside the PC girder as shown in Figure 5.14(a).



(a) CR800 DAS Box 1 (Main DAS)



(b) DAS Box 2 (Secondary DAS)

Figure 5.14. VWSG Connected to DAS at Precast Plant

After concrete reached the required compressive strength necessary for release, the prestressing force was released and the VWSG were allowed to collect the strain variation for at least one hour. Finally, the girders were moved to the yard for storage until being delivered to the bridge site.

5.2.6.3. Precast prestressed panels

A VWSG was installed within two PC/PS panels at the precast plant. These panels were placed at the mid-span section of span 2-3, between girder lines 2 and 3 and girder lines 3 and 4, respectively. Once the panels were set on the girders, the two VWSG remained perpendicularly oriented to the girders' longitudinal axis [Figure 5.5 and Figure 5.6(a)]. Figure 5.15 shows the detail of a VWSG installed at mid-height of the precast panels.



(a) Before Concrete Placement



(b) After Concrete Placement

Figure 5.15. VWSG Installed within PC/PS Panels

5.2.6.4. CIP deck

A total of twenty-two VWSG were installed within the CIP RC deck. Twenty of them were installed along the girders' longitudinal direction as specified in Figure 5.6a. Figure 5.16 shows the two PC/PS panels that were instrumented with VWSG along the perpendicular direction of the bridge. Figure 5.17 shows details of the VWSG employed within the CIP deck at mid-span and near-support sections.



Figure 5.16. Instrumented PC/PS Panels

The two last VWSG were transversely placed at 4.5 in (114 mm) from the bottom of the instrumented panels. One was located between girder lines 2 and 3, and the second between girder lines 3 and 4 (Figure 5.6a). DAS box 1 and DAS box 2 were situated on the interior sides of bent 2 and bent 3 pier caps. The 86 VWSG were split into two groups of 43 sensors that were connected to each DAS box (Figure 5.18). More details about the VWSG connected to each CR800 DAS box are given in Appendix C. After all the VWSG were placed within the deck, the CR800 DAS were anchored to the interior faces of the bents' pier caps.



(a) Mid-span Section



(b) Near Support Section

Figure 5.17. VWSG Installed on CIP RC Deck



Figure 5.18. Bridge A7957 VWSG Instrumentation

5.2.7. RFID Corrosion Sensors

Two RFID corrosion sensors (Figure 4.11), identified in Figure 5.19 as RFID corrosion sensors 1 and 2, were embedded at two different locations within the south side of the CIP RC deck. The purpose of the sensors is to detect two critical chloride

concentration levels at each location. The first value of chloride concentration will mark the onset of corrosion. The second value will be used to establish a correlation between the chloride ingress and the area of reinforcing steel that might be lost at that moment.

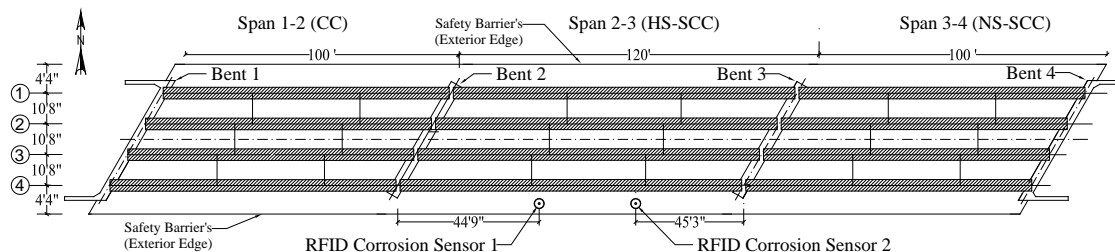


Figure 5.19. Bridge A7957 RFID Corrosion Sensors Installation (Plan View)

Table 5.7 presents the location's coordinates within the RC deck where the sensors were installed. Corrosion sensor 1 was placed 44 ft. 9 in. (13.7m) from the center line of bent 2 (Figure 5.19), along the direction of the safety barriers' longitudinal axis. This sensor was located 0.25 in. (0.6 cm) from the top surface of the deck, and at a distance of 22.0 in. (55.9 cm) from the exterior edge of the safety barrier (Figure 5.20).

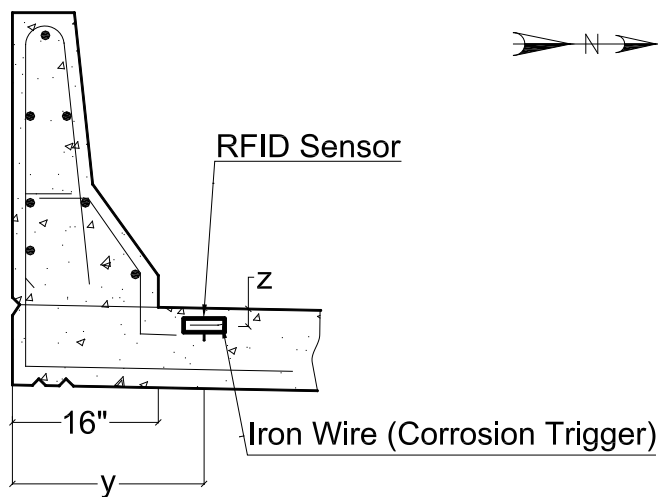


Figure 5.20. Bridge A7957 RFID Corrosion Sensors Installation (Elevation)

The second sensor was set 45 ft. 3 in. from the center line of bent 3, along the direction of safety barrier's principal axis. This sensor was separated 0.50 in. (1.3 cm) from the top surface of the deck and placed at a distance of 18.25 in. (46.4 cm) from the

exterior edge of the safety barrier (as reported in Table 5.7). Figure 5.21 shows an RFID corrosion sensor installed within the CIP RC deck of Bridge A7957 before concrete placement.

Table 5.7. RFID Sensors' Coordinates through CIP RC Deck of Bridge A7957

<i>Sensor No</i>	<i>Y</i>	<i>Z</i>
1	22"	¼"
2	18 ¼"	½"



Figure 5.21. RFID Installed on CIP RC Deck (Before Concrete Placement)

5.3. INTERMEDIATE BENT CONSTRUCTION

The first phase of the construction monitoring process of Bridge A7957 included the two intermediate bents. Bent no. 2 consisted of MoDOT's standard B mix while bent no. 3 was designed using MoDOT's B-2 mix with a 50% fly ash replacement level. The concrete temperature development profiles were recorded and analyzed between the two mixes. Each bent was constructed in two phases. First, the columns and web wall were poured. After sufficient strength was achieved, the pier cap was cast. Table 5.8 displays the construction schedule for the intermediate bents.

Table 5.8. Intermediate Bents Construction Schedule

Activity	Date
Instrumentation of bent 3 columns and web wall	6/28/2013
Pour of bent 3 columns and web wall	7/3/2013
Instrumentation of bent 2 columns and web wall	7/11/2013
Pour of bent 2 columns and web wall	7/12/2013
Instrumentation of bent 3 pier cap	7/23/2013
Pour of bent 3 pier cap	7/25/2013
Instrumentation of bent 2 pier cap	7/29/2013
Pour of bent 2 pier cap	7/30/2013

5.3.1. Mix Designs

Two mix designs were used in the intermediate bents. Bent 2 consisted of MoDOT's class B mix while bent 3 consisted of the same class B mix, modified with 50% fly ash replacement; mix IDs for bents 2 and 3 are 12CDB00A084 and 13CDHFVA003, respectively. Both mixes were batched by Osage County Concrete of Linn, MO. The design compressive strength for bents 2 and 3 was 3,000 psi (20.7 MPa). The mix designs are presented in Table 5.9. Air content and slump tests were performed prior to each pour.



Figure 5.22. Intermediate Bent QC/QA Specimens

Twenty-four 4 x 8 in. (100 x 200 mm) cylinders were collected for maturity studies of the compressive strength at 1, 3, 7, 14, 28, and 56 days as shown in Figure 5.22. The cylinders were field cured both at the job site as well as Missouri S&T to simulate the exposure conditions of the bridge substructure elements.

Table 5.9. Intermediate Bents Mix Designs

Type	Material	Bent 2 (lb./yd ³)	Bent 3 (lb./yd ³)
Coarse Aggregate	Choteau-Burlington-Cedar Valley – Gradation D Ledges 1A, 1B, 1, 2, 3	1840	1750
Fine Aggregate	Missouri River/Class A	1225	1242
Cementitious Material	Portland Cement – Type I/II	425	325
	Fly Ash – Class C	105	325
Water	--	248	213
Chemical Admixtures	Air Entraining Agent	6 oz./yd ³	6.5 oz./yd ³
	Water Reducer	11 oz./yd ³	13 oz./yd ³
w/cm	--	0.45	0.33
Design Air Content (%)	--	6.0	6.0

Conversions: 1 lb./yd³ = 0.5933 kg/m³, 1.0 oz./yd³ = 0.03708 kg/m³

5.3.2. Data Collection

Temperature data was recorded during each of the four castings of the intermediate bents identified previously in Table 5.8. After the thermocouples were installed, they were hooked up to the Compact RIO system. For the construction of the columns and web walls, the solar panel was connected after the pour was complete; the solar panel was connected before the pour of the pier caps. Data was collected for approximately 24-48 hours from the start of each pour. Figure 5.23 shows the DAS collecting data during the intermediate bent construction.



(a) Bent 3 Pier Cap



(b) Bent 2 Pier Cap

(c) Bent 3 Columns and Web Wall

Figure 5.23. Data Collection at Intermediate Bents

5.4. PC/PS GIRDERS AND PANELS FABRICATION

Six out of twelve PC/PS girders were instrumented at the cluster locations displayed in Figure 5.5 and Figure 5.6 (See Report D for additional details). A total of 86 VWSG with built-in thermistors, type EM-5, manufactured by Roctest Inc., were employed to monitor the stress variation as well as temperature changes in the girders, panels and CIP deck from fabrication through service life. The VWSG were installed prior to casting of the PC girders and were limited to girder lines 3 and 4 of the bridge (Figure 5.5). The CIP deck was instrumented at 16 different locations before concrete placement. A preconstruction planning meeting was held on November 16th, 2012, at Missouri S&T. The concrete producer, fabricator, contractor, and Missouri S&T researchers participated to clarify any details specific to the construction of the bridge

and its components. The bridge girders and panels were fabricated from July 26th through Aug 22nd, 2013 at the County Materials Corporation precast plant in Bonne Terre, MO. For the three spans, the PC/PS girders located on lines 3 and 4 (Figure 5.5) were selected to be monitored during their fabrication. Table 5.10 lists the construction timeline and the estimated steam curing time for the precast PC/PS girders and panels of Bridge A7957.

Table 5.10. PC/PS Girders Construction Timeline

Activities	Date
Instrumentation of span 1-2 girder 4 (S1-G4)	7/26/13
Pour of S1-G4 (steam cured for 16 hours)	7/29/13
Release of S1-G4	7/30/13
Instrumentation of span 1-2 girder 3 (S1-G3)	7/31/13
Pour of S1-G3 (steam cured for 16 hours)	8/1/13
Release of S1-G3, Instrumentation of span 3-4 girder 4 (S3-G4)	8/2/13
Pour of S3-G4 (steam cured for 38 hours)	8/3/13
Release of S3-G4, Instrumentation of span 3-4 girder 3 (S3-G3)	8/5/13
Pour of S3-G3 (steam cured for 16 hours)	8/6/13
Release of S3-G3, Instrumentation of span 2-3 girder 4 (S2-G4)	8/7/13
Pour of S2-G4 (steam cured for 88 hours)	8/8/13
Release of S2-G4, Instrumentation of span 2-3 girder 3 (S2-G3), Pour of S2-G3 (steam cured for 38 hours)	8/13/13
Release of S2-G3	8/15/13
Instrumentation of precast PC panels Pour of instrumented PC/PS panels (steam cured for 15 hours)	8/21/13
Release of PC/PS panels	8/22/13

5.4.1. Mix Designs

Three different concrete mixtures were utilized in the fabrication of the girders. The girders of the first span (span 1-2) were fabricated using a conventional concrete (CC) mixture with a specified strength of 8,000 psi (55.2 MPa). The concrete mix ID of the first span girders was 110A10A002CM. The girders in the second span (span 2-3), fabricated with HS-SCC, have a target compressive strength of 10,000 psi (68.9 MPa). The mix ID of the girders of this span was 13SECSPE001. The third span (span 3-4) used girders fabricated of NS-SCC with a specified compressive strength of 8,000 psi (55.2 MPa). The mix ID corresponding to the girders of the last span was 13SECSPE002.



(a) Slump flow and J-Ring Tests



(b) Column Segregation

Figure 5.24. Fresh Property Tests (Concrete Mixtures of Spans 2-3 and 3-4)

The mix designs are listed in Table 5.11. Air content and slump flow tests were conducted prior to each pour of the girders of span 1-2. In the case of the girders of spans 2-3 and 3-4, air content, slump flow, column segregation, and J-ring flow tests were also performed before concrete placement. Thirty 4 x 8 in (100 mm x 200 mm) cylinders were collected to conduct maturity studies on the compressive strength at 1, 3, 7, 14, 28, 56, load test 1, 1 year, and load tests 2 and 3. Furthermore, six 6 x 6 x 21 in (150 x 150 x 525 mm) beam specimens were made for each instrumented girder to obtain the flexural strength of concrete at 28 days and at the time when the live load tests 1 and 2 are executed.

Table 5.11. PC/PS Girders Concrete Mixture Comparison

Type	Material	Span 1-2 (CC)* (lb./yd ³)	Span 2-3 (HS-SCC) (lb./yd ³)	Span 3-4 (NS-SCC) (lb./yd ³)
Coarse Aggregate	Lead Belt, Park Hills Stone Masonry Grade E Dolomite	1780 [#]	1340 [§]	1476 [§]
Fine Aggregate	Weber, Cristal City Sand/Class A Ledges 4-1	1085	1433	1433
Cement	Portland Cement – Type I (Holcim, Ste. Genevieve Plant)	800	850	750
Water	---	256	280	260
Chemical Admixtures	Air Entraining Agent	8 oz./yd ³	17.0 oz./yd ³	17.0 oz./yd ³
	Type D Water Reducer (Recover)	9.2 oz./yd ³	25.5 oz./yd ³	25.5 oz./yd ³
	Type F High Range Water Reducer (Adva Cast 575)	17.20 oz./yd ³	76.5 oz./yd ³	67.5 oz./yd ³
w/c	---	0.32	0.33	0.35
Design Air Content (%)	---	5.5	5.0	5.0

*: CC corresponds to MoDOT's class A-1 mix.

#: MSA was limited to ¾".

§: MSA was limited to ½".

Two 4 x 24 in (100 x 600 mm) creep, shrinkage and coefficient of thermal expansion (CTE) specimens were fabricated prior to casting of S1-G4, S3-G3, and S2-G3. Figure 5.24 shows the fresh property tests conducted on the PC/PS girders of spans 2-3 and 3-4. Figure 5.25 shows the specimens collected during the fabrication of one of the girders mentioned previously. The PC/PS panels were fabricated with a MoDOT class A-1 mix. The design compressive strength of the mixture was 6,000 psi (41.4 MPa). Eighteen cylinders 4 x 8 in. (100 mm x 200 mm) were cast to conduct compressive strength tests at 1 day, 28 days, load test 1, 1 year, load test 2, and load test 3. The

cylinders were field cured both at the job site as well as at Missouri S&T to simulate the same exposure conditions of the bridge girder elements.



Figure 5.25. PC/PS Girders QC/QA Specimens

5.4.2. Data Collection

The two CR800 DAS were taken to County Materials, the fabricators' precast plant, in Bonne Terre, Missouri, to record data from the VWSG. The VWSG were connected to the CR800 DAS prior to casting, and temperature and strain readings were recorded from the pour until after release of the PC girders. Data was collected for at least one hour after the strands were released. Figure 5.26 shows the DAS boxes reading data during the fabrication of one of the girders.



Figure 5.26. Data Collection During the PC/PS Girders Fabrication

After releasing the tendons (Figure 5.27), deflection data was recorded to obtain the camber of the girders (Figure 4.9).



Figure 5.27. Release of PC/PS Girder

Finally, the girders were moved to the yard for storage until they were shipped and delivered to the bridge jobsite (Figure 5.28).



Figure 5.28. Girders Storage at Precast Plant

5.5. BRIDGE CONSTRUCTION

This stage of the project included monitoring the temperature and stresses of the different superstructure components of the bridge according to the instrumentation plan. The different monitoring phases included the girders erection, concrete placement within the CIP RC deck, and safety barriers.

5.5.1. Girders Erection

On September 24th, 2013, the first eight PC girders were shipped and placed on spans 1-2 and 2-3. Figure 5.29 shows some of the girders being delivered to the bridge jobsite. One HS-SCC and one NS-SCC PC/PS girder were selected to be monitored during their erection.



Figure 5.29. Shipping of the PC Girders to the Bridge Jobsite

Before the girders were lifted and set onto their final locations, CR800 DAS box 1 was strapped to the top flange of the girder as shown in Figure 5.30. The VWSG were connected to the DAS (Figure 5.30) to measure strain and temperature data until approximately one hour after the erection of the girders.



Figure 5.30. VWSG Sensors Connected to CR800 DAS

Figure 5.31 shows girder 4 of span 2-3 (HS-SCC) during the erection (September 24th, 2013). The data was read from the VWSG sensors placed at mid-span and near the east support sections.



Figure 5.31. Lifting of HS-SCC PC Girder 4 (Span 2-3)

Figure 5.32 shows the PC girders of the first two spans placed atop their supports. This activity was accomplished on September 24th, 2013.



Figure 5.32. Conventional Concrete and HS-SCC PC Girders Placed on Supports

On September 25th, 2013, the last four PC/PS girders were shipped and placed on span 3-4. The VWSG sensors installed at mid-span and near the west-end sections of girder 4 collected data during the erection. Figure 5.33 shows the lifting and erection of the girder.



(a) NS-SCC PC/PS Girder 4 with DAS



(b) PC/PS Girders Placed on Their Supports

Figure 5.33. Lifting and Setting of NS-SCC PC Girders

5.5.2. CIP RC Deck

After the PC girders were erected, the contractor started setting the steel diaphragms and precast concrete panels as shown in Figure 5.34. Steel channels C15x33.9 were employed as the intermediate steel diaphragms that transversely connect the PC girders (Figure 5.34).



Figure 5.34. Diaphragm and PC/PS Panels Erection

The deck's reinforcing steel was placed, and the rest of the VWSG sensors were set within the girder's mid-span and near support sections according to the instrumentation plan (Figure 5.5). Figure 5.35(a) and Figure 5.35(b) show how the VWSG wires were gathered and passed through a PVC pipe. Finally, the wires were

hooked up to the CR800 DAS boxes that were previously anchored on the interior faces of bents 2 and 3 [Figure 5.35(c) and Figure 5.35(d)].



(a) VWSG Wires Passed through Formwork



(b) VWSG Collected Through PVC Pipe



(c) VWSG Wires Connected to CR800 DAS Modules



(d) CR800 DAS Anchored to Bent 3 Pier Cap

Figure 5.35. Installation of VWSG within CIP Deck and CR800 DAS Boxes



Figure 5.36. Concrete Placement on Intermediate RC Diaphragm

The intermediate bents RC diaphragms were cast before the CIP RC deck (Figure 5.36). This procedure was executed to give continuity to the RC and PC bridge superstructure elements. After the RC diaphragms were cast, the contractor poured the RC deck. Figure 5.37 shows the equipment employed during the concrete placement and some of the crew members finishing the surface of the CIP deck.



Figure 5.37. Concrete Placement on CIP RC Deck

RFID corrosion sensors 1 and 2, were placed at the locations described in Section 5.2.7. These sensors were set within the CIP RC deck right after the concrete finishing equipment worked the concrete surface located above the locations selected to be instrumented. Figure 5.38 shows one of the corrosion sensors embedded within the south side of Bridge A7957. More details about the installation of the RFID corrosion sensors on Bridge A7957 can be found in Myers and Hernandez (2014).



Figure 5.38. RFID Corrosion Sensor Embedded within CIP Deck

Figure 5.39 displays the final appearance of the CIP RC deck of Bridge A7957 after concrete was placed in October 21, 2014.



Figure 5.39. Finished Surface of CIP RC Deck

5.5.2.1. Mix design

A MoDOT modified B-2 concrete mixture (identified as mix 12CDMB2A087) with a specified design strength of 4,000 psi (27.6 MPa) was employed to cast the RC deck. The deck was poured on October 21st, 2013. Osage County Concrete of Linn, MO, produced the concrete mix. The mix proportions are listed in Table 5.12.

Table 5.12. CIP RC Deck's Concrete Mix Proportions

Type	Material	Design Weight (lb./yd ³)	Batched Weight (lb./yd ³)
Coarse Aggregate	Capital Quarries Holt Summit, MO	1895	1932
Fine Aggregate	Natural Sand Class A Capital Sand. Jefferson City, MO	1170	1214
Cementitious Material	Portland Cement – Type I/II Continental Hannibal, MO	450	450
	Fly Ash – Class C Headwaters	150	150
Chemical Admixtures	Air Entraining Agent Daravair 1400	4.5 oz./yd ³	4.5 oz./yd ³
	Water Reducer Type A Adva140	2.0 oz./cwt	2.0 oz./cwt
Water	--	220	175
w/cm	--	0.37	0.29

Conversions: 1 lb./yd³ = 0.5933 kg/m³, 1.0 oz./yd³ = 0.03708 kg/m³, 1.0 oz./cwt = 6.5 oz./yd³

Concrete temperature, air content and slump tests were conducted prior to casting the deck. Twenty-four 4 x 8 in. (100 mm x 200 mm) concrete cylinders (Figure 5.40) were collected to obtain the compressive strength at different ages (3, 7, 14, 28, 56, load test 1, 1 year, and load test 2). In addition, three 12 x 12 x 3 in. (305 x 305 mm x 76 mm) abrasion test specimens (Figure 3.16), and three 3.5 x 4.5 x 16 in. (89 x 114.3 x 406.4 mm) freeze-thaw specimens (Figure 3.12) were fabricated. Finally, five ponding specimens were collected according to the detail of Figure 3.13 and Figure 3.14. RFID corrosion sensors 3 and 4 were installed in only two ponding specimens (Figure 5.41).



(a) Compression Test Specimens



(b) Freeze-Thaw, Abrasion and Ponding Test Molds



(c) Curing Freeze-Thaw, Abrasion and Ponding Test Specimens

Figure 5.40. CIP Deck QC/QA Specimens Collected During Concrete Placement

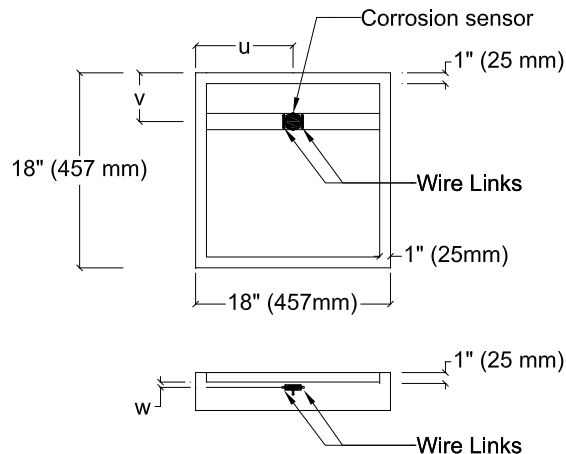


Figure 5.41. Detail of RFID Corrosion Sensor Installed in Ponding Test Specimens

The coordinates of the location where the RFID corrosion sensors were installed within the ponding specimens are listed in Table 5.13.

Table 5.13. RFID Sensors' ID Coordinate Locations within Ponding Specimens

Sensor ID	RFID ID	Specimen ID	u (in.)	v (in.)	w (in.)
3	61830DF	C-SEN2-001-F	9.00	4.50	0.25
4	618301F	C-SEN2-002-F	9.00	4.50	0.50

u, v, w: Coordinates defining the locations where the RFID sensors were installed (Figure 5.41).
Conversion: 1 in. = 25 mm

5.5.2.2. Data collection

On October 17th, 2013, the eighty-six VWSG sensors were fixed to both CR800 DAS according to the instrumentation plan and details of Figure 5.5 and Figure 5.6. Since this date, these sensors have been continuously collecting temperature and strain data within the superstructure elements of Bridge A7957. Temperature and strain data corresponding to the cast of the RC deck, approach slabs, and safety barriers are available and will be used to compare any trends in the responses of the different super structure elements.

5.5.3. Approach Slab Concrete Placement

The approach slabs were poured on December 4, 2013. No compression cylinders were made by the researchers during the casting of this part of the structure. However, temperature and strain data was recorded by the sensors embedded within the structure.

5.5.4. Safety Barrier Curbs

The safety barrier's concrete was poured on December 19, 2013. Fifteen 4 x 8 in. (100 mm x 200 mm) concrete cylinders were collected during the concrete placement on this part of the structure. The compressive strength was programmed to be obtained at different ages (7, 28, 56, load test 1, and 1 year). Figure 5.42 shows the final view of Bridge A7957 after it was completed.



Figure 5.42. Bridge A7957 Completed

5.6. PROBLEMS ENCOUNTERED

At the precast plant, the girders' instrumentation was conducted successfully and took approximately 4 hours per girder. The VWSG sensor installation carried out at the bridge site including the CIP deck slab and routing of wiring was successful. This installation took approximately 3 days in total. However, there were some problems encountered throughout the instrumentation program. At the precast plant, one VWSG was accidentally broken during placement within the section located at girder 3's mid-span of span 2-3 (HS-SCC), layer TF (Table 5.5). This sensor, labeled as "S2-G3-M5", was connected to CR800 DAS 2. No data was collected during fabrication for this sensor.

At the bridge site, the sensor placed at the mid-span section of girder 4 (span 1-2), layer CGC presented a failure after it was connected to the CR800 DAS1 secured to the interior face of bent 2. This sensor, labeled as “S1-G4-M4”, did not collect any data before and after the deck was poured.

6. RESEARCH PROGRAM RESULTS

6.1. MATERIAL TEST RESULTS

The following section contains preliminary material results from the trial mixes and QC/QA specimens from the bridge substructure and superstructure elements. Also included are the hydration profiles from the intermediate bents.

6.1.1. Trial Mixes

6.1.1.1. HVFAC

6.1.1.1.1. Fresh properties

The HVFAC trial mix was batched on January 8, 2013 at Osage County Materials in Linn, MO. Fresh properties of the mix were reported and are listed in Table 6.1. The air content closely matches the design air content of 6.0%. The lower slump value compared to the HVFAC mixes in the intermediate bents (Table 6.1) could be explained by the colder weather and concrete temperatures during the trial mix batching.

Table 6.1. HVFAC Trial Mix Fresh Properties

Air Temp. (°F/°C)	64/18
Concrete Temp. (°F/°C)	64/18
Slump (in.)	2.5
Air Content (%)	5.3

Conversions: 1 in. = 25.4 mm

6.1.1.1.2. Hardened properties

The researchers conducted compressive strength and modulus of elasticity tests on the HVFAC trial mix at 7 and 28 days. The contractor, Fred Weber, Inc., also collected compressive strength results at 1, 2, 3, 4, 7, and 28 days. The rate of strength gain for HVFAC is expected to be slower than that of CC. Compressive strengths at 56 days are typically reported to address this trend; however, for the trial mix investigated, a 56-day test was not conducted. Results for the peak compressive stress, f'_c , are shown in Table

6.2. Slight variations between the university and contractor in compressive strength occurred, possibly due to curing conditions, end capping conditions, and the selected load rate from ASTM C39 (ASTM C 39 2012).

Table 6.2. HVFAC Trial Mix Compressive Strength

Concrete Age (days)	Compressive Strength (psi)	
	Contractor	University
1	100	N/A
2	1000	N/A
3	2330	N/A
4	3070	N/A
7	4440	3977
28	6240	5967

Conversion: 1000 psi = 6.895 MPa

Measured values for the modulus of elasticity at the time of testing were compared with empirical estimates from ACI 318-11 and AASHTO 2012. These empirical formulas account for the unit weight of concrete (w_c) (pcf for ACI, kcf for AASHTO), compressive strength (f'_c) (psi for ACI, ksi for AASHTO), and the type of aggregate (K_I). Since additional testing was not performed on the dolomitic limestone aggregate, K_I was taken as 1.0. Empirical equations for MOE from ACI 318-11 and AASHTO 2012 are provided in Equations (6.1) and (6.2), respectively (ACI 318-11, AASHTO 2012).

$$E_c = 33w_c^{1.5}\sqrt{f'_c} \quad (6.1)$$

$$E_c = 33,000K_1w_c^{1.5}\sqrt{f'_c} \quad (6.2)$$

ACI uses units of pounds and feet while the AASHTO formula uses kips and feet. The variable, K_1 , is a correction factor for source of aggregate, and is typically taken as 1.0, unless determined by physical testing (AASHTO 2012). Measured and predicted values for the modulus of elasticity in units of psi for the HVFAC trial mix are listed in Table 6.3. Both the ACI and AASHTO predictions underestimated the MOE. The

modulus of elasticity of concrete can have significant variability due to concrete strength, concrete age, aggregate and cement properties, rate of loading, type and size of specimen, and the definition of the elastic modulus, be it initial, tangent, or secant modulus (Pauw 1960).

Table 6.3. HVFAC Trial Mix Measured and Predicted Modulus of Elasticity

Age (days)	Calculated	ACI Prediction	AASHTO Prediction
7	4,137,169	3,550,527	3,550,527
28	4,766,590	4,349,036	4,349,036

Conversion: 1000 psi = 6.895 MPa

6.1.1.2. HS-SCC

6.1.1.2.1. Fresh Properties

Fresh properties from the HS-SCC trial mix conducted at County Materials Corporation on January 31, 2013 are provided below in Table 6.4. The slump flow and passing ability were on the low end of typical SCC mixtures, in part due to the colder temperatures (ACI 237 2007). The segregation percentage was 0.0% as there was a slightly larger amount of coarse aggregate in the top third as opposed to the bottom third of the column.

Table 6.4. HS-SCC Trial Mix Fresh Properties

Air Temp. (°F/°C)	46/8	
Concrete Temp. (°F/°C)	65/18	
Air Content (%)	5.6	
Slump Flow (in.)	21	
J-Ring (in.)	19	
Segregation Column	Top (lb.)	8.96
	Bottom (lb.)	8.88
	S (%)	0.00

Conversions: 1 in. = 25.4 mm, 1 lb. = 0.4536 kg

6.1.1.2.2. Hardened properties

Compressive strength, modulus of elasticity, and splitting tensile strength (STS) tests were performed at 1, 7, and 28 days. The average results are presented in Table 6.5. The modulus of elasticity was compared to empirical estimates from ACI 318-11 and ACI 363R-10 graphically displayed in Figure 6.1. The ACI 318-11 [Equation (6.1)] model is typically not reliable for concrete strengths in excess of 8,000 psi (55 MPa) because of the data it is based on (ACI 318 2011). The ACI 363R-10 model proposed by Martinez et al. (1982) [Equation (6.3)] was implemented as a lower bound for HSC concrete for concrete strengths ranging from 3,000 to 12,000 psi (20.7 to 82.7 MPa) (ACI 363 2010). In the case of HS-SCC, it provides a reasonably accurate estimate. Tomosawa et al. proposed a separate ACI 363R-10 model [Equation (6.4)] which accounts for the aggregate source as well as type of cementitious material; it provides a lower-bound estimate for HS-SCC. For the listed equations, E_c is the modulus of elasticity (psi), f'_c is the compressive strength of concrete (psi), and w is the concrete unit weight (pcf). The variable k_1 is taken as 1.2 for crushed limestone and calcined bauxite aggregates; 0.95 for crushed quartzite, crushed andesite, crushed basalt, crushed clay slate, and crushed cobble stone aggregates; and 1.0 for other aggregates. The variable k_2 is taken as 0.95 for silica fume, slag cement, and fly ash fume; 1.10 for fly ash; and 1.0 for other types of admixtures (ACI 363 2010). The dolomite and Portland cement used in the HS-SCC trial mix correspond to k_1 and k_2 values of 1.0 and 1.0, respectively.

$$E_c = 40,000\sqrt{f'_c} + 10^6 \quad (6.3)$$

$$E_c = 4.86 * 10^6 k_1 k_2 \left(\frac{w}{150} \right)^2 \left(\frac{f'_c}{8700} \right)^{(1/3)} \quad (6.4)$$

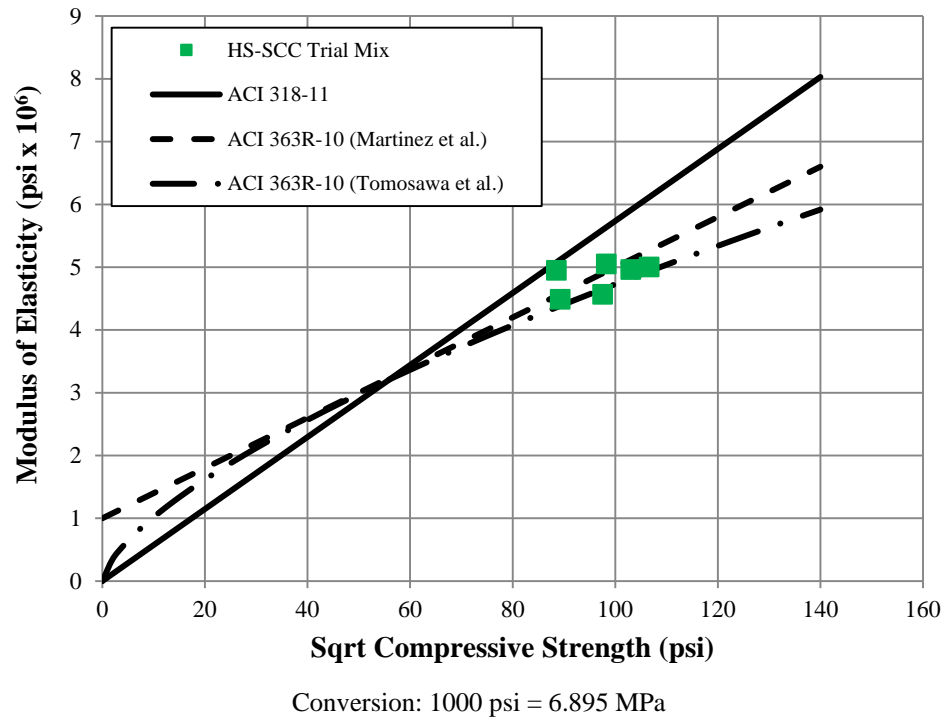


Figure 6.1. HS-SCC Trial Mix Modulus of Elasticity vs. Compressive Strength

Table 6.5. HS-SCC Trial Mix Hardened Properties

Age of Concrete (days)	Compressive Strength (psi)	Modulus of Elasticity (psi)	Splitting Tensile Strength (psi)
1	7,996	4,527,561	567
7	9,658	4,977,283	579
28	10,957	5,008,516	537

Conversion: 1000 psi = 6.895 MPa

The splitting tensile strengths of the HS-SCC were compared to empirical estimates from ACI-318-11 [Equation (6.5)] and ACI 363R-10 [Equation (6.6)] as shown in Figure 6.2. Equation (6.6) below, proposed by Carrasquillo et al. (1981) in ACI 363R-10, is valid for concrete strengths ranging from 3,000 to 12,000 psi (21 to 83 MPa). Myers and Carrasquillo suggested Equation (6.7) from ACI 363R-10 specifically for member-cured dolomitic limestone (ACI 363 2010). For Equations (6.5) through (6.7), f_t is the splitting tensile strength (psi), and f'_c is the compressive strength of concrete (psi).

$$f_t = 6.7\sqrt{f'_c} \quad (6.5)$$

$$f_t = 7.4\sqrt{f'_c} \quad (6.6)$$

$$f_t = 8.66\sqrt{f'_c} \quad (6.7)$$

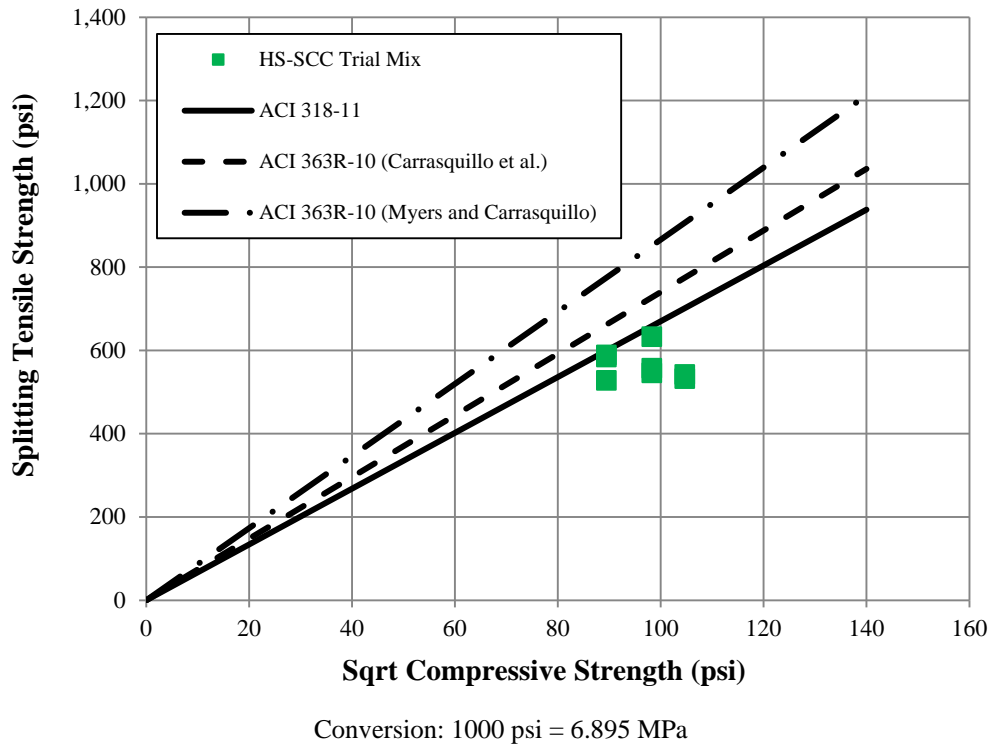


Figure 6.2. HS-SCC Trial Mix Splitting Tensile Strength vs. Compressive Strength

The ACI 318-11 model more closely correlates to the data obtained. The STS has been shown to have significant variability depending on the aggregates, paste, and interface zone (Wight and MacGregor 2005). However, post-failure images of STS testing reveal that the failure plane extended through the aggregate (Figure 6.3). Thus the bond between the aggregates and paste is greater than the strength of the aggregate themselves. Furthermore, Myers et al. (2012) found no variability between HSC and HS-SCC with dolomitic limestone, and both mixtures fell below the ACI 318-11 prediction.



Figure 6.3. Splitting Tensile Strength Failure Plane

6.1.1.3. NS-SCC

6.1.1.3.1. Fresh properties

The NS-SCC trial mix was batched on March 8, 2013 at County Materials Corporation in Bonne Terre, MO. Fresh properties recorded are listed in Table 6.6. The slump flow and passing ability are larger than those measured during the HS-SCC trial mix in part due to the warmer temperatures and higher w/cm ratio. ACI 237r-07 recommends a maximum segregation percentage of 10%; the segregation of 8.2% met this value.

Table 6.6. NS-SCC Trial Mix Fresh Properties

Air Temp. (°F/°C)	53/12	
Concrete Temp.	not recorded	
Air Content (%)	8.2	
Slump Flow (in.)	25	
J-Ring (in.)	25	
Segregation Column	Top (lb.)	8.66
	Bottom (lb.)	9.41
	S (%)	8.20

Conversions: 1 in. = 25.4 mm, 1 lb. = 0.4536 kg

Khayat and Mitchell (2009) found that an increase in the w/cm ratio of SCC mixes leads to a reduction in static stability and thus increased segregation. The w/cm

ratios of the HS-SCC and NS-SCC were 0.33 and 0.35, respectively, which support that trend.

6.1.1.3.2. Hardened properties

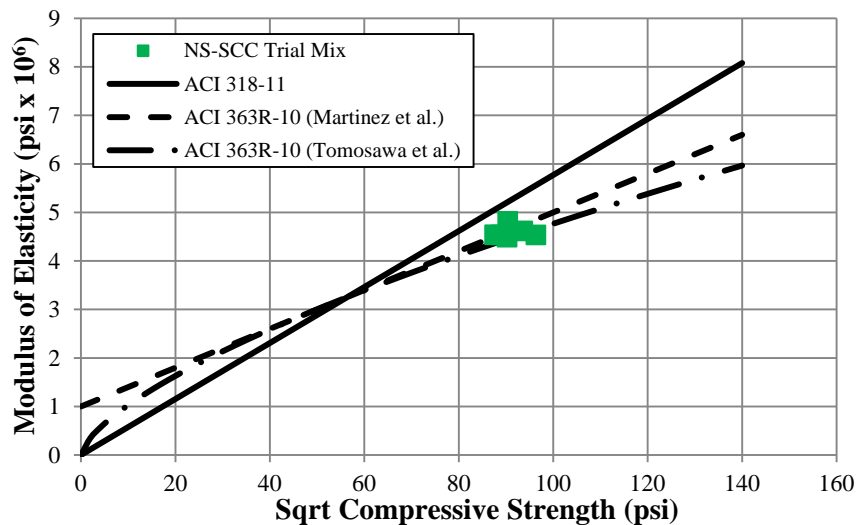
The resulting average hardened mechanical properties of the NS-SCC mix including compressive strength, modulus of elasticity, and splitting tensile strength are displayed in Table 6.7.

Table 6.7. NS-SCC Trial Mix Hardened Properties

Concrete Age (days)	Compressive Strength (psi)	Modulus of Elasticity (psi)	Splitting Tensile Strength (psi)
3	7497	4,513,258	454
7	8163	4,539,066	489
28	9179	4,717,905	633

Conversion: 1000 psi = 6.895 MPa

The modulus of elasticity and splitting tensile strength were compared against ACI 318-11 and ACI 363R-10 equations previously mentioned in Sections 6.1.1.1.2 and 6.1.1.2.2 and are illustrated in Figure 6.4 and Figure 6.5, respectively.



Conversion: 1000 psi = 6.895 MPa

Figure 6.4. NS-SCC Trial Mix Modulus of Elasticity vs. Compressive Strength

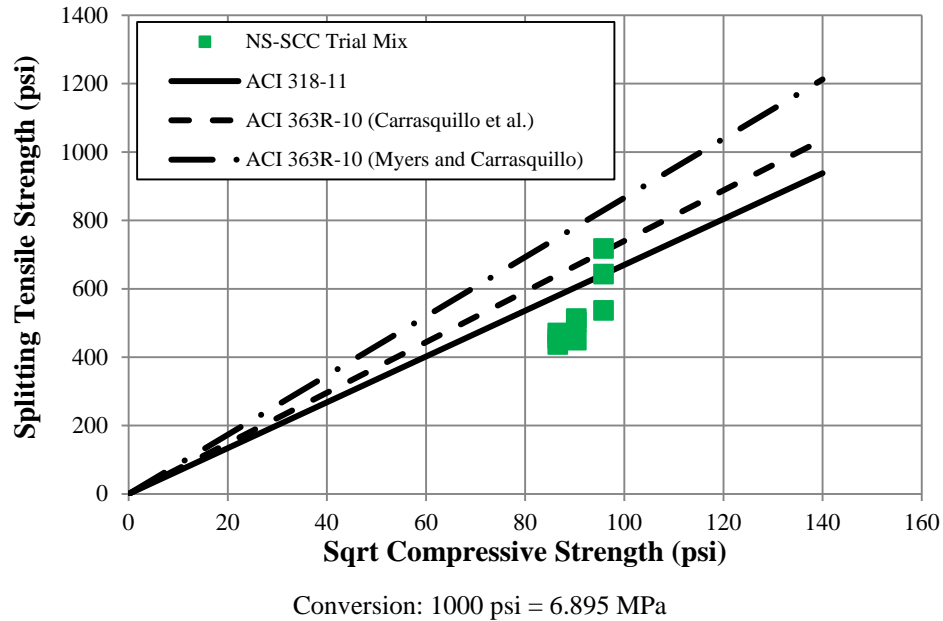


Figure 6.5. NS-SCC Trial Mix Splitting Tensile Strength vs. Compressive Strength

The MOE of the NS-SCC mix straddles the ACI 363R-10 equation proposed by Martinez et al., and can be conservatively estimated by the ACI 363R-10 estimate suggested by Tomosawa et al. These observations are similar to those from the HS-SCC trial mix.

In general, all three splitting tensile strength models overestimate the STS, with the ACI model being the best predictor. As expected, there is considerable variability in STS test results. The variations in aggregate sources could explain the variation between the test results and the ACI 363R-10 (Myers and Carrasquillo) equation, which was suggested for dolomitic limestone.

6.1.2. Intermediate Bents (HVFAC)

The intermediate bents were constructed in four phases previously presented in Table 5.8. Fresh properties were recorded and QC/QA specimens were collected for maturity studies of compressive strength. Lastly, the hydration profiles from each structural element were collected via the Compact RIO data acquisition system.

6.1.2.1. **Fresh properties**

The intermediate bents were constructed during the month of July 2013. Fresh properties, including air content and slump, were performed prior to each pour for the intermediate bents and are listed in Table 6.8.

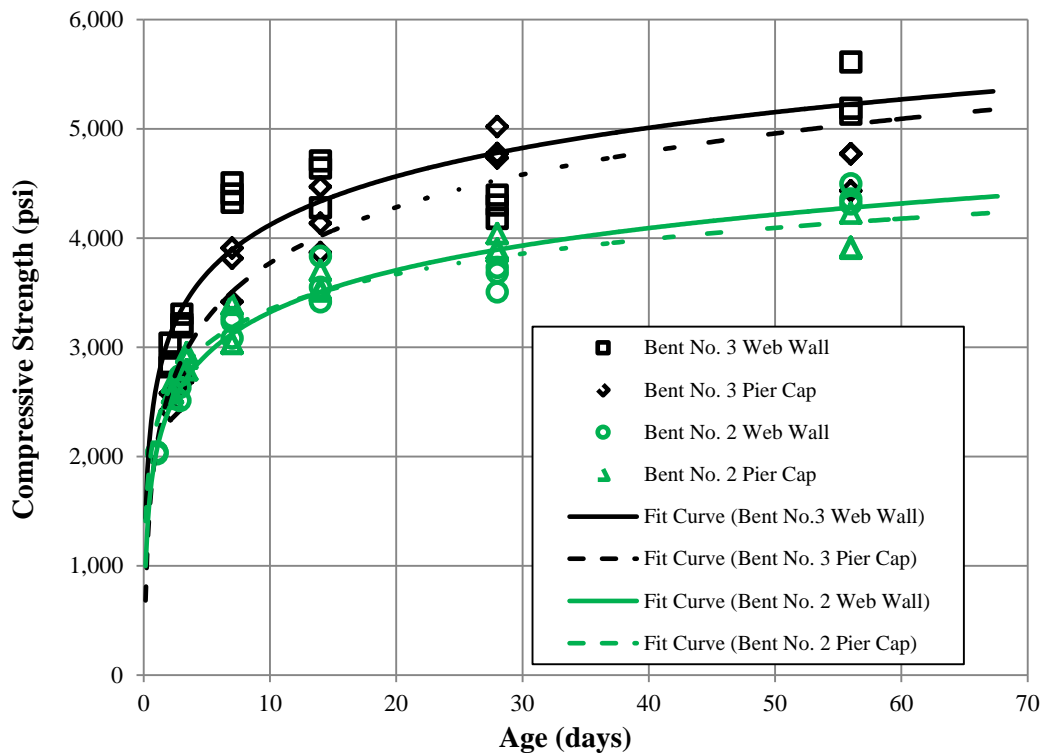
Table 6.8. Intermediate Bents Fresh Properties

	Bent 2 Web Wall	Bent 2 Pier Cap	Bent 3 Web Wall	Bent 3 Pier Cap
Air Temp. (°F/°C)	79/26	70/21	76/24	67/19
Concrete Temp. (°F/°C)	78/26	75/24	79/26	79/26
Slump (in.)	4	5.5	5.75	3
Air Content (%)	5.6	7.6	6.6	5.5

Conversions: 1 in. = 25.4 mm

6.1.2.2. **Hardened properties**

The time development of the compressive strength is illustrated in Figure 6.6.



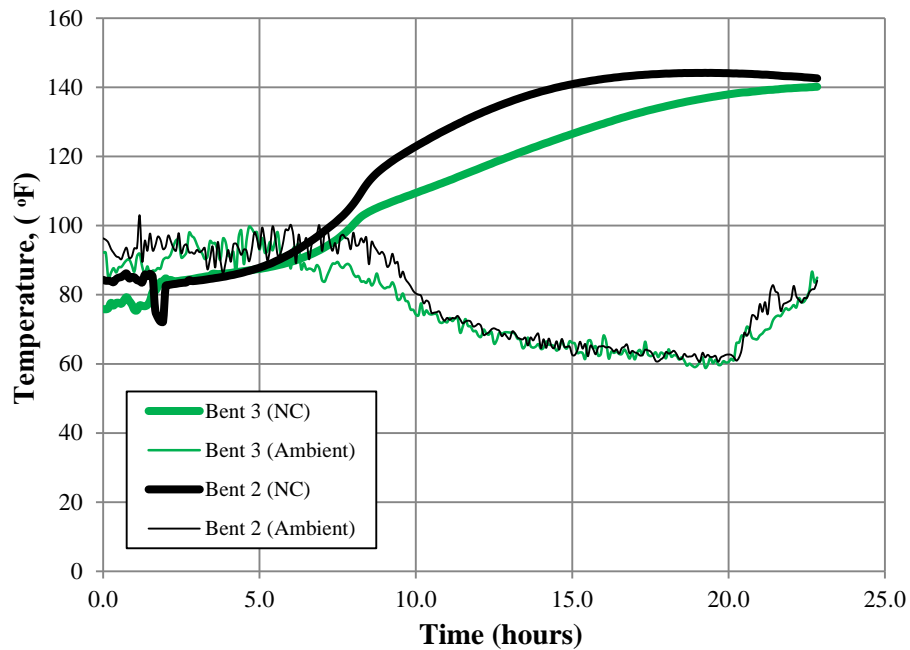
Conversion: 1000 psi = 6.895 MPa

Figure 6.6. Intermediate Bents Compressive Strength vs. Age

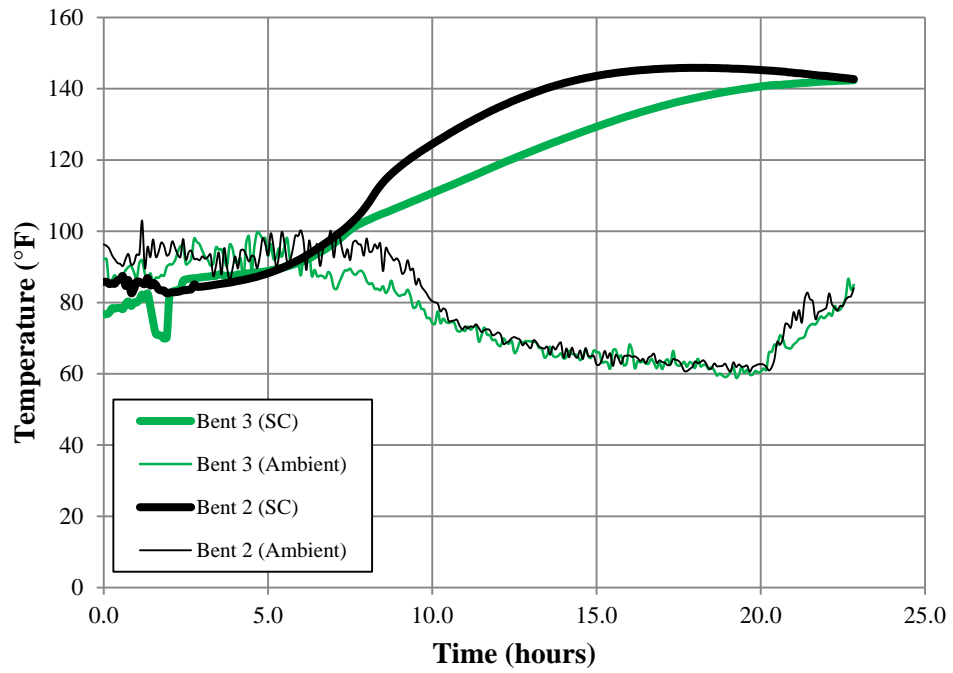
Bent 3 had a 28-day design compressive strength of 3,000 psi (28 MPa) while bent 2's specified compressive strength was 3,000 psi (21 MPa). Trendlines were applied to the tested data from each pour to develop a sense of the long-term strength gaining characteristics of each mix. The HFVAC mixes do not appear to level off to the extent of the CC mix, evidence of the high replacement level of fly ash.

6.1.2.3. Hydration profiles.

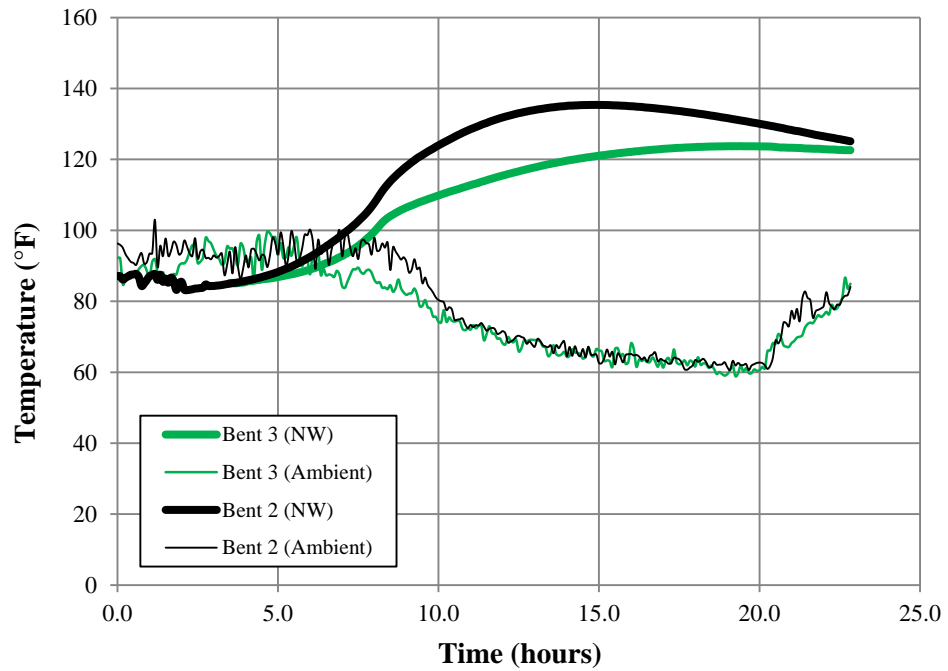
The temperature development profiles were recorded from the start of each pour using thermocouple wires. The locations of the embedded thermocouples were presented in (Section 5.2.6.1). Figure 6.7 presents hydration profiles from the construction of the columns and web wall. Figure 6.8 illustrates the temperature development in the pier caps. The trends in the columns and web walls of the two bents indicate that a 50% fly ash replacement has a negligible effect on setting time, but reduces the amount of heat released and the time at which the peak of the hydration curve occurs. These observations support the findings of Wang et al. (2006). When examining the heat generation in the pier caps, similar trends are noted with the exception that the peak of the hydration curve is delayed with respect to the conventional concrete mix.



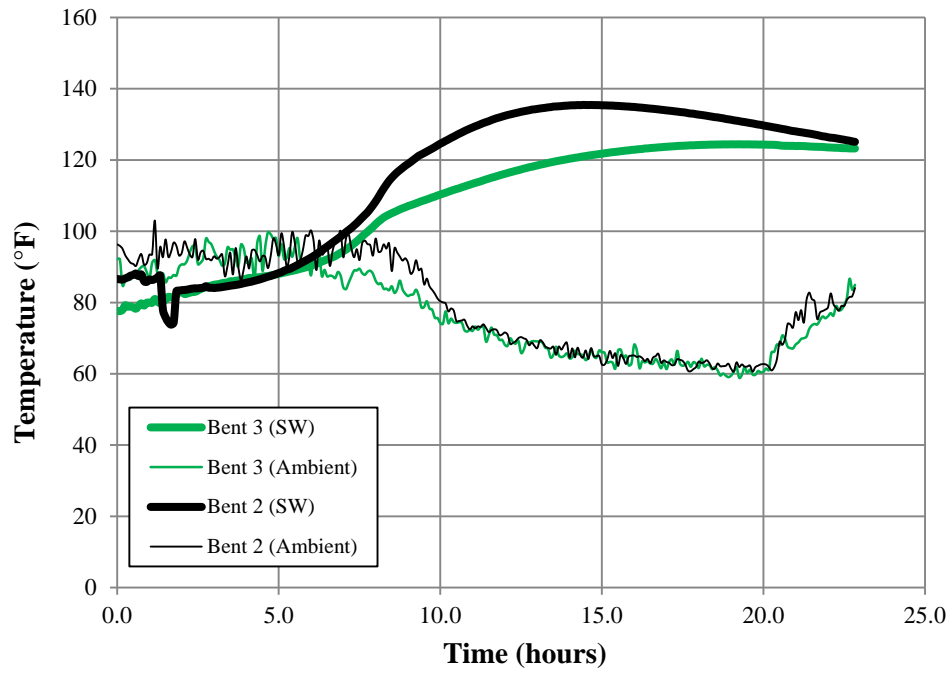
(a) North Column



(b) South Column



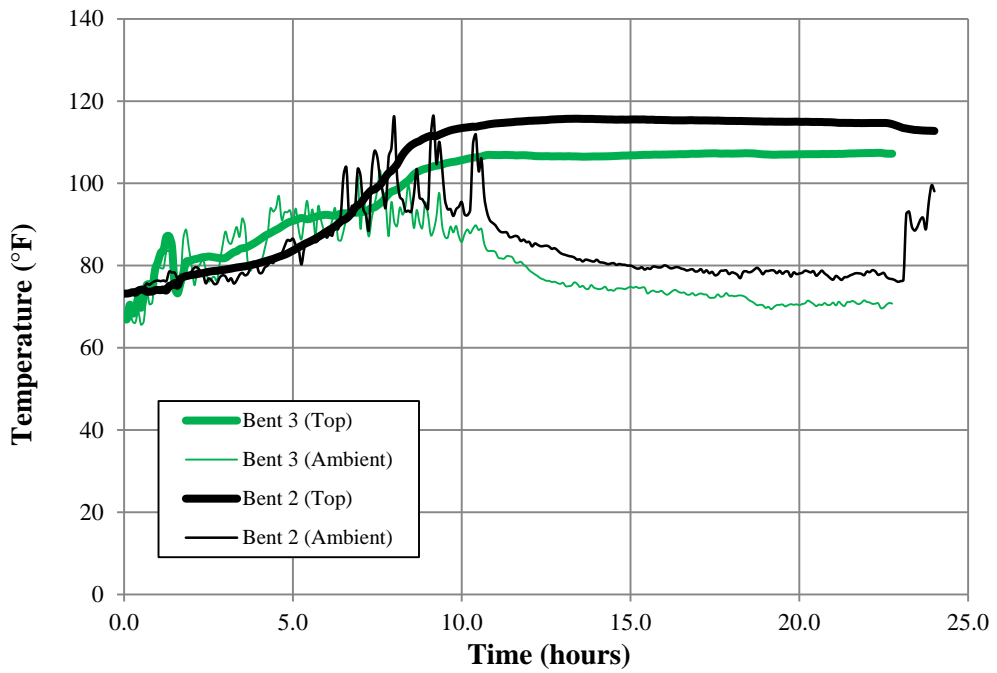
(c) North Web Wall



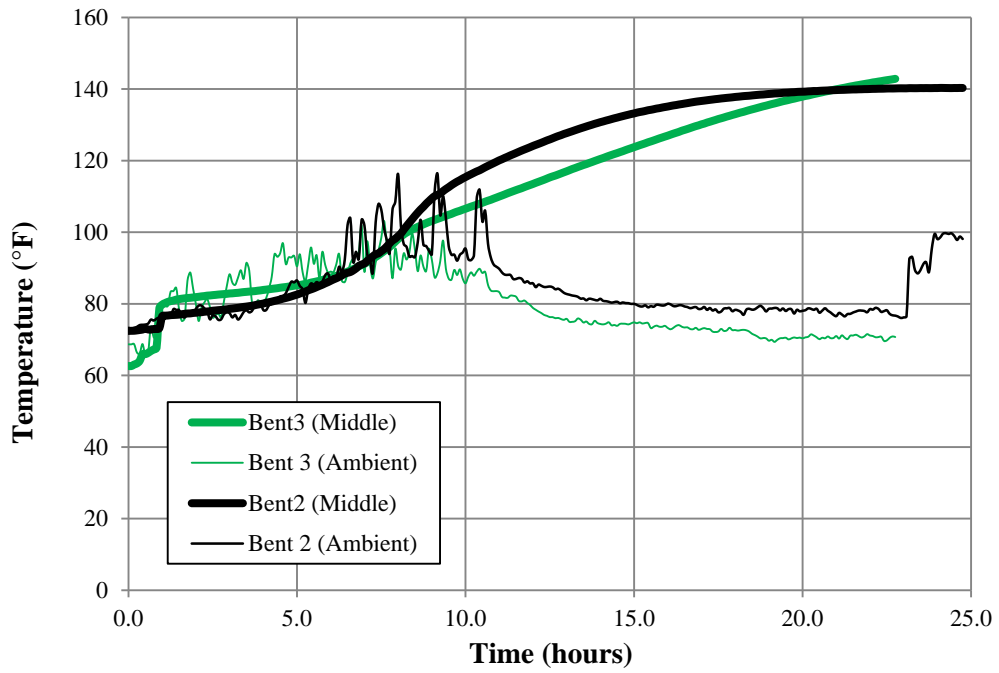
(d) South Web Wall

Conversion: °C = (°F)(5/9)+32

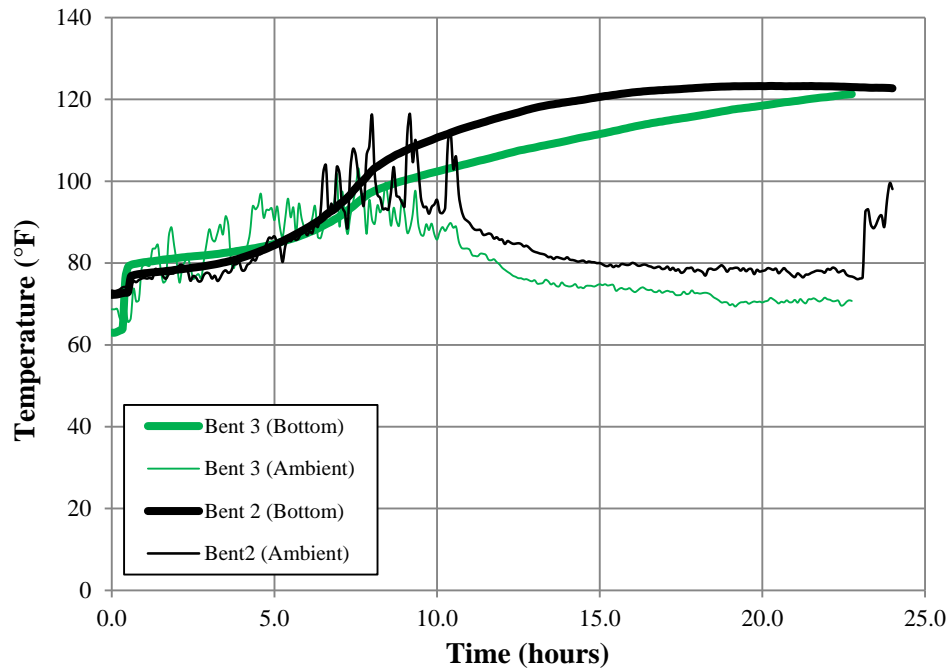
Figure 6.7. Intermediate Bents Hydration Profiles: Columns and Web Wall



(a) Top of Pier Cap



(b) Middle of Pier Cap



(c) Bottom of Pier Cap

Conversion: $^{\circ}\text{C} = (^{\circ}\text{F})/1.8 + 32$

Figure 6.8. Intermediate Bents Hydration Profiles: Pier Cap

The hydration rate is defined as the temperature rise per 100 lbs (45.4 kg) of cementitious material per cubic yard, defined in Equation (6.8). The difference in temperature (peak concrete temperature minus initial concrete temperature) in each profile was calculated and divided by the amount of cementitious material per cubic yard in the respective mixture. The amount of cementitious material per cubic yard in bents 2 and 3 was 530 and 650, respectively. Table 6.9 lists the hydration rates at each of the investigated locations for bents 2 and 3.

$$= \frac{\text{Peak Temperature} - \text{Initial Temperature}}{100 \text{ lbs. cementitious material per } yd^3} \quad (6.8)$$

Approximately 23 hours after pour of the bent 3 pier cap, the DAS was accidentally disconnected when the formwork was removed by the contractor. Missouri S&T did not return to the construction site until 2 days after the pour, and consequently hydration data from roughly 23-48 hours after casting was lost. However, temperature development profiles from the other intermediate bent pours leveled off after roughly 20-26 hours, thus bent 3 was nearing the peak of the hydration process when the DAS was disconnected.

Table 6.9. Intermediate Bents Hydration Rates

Location	Hydration Rates				Percent Reduction
	Bent 2		Bent 3		
	(°F/cwt)	(°C/cwt)	(°F/cwt)	(°C/cwt)	
North Column	11.47	6.37	8.67	4.82	24.4
South Column	11.77	6.54	8.63	4.79	26.7
North Web Wall	9.77	5.43	5.93	3.29	39.3
South Web Wall	9.71	5.39	6.31	3.51	35.0
Top Pier Cap	7.68	4.86	4.37	2.43	43.1
Middle Pier Cap	12.32	6.85	N/A	N/A	N/A
Bottom Pier Cap	9.11	5.06	6.51	3.61	28.6

In Figure 6.8, the temperature rises in the top and bottom of the pier cap for bent 3 appear to be leveling off, and thus the hydration rates will be very similar to that if additional data was collected. However, for the thermocouple located at the middle of the

pier cap in bent 3 (Figure 6.8b), the temperature rise does not appear to level off, and so the hydration rate was not calculated.

The high fly ash replacement significantly reduced the heat generation within the intermediate bents. The percent reduction in the heat of hydration process was calculated as a percentage of the intermediate bent 2 as shown in Table 6.9. There was a 24-43% reduction in heat generation when a 50% fly ash replacement level was used.

6.1.3. Bridge Girders

6.1.3.1. Fresh properties

The PC/PS girders were constructed during July 29th through August 13th 2013 (Table 5.10). Fresh properties, including air content, slump, and temperature were performed prior to each pour of the girders fabricated with conventional concrete. Slump flow, J-Ring and segregation column tests were conducted for the NS-SCC and HS-SCC girders. The fresh properties for the instrumented girders of the three spans are listed in Table 6.10.

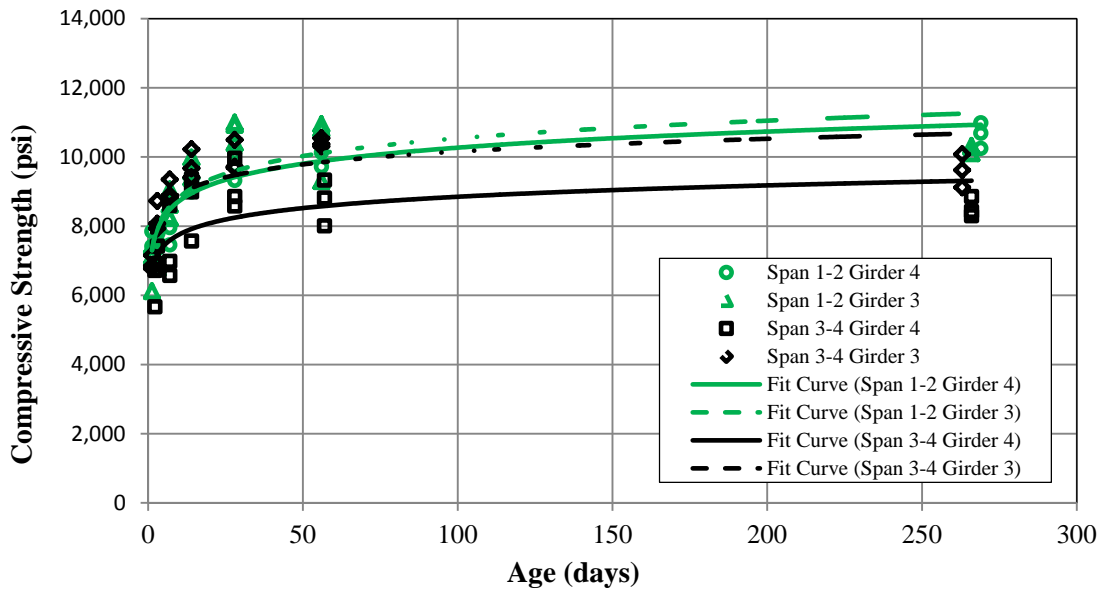
Table 6.10. PC/PS Girders Fresh Properties

	Span 1 Girder 4	Span 1 Girder 3	Span 3 Girder 4	Span 3 Girder 3	Span 2 Girder 4	Span 2 Girder 3	
Air Temp. (°F/°C)	71/22	71/22	78/26	74/23	76/24	78/26	
Concrete Temp. (°F/°C)	72/22	72/22	83/28	81/27	83/28	84/29	
Slump (in.)	9	9	N/A	N/A	N/A	N/A	
Air Content (%)	6.9	6.9	8.3	5.4	8.3	7.9	
Slump Flow (in.)	N/A	N/A	27	25	23	27	
J-Ring (in.)	N/A	N/A	25	24	24	26.5	
Segregation Column	Top (lb.)	N/A	N/A	7.70	-	8.85	-
	Bottom (lb.)			7.49	-	8.90	-
	S (%)			0.00	-	0.56	-

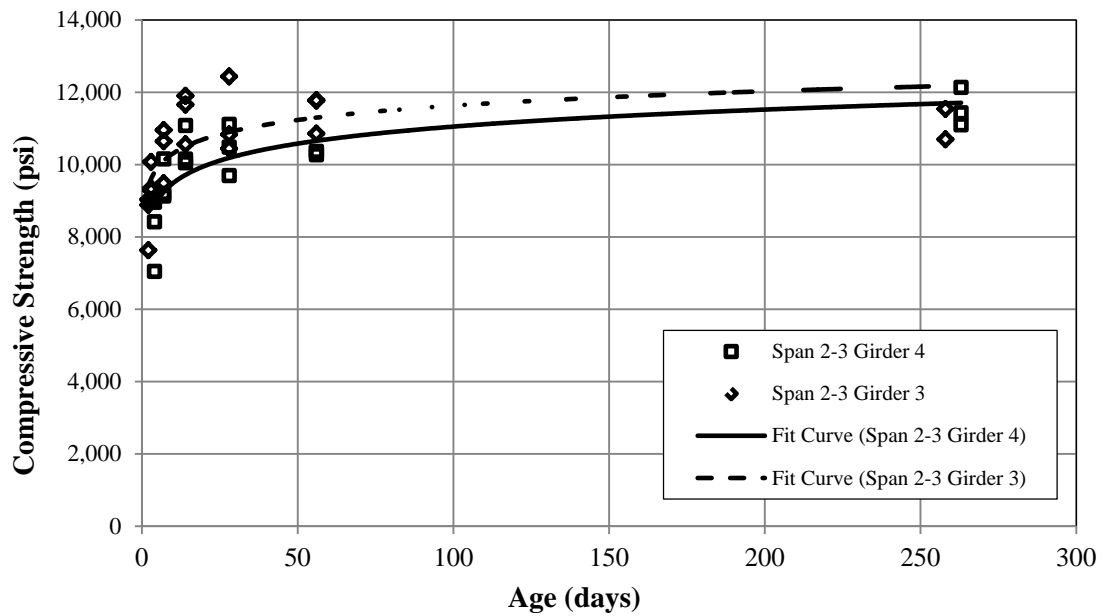
Conversions: 1 in. = 25.4 mm, 1 lb. = 0.4536 kg

6.1.3.2. Compressive strength.

The development of the compressive strength through time is displayed in Figure 6.9.



(a) CC vs. NS-SCC PC/PS Girders



(b) CC vs. HS-SCC PC/PS Girders

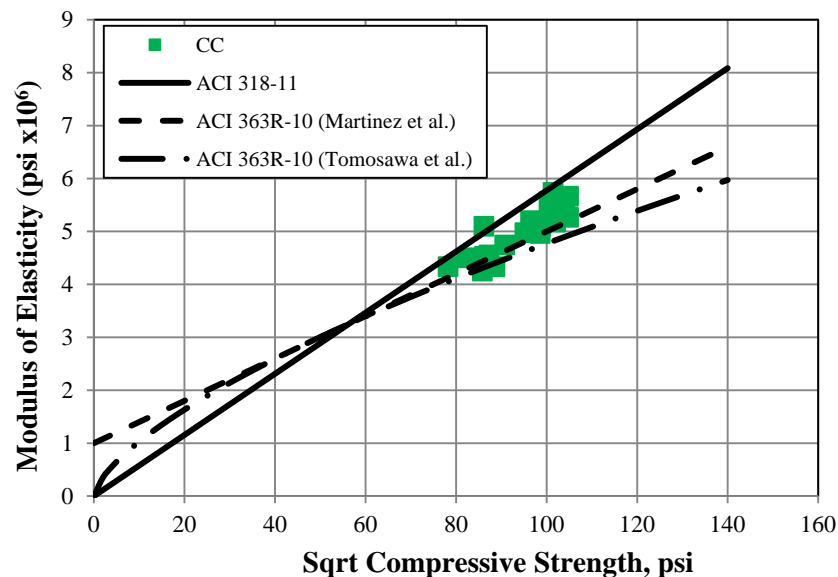
Conversion: 1000 psi = 6.895 MPa

Figure 6.9. PC/PS Girders Compressive Strength vs. Age

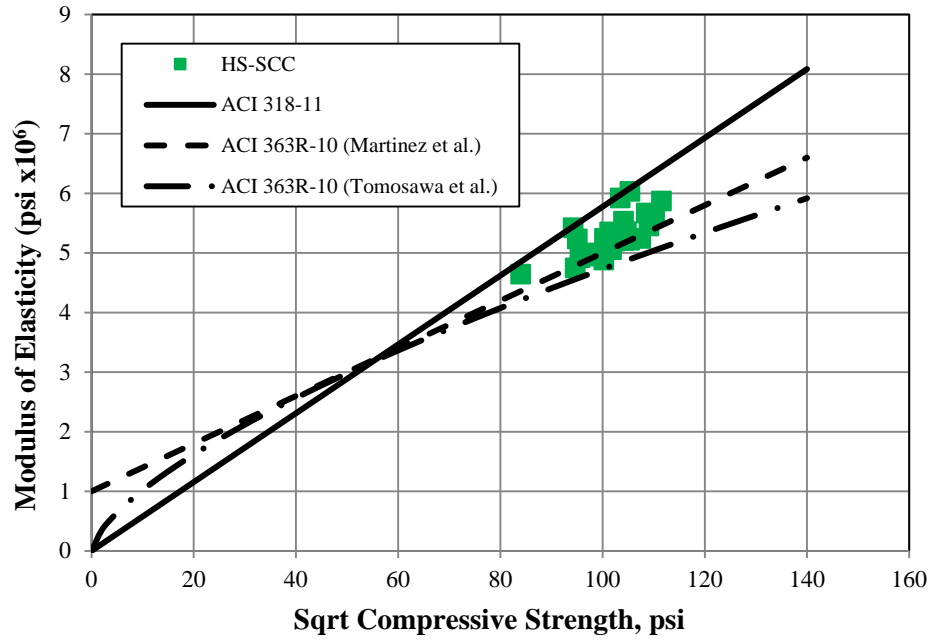
Spans 1-2 (CC) and 3-4 (NS-SCC) girders had a 28-day specified compressive strength of 8,000 psi (55.2 MPa) while Span 2-3's design compressive strength was 10,000 psi (68.9 MPa). Trendlines were plotted for the tested data of each pour. Figure 6.9(a) presents a strength development comparison of the girders in span 1-2 (CC) and span 3-4 (NS-SCC). In both cases the compressive strength developed at 28 days was higher than the design compressive strength. Figure 6.9(b) displays the compressive strength development in the case of the girders of span 2-3 (HS-SCC). At 28 days, the HS-SCC girders reached a higher compressive strength than the specified compressive strength.

6.1.3.3. Modulus of elasticity.

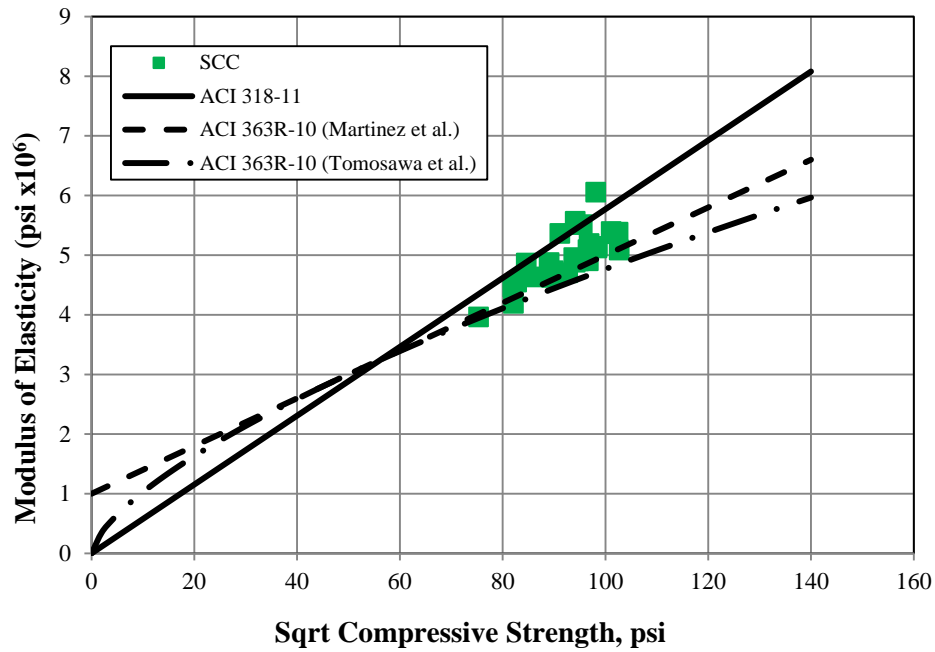
The modulus of elasticity data was plotted against the square root of compressive strength shown in Figure 6.10. The data was compared to ACI 318-11 according to Equation (6.1), and ACI 363R-10 [Equations (6.3) and (6.4)] estimates. Similar trends are observed when the three different concrete mixes used are compared. The ACI 363R-10 model proposed by Martinez et al. (1982) provides an accurate estimate for the MOE of the three mixes employed to fabricate the girders, while the Tomosawa et al. (1993) equation of ACI 363R-10 is a lower bound predictor. The ACI 318-11 equation in the majority of the tests conducted overestimates the modulus of elasticity.



(a) Span 1-2 Girders (Conventional Concrete)



(b) Span 2-3 Girders (High-Strength Self-Consolidating Concrete)



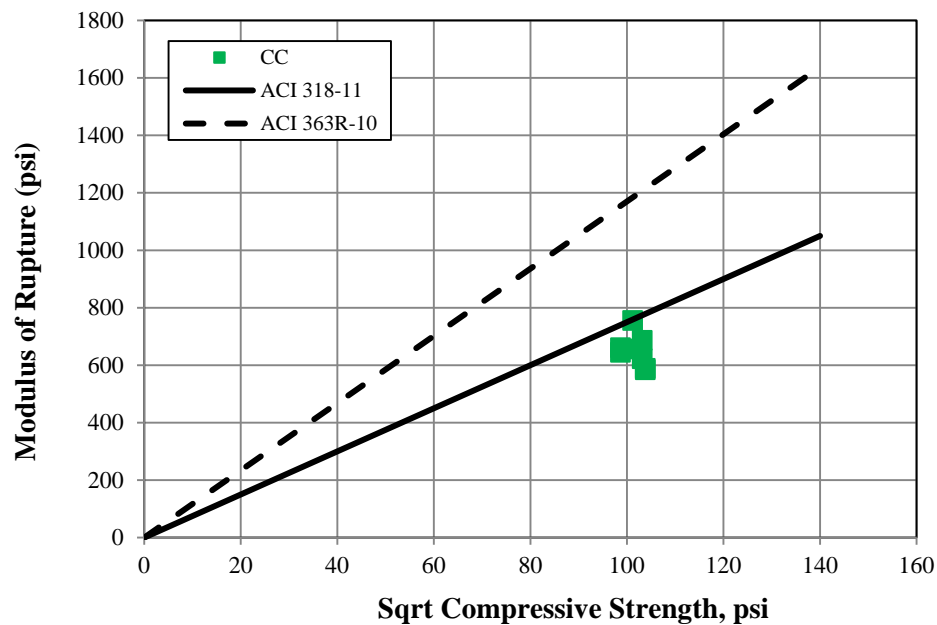
(c) Span 3-4 (Self-Consolidating Concrete)

Conversion: 1000 psi = 6.895 MPa

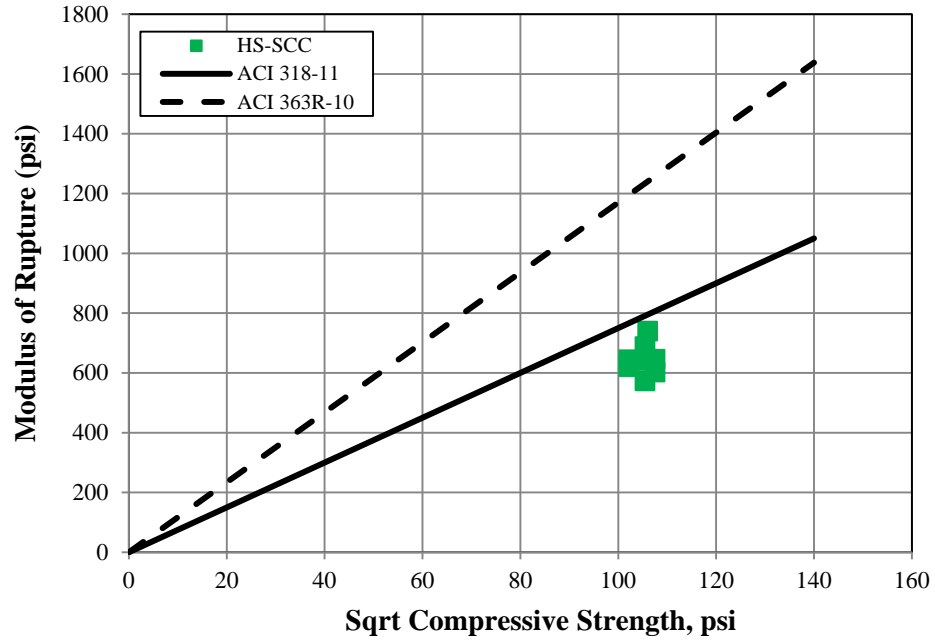
Figure 6.10. PC/PS Girders Modulus of Elasticity vs. Compressive Strength

6.1.3.4. Modulus of rupture.

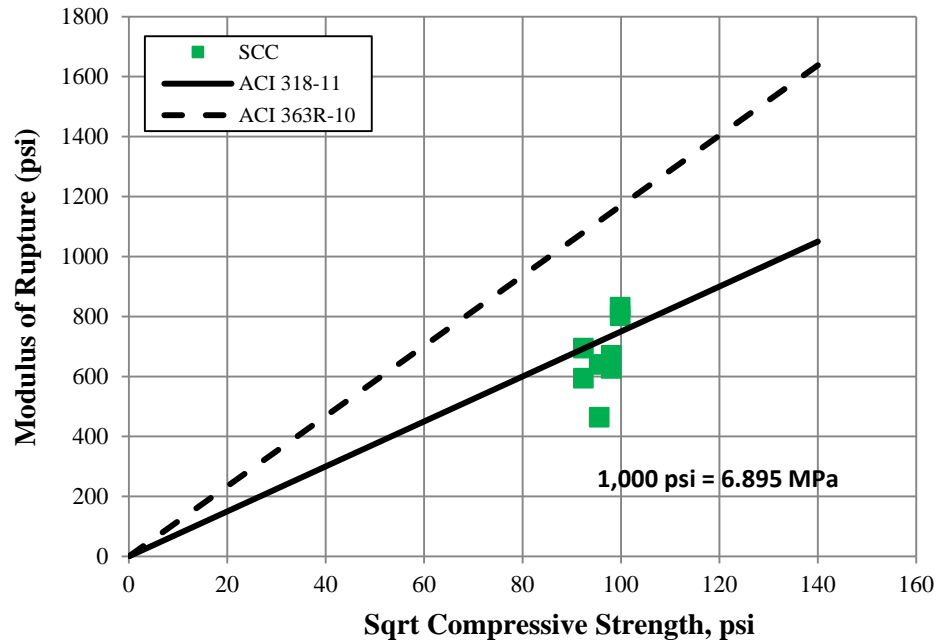
For each span, two tests per girder (girders 3 and 4) were conducted at 28 days and on the same day when the first live load test was conducted on the bridge. Figure 6.11 presents the modulus of rupture versus the square root of compressive strength for the 8 tests run per mix. Despite the validity of the ACI 318-11 empirical model for concrete strengths up to approximately 8,000 psi (55.2 MPa), it appropriately estimates the MOR for the three mixes used. The HSC model in ACI 363R-10 significantly overestimates the MOR. The reduction of the MOR, compared to the ACI 363R-10 model, in the case of the girders fabricated with HS-SCC is associated to the smaller volume of coarse aggregate used in the mix.



(a) Span 1-2 Girders (Conventional Concrete)



(b) Span 2-3 Girders (High-Strength Self-Consolidating Concrete)



(c) Span 3-4 (Self-Consolidating Concrete)

Conversion: 1000 psi = 6.895 MPa

Figure 6.11. PC/PS Girders Modulus of Rupture vs. Compressive Strength

6.1.3.5. Coefficient of thermal expansion.

The coefficient of thermal expansion (CTE) is defined as the rate at which concrete contracts or expands with temperature changes. The CTE gives the amount of strain variation within a structure that occurs from changes in temperature. Since coarse aggregate makes up the bulk of concrete, the coarse aggregate's CTE is the most influential factor in concrete's CTE, as well as quantity of aggregate in the mix. The CTE was obtained for one specimen of each mixture. As it is shown in Table 6.11 and Figure 6.12, the CC exhibited a reduced thermal change compared to the other mixtures due to the quantity of coarse aggregate in the mix.

Table 6.11. Measured Coefficient of Thermal Expansion

Mixture	Placement Date	Coefficient of Thermal Expansion	
		$\mu\epsilon/^{\circ}\text{F}$	$\mu\epsilon/^{\circ}\text{C}$
CC (Span 1-2)	7/29/2013	4.97	8.94
HS-SCC (Span 2-3)	8/13/2013	5.51	9.91
NS-SCC (Span 3-4)	8/6/2013	6.28	11.3

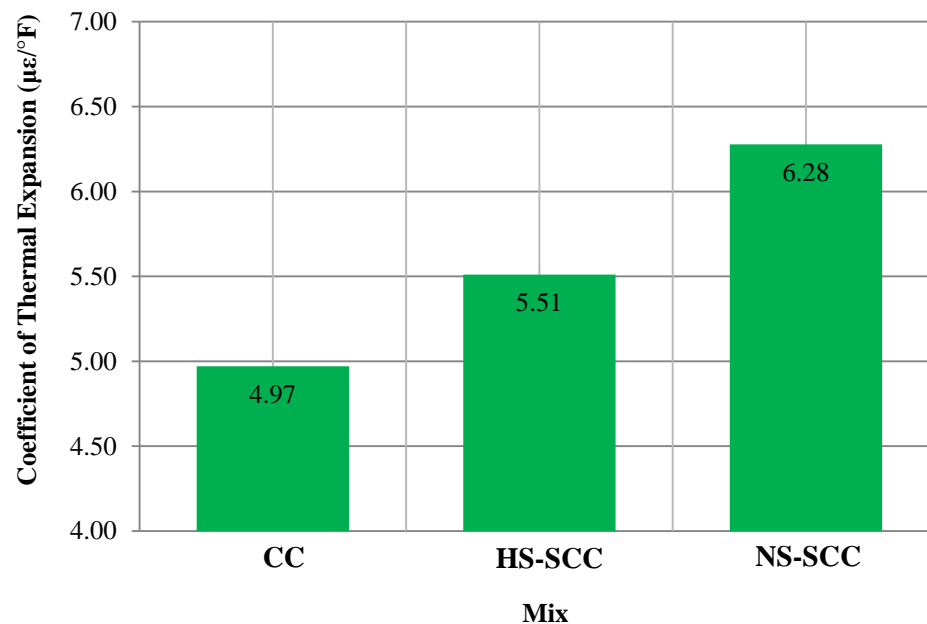


Figure 6.12. Coefficient of Thermal Expansion

6.1.3.6. Creep.

ACI 209 (2005) defines creep as the time dependent increase in strain under a sustained constant load that takes place after the initial strain at loading. In case of concrete, the constant stress is due to the prestress force, self-weight, and superimposed dead loads. Table 6.12 summarizes the loads applied to the creep specimens.

Table 6.13 provides the results that include creep strain, creep coefficient, and specific creep.

Table 6.12. Creep Test Summary

Mixture	Casting Date	Curing Type	Design Compressive Strength (ksi)	Loading Force (kip)	Stress Level (ksi)
CC (Span 1-2)	7/29/2013	Steam Curing	8	20	3.2
HS-SCC (Span 2-3)	8/13/2013	Steam Curing	10	25	4
NS-SCC (Span 3-4)	8/6/2013	Steam Curing	8	20	3.2

Conversions: 1 ksi = 6.89476 MPa, 1 kip = 4.4482 kN

The data presented in Table 6.14 show that the HS-SCC underwent a greater amount of creep than NS-SCC and CC. This is due to the fact that its ratio of sand to total aggregate content is greater than the ratio present in both of NS-SCC and CC. In other words, the percentage of coarse aggregate in HS-SCC is less than in NS-SCC and CC.

The values of HS-SCC, NS-SCC, and CC were compared to empirical models. The models implemented were AASHTO LRFD (2007), ACI 209 (1997), and a method recommended by NCHRP 628 for determining the creep of self-consolidating concrete. The AASHTO LRFD (2007) model for determining creep of CC was updated by NCHRP 426 (Tadros et al. 2003). The empirical model is presented in Equations (6.9) through (6.13) below.

Table 6.13. Creep Results.

Creep Strain (microstrain)				
Mixture	Days After Loading			
	3	28	56	120
CC	87.944	106.944	116.088	125.76
HS-SCC	126.505	160.62	169.75	192.2
NS-SCC	88.337	104.372	114.644	119.46
Percentage of 120 Day Creep				
CC	69.99	84.79	92.3	100
HS-SCC	65.78	83.52	88.27	100
NS-SCC	73.73	87.11	95.69	100
Measured Creep Coefficient				
CC	1.08	1.31	1.43	1.55
HS-SCC	1.11	1.40	1.48	1.68
NS-SCC	1.10	1.30	1.43	1.49
Specific Creep ($\mu\epsilon/\text{psi}$)				
CC	0.03	0.035	0.0375	0.04
HS-SCC	0.032	0.040	0.043	0.048
NS-SCC	0.028	0.034	0.037	0.039

$$\psi(t, t_i) = 1.9k_s k_{hc} k_f k_{td} t_i^{-0.118} \times A \quad (6.9)$$

$$k_s = 1.45 - 0.13 \left(\frac{V}{S} \right) \geq 0.0 \quad (6.10)$$

$$k_{hc} = 1.56 - 0.008H \quad (6.11)$$

$$k_f = \frac{5}{1 + f'_{ci}} \quad (6.12)$$

$$k_{td} = \left(\frac{t}{61 - 4f'_{ci}} \right) \quad (6.13)$$

Where:

$\psi(t,t_i)$: creep coefficient

ks: factor for volume to surface ratio of the specimen

k_{hc}: factor for humidity for creep

k_f: factor for the concrete strength

k_{td}: factor for time development

V/S: volume to surface ratio(in.)

H: relative humidity (%)

f'ci: compressive strength at release (psi)

t_i: age (days) in which the load is applied

t: concrete maturity age (days)

The ACI 209 (2008) model developed for conventional concrete creep is shown in Equations (6.14) through (6.22) below.

$$\nu_u = 2.35\gamma_c \quad (6.14)$$

$$\gamma_{cr} = \gamma_{la}\gamma_{\lambda}\gamma_{v/s}\gamma_s\gamma_{\psi}\gamma_{\alpha} \quad (6.15)$$

$$\gamma_{la} = 1.25(t_{la})^{-0.118} \quad (6.16)$$

$$\gamma_{la} = 1.13(t_{la})^{-0.094} \quad (6.17)$$

$$\gamma_{\lambda} = 1.27 - 0.0067\lambda \quad (6.18)$$

$$\gamma_{v/s} = 2/3(1 + 1.13e^{-0.54(\frac{v}{s})}) \quad (6.19)$$

$$\gamma_s = 0.82 + 0.067s \quad (6.20)$$

$$\gamma_{\psi} = 0.88 + 0.0024\psi \quad (6.21)$$

$$\gamma_{\alpha} = 0.46 + 0.09\alpha \leq 1.0 \quad (6.22)$$

Where:

γ_{la} : correction factor for the age of loading

γ_{λ} : correction factor for ambient relative humidity

$\gamma_{v/s}$: correction factor for the volume to surface ratio

γ_s : correction factor for the slump

γ_{ψ} : correction factor for fine aggregate percentage

γ_{α} : correction factor for air content

t_{la} : concrete age at loading (days)

λ : ambient relative humidity (%)

V/S: volume to surface ratio (in.)

s: slump (in.)

ψ : ratio of fine aggregate to total aggregate by weight (%)

α : air content (%)

NCHRP 628 (Khayat and Mitchell 2009) developed a modified expression for AASHTO LRFD (2007) to determine the creep of SCC. This expression is presented in Equations (6.23) through (6.27). The expression utilizes the same variables as the AASHTO LRFD expression except A is a factor for the cement type; A is 1.19 for Type I/II cement and 1.35 for Type III with 20% fly ash binder. In addition, all variables in this method are in the metric (SI) system; therefore, V/S is in mm and f'_{ci} is in MPa.

$$\psi(t, t_i) = 1.9k_s k_{hc} k_f k_{td} t_i^{-0.118} \times A \quad (6.23)$$

$$k_s = 1.45 - 0.13 \left(\frac{V}{S} \right) \geq 0.0 \quad (6.24)$$

$$k_{hc} = 1.56 - 0.008H \quad (6.25)$$

$$k_f = \frac{35}{7 + f'_{ci}} \quad (6.26)$$

$$k_{td} = \left(\frac{t}{61 - 0.58f'_{ci} + t} \right) \quad (6.27)$$

Table 6.14 shows the measured to theoretical creep values for CC, HS-SCC, and NS-SCC. As can be concluded from the table, CC, HS-SCC, and NS-SCC measured creep coefficients at 120 days were lower than the predicted values using AASHTO (2007), higher than values determined by ACI 209 model, and lower than predicted values obtained by NCHRP 628.

Table 6.14. Measured & Predicted Creep Coefficient at 120 days

Material	CC	HS-SCC	NS-SCC
Measured	1.55	1.68	1.49
AASHTO LRFD 2007	1.88	1.8	1.95
ACI 209-08	0.73	0.82	0.73
NCHRP 628	2.06	1.97	2.14

6.1.3.7. Shrinkage

The shrinkage of concrete is the decrease in volume of hardened concrete with time which includes drying shrinkage, autogenous shrinkage, and carbonation. The shrinkage monitored by the specimens was drying shrinkage. Drying shrinkage is unrelated to load application or thermal effects. The amount of water contained in most concrete mixes is more than is needed for the complete hydration of the cementitious materials. This excess water leaches to the surface and evaporates as a function of time. As the excess water makes it to the surface and evaporates the concrete structure is reduced in volume. The rate of volume reduction occurs initially at a high rate and later diminishes with time. This is due to both the lack of excess water and increase in stiffness as the concrete cures. The results for the drying shrinkage data are presented in Table 6.15 through Table 6.17. Furthermore, the empirical results derived from shrinkage equations recommended by AASHTO (2007), ACI 209R (2008), and NCHRP Report 628 developed by Khayat and Mitchell (2009) for modifications to the AASHTO LRFD (2004) for SCC are documented within the tables.

The AASHTO LRFD (2007) developed for HSC by Tadros et al. (2003). The empirical model is presented in Equation (6.28) through (6.32).

$$\varepsilon_{sh} = k_s k_{hs} k_f k_{td} 0.48 \times 10^{-3} \quad (6.28)$$

$$k_s = \left[\frac{\frac{t}{26e^{0.36\left(\frac{V}{S}\right)} + t}}{\frac{t}{45 + t}} \right] \left[\frac{1064 - 94\left(\frac{V}{S}\right)}{923} \right], \quad \frac{V}{S} \leq 6.0 \text{ in} \quad (6.29)$$

$$k_{hs} = 2 - 0.014H \quad (6.30)$$

$$k_f = \frac{5}{1 + f'_{ci}} \quad (6.31)$$

$$k_{td} = \left(\frac{t}{61 - 4f'_{ci}} \right) \quad (6.32)$$

Where:

ε_{sh} : drying shrinkage

k_s : factor for volume-to-surface ratio of the specimen for shrinkage

k_{hs} : factor for humidity for shrinkage

k_f : factor for the concrete strength

k_{td} : factor for time development

V/S : volume to surface ratio (in.)

H : relative humidity (%)

f'_{ci} : compressive strength at release (psi)

t : concrete maturity age (days)

The ACI 209 (1997) model developed for conventional concrete shrinkage is displayed in Equations (6.33) through (6.42).

$$(\varepsilon_{sh})_u = 780\gamma_{sh} \times 10^{-6} \quad (6.33)$$

$$\gamma_{sh} = \gamma_\lambda \gamma_{V/S} \gamma_S \gamma_\psi \gamma_c \gamma_\alpha \quad (6.34)$$

$$\gamma_{\lambda} = 1.4 - 0.0102\lambda \text{ for } 40 \leq \lambda \leq 80 \quad (6.35)$$

$$\gamma_{\lambda} = 3 - 0.030\lambda \text{ for } 80 \leq \lambda \leq 100 \quad (6.36)$$

$$\gamma_{\frac{V}{S}} = 1.2e^{-\frac{0.12V}{S}} \quad (6.37)$$

$$\gamma_S = 0.89 + 0.041s \quad (6.38)$$

$$\gamma_c = 0.75 + 0.00036c \quad (6.39)$$

$$\gamma_{\psi} = 0.3 + 0.014\psi \text{ for } \psi \leq 50\% \quad (6.40)$$

$$\gamma_{\psi} = 0.9 + 0.002\psi \text{ for } \psi > 50\% \quad (6.41)$$

$$\gamma_{\alpha} = 0.95 + 0.008\alpha \text{ for } \alpha \leq 1.0 \quad (6.42)$$

Where:

γ_{λ} : correction factor for ambient relative humidity

$\gamma_{V/S}$: correction factor for the volume to surface ratio

γ_s : correction factor for the slump

γ_{cc} : correction factor for cement content

γ_ψ : correction factor for fine aggregate percentage

γ_a : correction factor for air content.

λ : ambient relative humidity (%).

V/S : volume to surface ratio (in.)

s : slump (in.)

ψ : ratio of fine aggregate to total aggregate by weight (%)

c : cement content (lbs/ft³)

α : air content (%)

NCHRP 628 (Khayat and Mitchell 2009) developed a modified expression for AASHTO LRFD (2004) model to determine the shrinkage of SCC. This expression is presented in Equations (6.43) through (6.45). The expression utilizes the same variables as the AASHTO LRFD expression, except A is a factor for the cement type. A is 0.918 for Type I/II cement and 1.065 for Type III with 20% fly ash binder. In addition, all variables in this method are in the metric (SI) system; therefore, V/S is in mm.

$$\varepsilon_{sh} = k_s k_{hs} \left(\frac{t}{55 + t} \right) 0.56 \times 10^{-3} \times A \quad (6.43)$$

(Steamed cured)

$$k_s = \left[\frac{\frac{t}{26e^{0.0142\left(\frac{V}{S}\right)} + t}}{\frac{t}{45 + t}} \right] \left[\frac{1064 - 3.7\left(\frac{V}{S}\right)}{923} \right], \quad \frac{V}{S} \leq 6.0 \text{ in} \quad (6.44)$$

$$k_{hs} = 2 - 0.014H \quad (6.45)$$

Table 6.15 through Table 6.17 summarize the measured shrinkage strain at different days compared to prediction models.

Table 6.15. CC Shrinkage Strain

Method	Shrinkage Strain ($\mu\epsilon$)				
	7 days	14 days	28 days	56 days	180 days
Measured Shrinkage Strain	-136	-165	-165	-166	-175.5
AASHTO 2007	-85	-140	-206	-269	-339
NCHRP Report 628	-94	-164	-265.5	-383.5	-555
ACI 209R-08	-134	-229.8	-357	-495	-673

Table 6.16. HS-SCC Shrinkage Strain

Method	Shrinkage Strain ($\mu\epsilon$)				
	7 days	14 days	28 days	56 days	180 days
Measured Shrinkage Strain	-144	-166.5	-187	-198	-201.56
AASHTO 2007	-85	-138	-199	-254.6	-312.7
NCHRP Report 628	-82	-147	-244.5	-365.6	-555
ACI 209R-08	-137.7	-236	-367	-508	-691

Table 6.17. NS-SCC Shrinkage Strain

Method	Shrinkage Strain ($\mu\epsilon$)				
	7 days	14 days	28 days	56 days	180 days
Measured Shrinkage Strain	-138.5	-139	-143	-159	-180
AASHTO 2007	-86	-143	-214	-284	-364
NCHRP Report 628	-82	-147	-244.5	-365	-555
ACI 209R-08	-132	-225.8	-351	-486	-661

As can be seen from Tables 6-15 through 6-17, AASHTO 2007 provides a closer estimate for CC, HS-SCC, and NS-SCC after 28 days. NCHRP 628 and ACI 209 overestimate the amount of shrinkage strain after 28 days.

6.1.4. NASP Pullout Tests

The NASP test aims to assess the bonding abilities of seven wire prestressing strands in concrete. The pullout specimens were fabricated with the concrete mixes employed to cast the PC girders of spans 1-2 (CC) and 3-4 (NS-SCC) of Bridge A7957. Table 6.18 summarizes the NASP test results. There was little difference in bond performance between NS-SCC and CC at 0.001 in (0.025 mm) of strand slip. However, CC exhibits higher bond performance than NS-SCC at 0.1 in (2.54 mm) of strand slip. Since the loads had been normalized with respect to concrete strength, this difference is most likely due to other factors, such as a higher fine aggregate content in the NS-SCC mix than CC. In addition, that might have caused a less adhesion between the strand and concrete which leads to a lower slip load.

Table 6.18. Concrete NASP Results

Mix	Day	Specimen ID	$\sqrt{f_c}$ ($\sqrt{\text{psi}}$)	Load/ $\sqrt{f_c}$ at Slip of 0.001 in				Load/ $\sqrt{f_c}$ at Slip of 0.1 in			
				Load/ $\sqrt{f_c}$ (lb./ $\sqrt{\text{psi}}$)	Average (lb./ $\sqrt{\text{psi}}$)	Std. Dev. (lb./ $\sqrt{\text{psi}}$)	COV.	Load/ $\sqrt{f_c}$ (lb./ $\sqrt{\text{psi}}$)	Average (lb./ $\sqrt{\text{psi}}$)	Std. Dev. (lb./ $\sqrt{\text{psi}}$)	COV.
NS-SCC	28 days	SCC-1	104.96	82.9	93.14	18	19%	131.74	122.59	9	7%
		SCC-2		77.9				110.44			
		SCC-3		118.6				125.59			
CC	28 days	A-1-1	105.35	75.74	90.73	17	19%	152.72	151.14	6	4%
		A-1-2		81.61				157.12			
		A-1-3		114.85				143.59			

Conversion: 1 lb. = 4.45 N, 1 in. = 25.4 mm

6.1.5. Deck

6.1.5.1. Fresh properties

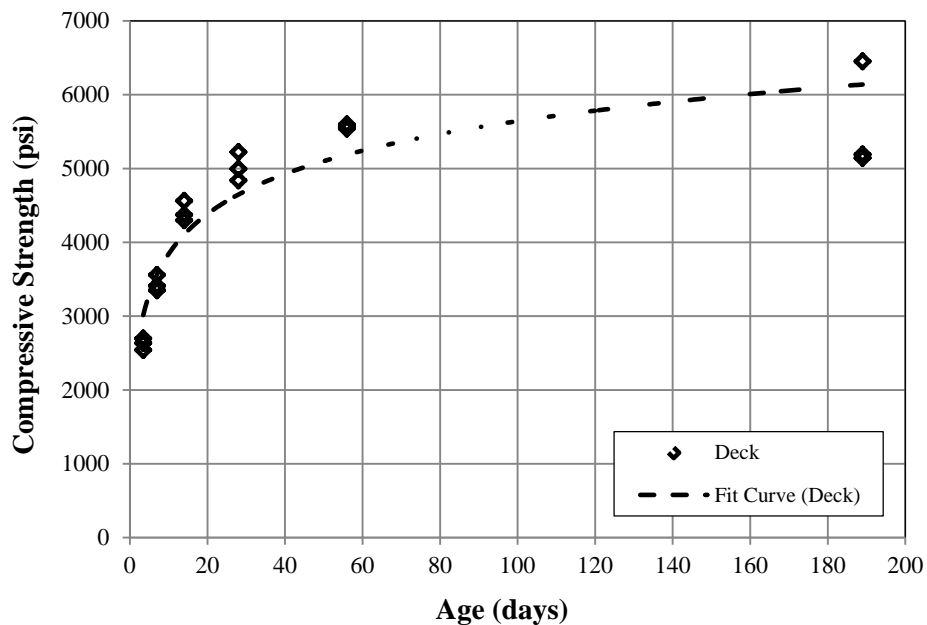
The CIP RC deck was cast on October 21st 2013 (Section 5.5.2). Fresh properties, recorded for batches 1 through 3, are presented in Table 6.19.

Table 6.19. Modified B-2 Concrete Mix Fresh Properties

	Batch 1	Batch 2	Batch 3
Air Temp. (°F/°C)	49/9	49/9	50/10
Concrete Temp. (°F/°C)	62/17	64/18	63/17
Slump (in.)	6.0	5.5	5.75
Air Content (%)	7.0	6.2	8.3

Conversions: 1 in. = 25.4 mm

6.1.5.2. Compressive strength



Conversion: 1000 psi = 6.895 MPa

Figure 6.13. Deck Compressive Strength vs. Age

Compressive strength tests were conducted at 3, 7, 14, 28, 56 days, and when the first live load test was executed. The compressive strength is plotted in Figure 6.13. The results obtained after 14 days exceeded the target strength of 4,000 psi (27.6 MPa) specified by MoDOT.

6.1.5.3. Abrasion resistance

The abrasion resistance results are illustrated in Figure 6.14 and Figure 6.15. The results obtained are consistent with trends found in previous studies. Figure 6.16 shows the specimen after the abrasion test.

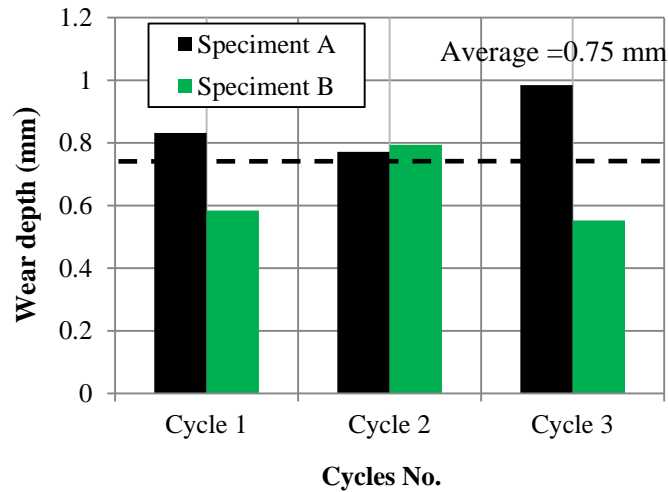


Figure 6.14. Depth of Wear Results

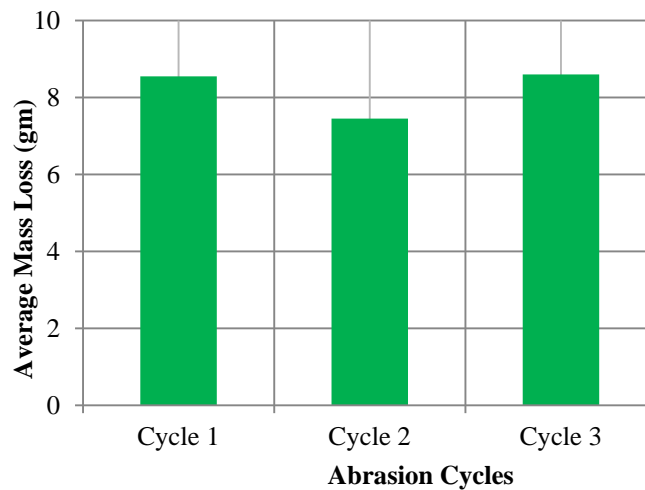


Figure 6.15. Average Mass Loss Results

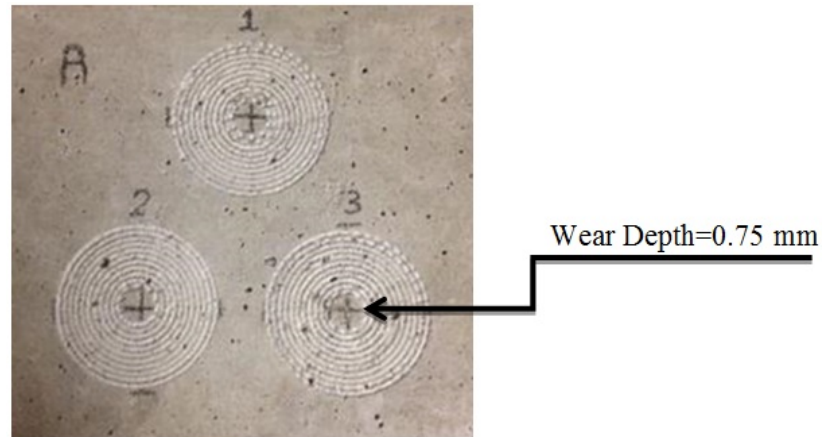


Figure 6.16. Specimen after Abrasion Test

6.1.5.4. Freeze and Thaw Resistance

The freeze-thaw resistance was investigated for deck concrete. The test results for each specimen are presented in Table 6.20 which illustrates the durability factor for every beam for the test specimens.

Table 6.20. Freeze and Thaw Results

Beam No.	Casting Date	Durability Factor
1	10/21/2013	84.6
2	10/21/2013	88.4
3	10/21/2013	87.9
Average		87.0

6.1.5.5. Ponding Test

The ponding test was performed in accordance with ASTM C 1543-10, (Standard Test Method for Determining the Penetration of Chloride Ion into Concrete by Ponding). The test results are shown in Figure 6.17. Using the scale set forth by Broomfield in 2007 (Table 3.6) the concrete of the deck were assigned corrosion risk based on the data collected in the chloride analysis as can be seen in Table 6.21. It may be observed that the chloride percentage by weight at 2.0 in. (50.8 mm) is negligible.

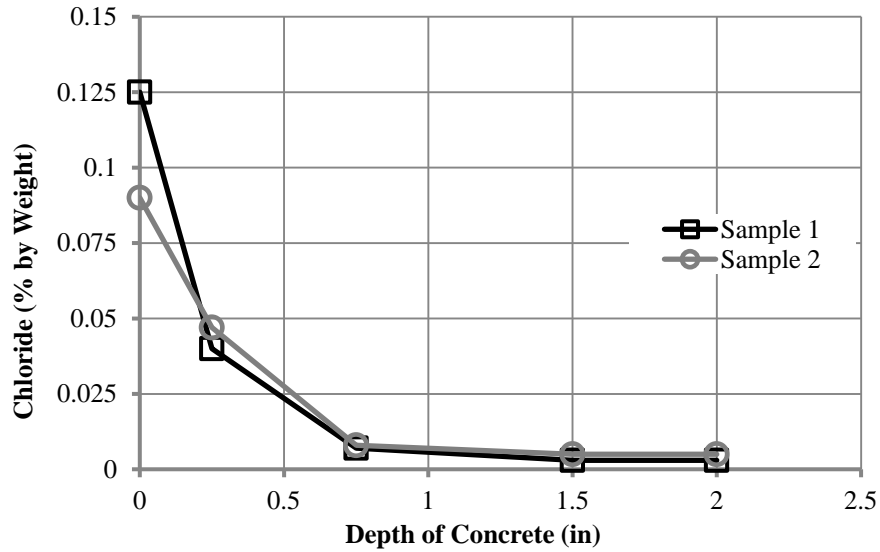


Figure 6.17 Chloride Concentration Profile

Table 6.21 Average Chloride Content at Specific Depths

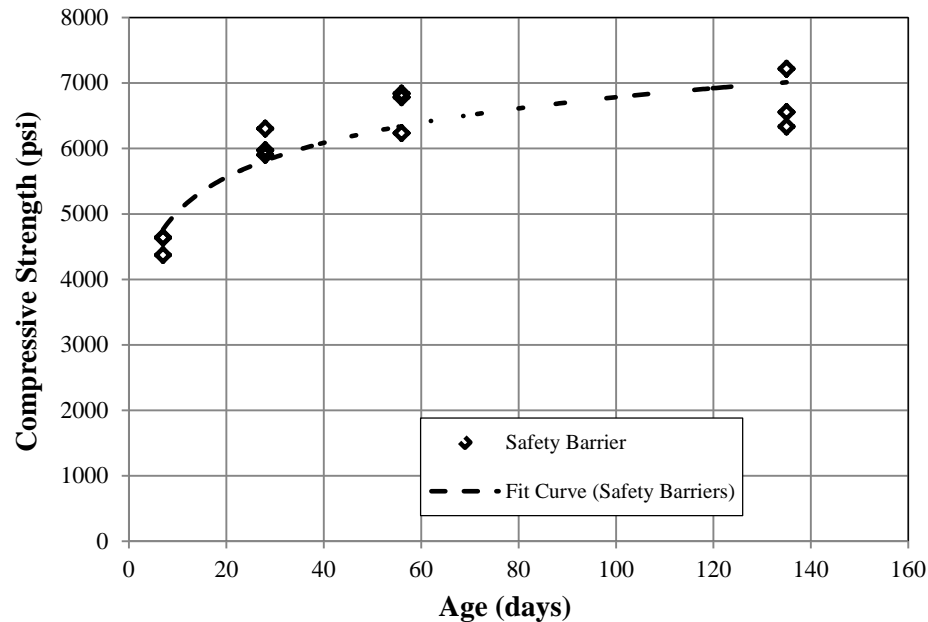
Depth (in)	Average Chloride Content (%)	Corrosion Risk
Surface	0.1075	Moderate
0.25	0.0435	Low
0.75	0.0075	Negligible
1.5	0.004	Negligible
2	0.004	Negligible

6.1.6. Safety Barriers

6.1.6.1. Compressive strength.

The safety barriers were cast on December 19th, 2013 (Section 5.5.4). Fresh properties were not recorded by the researchers. Compressive strength tests were executed at 7, 28, 56 days and when live load test 1 was conducted. The compressive strength against age is presented in Figure 6.18. The results obtained after 7 days

exceeded the design strength of 4,000 psi (27.6 MPa) specified by MoDOT (Class B-2 mix).



Conversion: 1000 psi = 6.895 MPa

Figure 6.18. Deck Compressive Strength vs. Age

6.2. SUMMARY AND CONCLUSIONS

6.2.1. Trial Mixes

The following conclusions were reached from the HVFAC, HS-SCC, and NS-SCC trial mixes:

- The modulus of elasticity of the HS-SCC trial mix closely matches the Martinez et al. equation of ACI 363R 2010 while the equation suggested by Tomosawa et al. in ACI 363R 2010 provides a lower bound estimate. The ACI 318 2011 equation overestimated the modulus of elasticity.
- The splitting tensile strength of the HS-SCC mix was overestimated by both the ACI 318 2011 and ACI 363R 2010 prediction equations. Post-test cross section images revealed that the aggregate failed before the interfacial bond zone between the paste and aggregate.

- The modulus of elasticity of the 8,000 psi (55.2 MPa) NS-SCC trial mix was accurately estimated by both the Tomosawa et al. and Martinez et al. prediction equations in ACI 363R 2010. Both of these curves intersected at roughly 8,000 psi.
- The ACI 318 2011 equation for the splitting tensile strength provides the best prediction for NS-SCC, while the ACI 363R 2010 equation overestimated the STS.

6.2.2. Intermediate Bents (HVFAC)

The following observations were documented regarding the HVFAC with 50% fly ash replacement:

- Raising the level of replacement fly ash from 20% to 50% reduced the heat generated by 24-43%.
- There was a negligible difference in the setting time of the HVFAC versus the CC mix with 20% fly ash replacement.
- There were mixed results when analyzing the time to reach the peak hydration temperature between the CC (Class B mix) and HVFAC.

6.2.3. Implementation Program

- The first full-scale structure implementation of high-strength self-consolidating concrete (HS-SCC) and high volume fly ash concrete (HVFAC) has been executed on the structure of Bridge A7957 through the Missouri Department of Transportation (MoDOT).
- High volume fly ash concrete, a sustainable material, at a 50% replacement level was used within one of the interior supports of this bridge. Coupled with the use of SCC, Bridge A7957 is expected to have a longer service life than traditional reinforced concrete structures.
- The instrumentation phase of the project has been effectively accomplished. Currently, maturity studies are being conducted on the different concrete mixes employed in the bridge to compare the differences among the development of

mechanical properties including: creep, shrinkage, thermal gradients, time dependent behavior and serviceability in the long-term.

- A series of live load tests have been conducted to establish a benchmark that will be used to monitor any change in the structure's response and to help validate design assumptions.

7. PRESTRESS LOSSES

7.1. INTRODUCTION

7.1.1. General

The prestress losses are the losses that occur in the tensile stress of prestress steel. These losses affect a prestressed section's performance. The tensile force in the tendon does not remain constant from the recorded value in the jacking gauge. It changes with time. These losses are classified into two categories: immediate and either long-term or time-dependent. Immediate losses take place when prestressing the tendon and then transferring the prestress to the concrete member. Both the elastic shortening (ES) and anchorage slip are immediate losses. In contrast, losses produce by creep of the concrete (CR), shrinkage of the concrete (SH), and relaxation of the tendon (RE) are considered time-dependent losses. A simple equation is presented in Equation (7.1) used to determine the total Prestress losses within concrete beam (PCI, 2010).

$$\Delta f_{Total} = \Delta f_{ES} + \Delta f_{SH} + \Delta f_{CR} + \Delta f_{RE} \quad (7.1)$$

Strand relaxation (RE) which is a loss in strand stress, can be computed if the relaxation-time relation is known. This relationship is sometimes supplied by the strand manufacturer. Equation (7.2) is typically used to compute this stress change. (Nawy, 2009). This equation is used in the case of low-relaxation strands.

$$\Delta f_{RE} = f_{jack} \frac{\log_{10} t}{45} \left(\frac{f'_{pi}}{f_{py}} - 0.55 \right) \quad (7.2)$$

The time t is the time, in hours, after initial stressing. The yield stress of the strand, f_{py} , is typically assumed to be 90% of f_{pu} for low-relaxation tendons, 85% of f_{pu} for stress-relieved tendons, and 80% of f_{pu} for prestressing bars (Nawy, 2009). If the pretensioning force is less than $0.55f_{pu}$, no losses due to relaxation will occur. However,

we generally would not design to this pretensioning force level because it is not efficient (Myers and Yang, 2005).

Elastic shortening produces the most significant effect on prestress losses. The concrete undergoes ES when the prestressing force is transferred from the end blocks of the casting bed to the girder after the concrete has sufficiently hardened. The strands are now shortened and the tensile force in the tendons is reduced because the strands are bounded to the concrete. These losses can be a significant portion of the total prestress losses and should be accurately accounted for in the design process. Under-predicting prestress losses can result in cracking at service loads. Over-predicting prestress losses can result in an overly conservative design for service load stresses. Equation (7.3) is utilized to determine the change in stress from elastic shortening. In design it is usually considered sufficient to estimate the elastic shortening loss by using gross section properties. Equation (7.4) can be used to estimate the stress of the concrete at release.

$$\Delta f_{ES,Steel} = n f_{cgs} = \frac{E_p}{E_{ci}} f_{cgs} \quad (7.3)$$

$$f_{cgs} = -\frac{P_0}{A_g} - \frac{P_0 e^2}{I_g} + \frac{M e}{I_g} \quad (7.4)$$

The f_{cgs} is the stress of the concrete at the centroid of the prestress strands, E_p is the modulus of elasticity of the prestressing strand and E_{ci} is the modulus of elasticity of the concrete at release. The P_0 is the estimated force at release. This force is specified differently in different specifications (Myers and Yang, 2005). The A_g and I_g represent the area and moment of inertia of the gross section, respectively. The e is the eccentricity of the strand, and M is any moment applied to the beam.

Finally, prestress losses due creep and shrinkage cause additional losses within the member over time. Creep and shrinkage are one of the critical factors for design of structural members due to the length change over time. Creep of the concrete causes a time-dependent change in strain throughout the depth of the member, where the cross-section is in compression under elastic effects due to application of sustained load, an

additional compressive strain will develop over time. The shortening will decrease the amount of prestressing force applied from the tendons to the concrete. In addition, concrete shrinkage will result in a similar time-dependent compressive strain and also cause a loss of tension in the pretensioning force.

This section presents measurements of prestress loss in the instrumented beams of this research program. Measurements of prestress losses due to elastic shortening at release of pre-tensioned strands are examined and total prestress loss in service is discussed, including time-dependent losses due to creep, shrinkage, and relaxation. Total measured prestress losses are compared to different current code models.

7.1.2. Measurement of Prestress Losses Using Internal Sensors (VWSGs)

VWSGs within each beam were used to measure prestress losses within the girders. These measurements are indirect in the sense that changes in stress were not actually measured. Instead, changes in concrete strain at the centroid of the pre-tensioned strands (c.g.s.) were measured using embedded gauges, and these results were converted to stress losses. To determine the prestress losses, the strain at the level of the c.g.s. of the prestressing steel, ϵ_{cgs} , was determined by interpolating the temperature corrected strain data from the sensors and multiplied by the MOE of the prestressing strands, E_{ps} , this is demonstrated in Equation (7.5). The MOE of pre-tensioned strands was taken as 28,500 ksi (196.5 GPa) in the Equation (7.5).

$$\Delta f_{p, Meas} = E_{ps} \cdot \epsilon_{cgs, meas} \quad (7.5)$$

The Equation (7.5) can be used to measure the losses due to elastic shortening, creep and shrinkage. However, the relaxation losses are not accounted in Equation (7.5) because these losses do not cause a direct change in strain in the concrete at the level of the strand. Therefore, these losses must be added analytically using Equation (7.2) for low relaxation strands. The corrected measured prestress losses are thus given in Equation (7.6).

$$\Delta f_{p, Meas} = E_{ps} \cdot \epsilon_{cgs, meas} + \Delta f_{p, Relaxation} \quad (7.6)$$

7.2. ELASTIC SHORTENING AT RELEASE

7.2.1. Background

Elastic shortening is the change in length of the girder due to applied compressive force of the strand. The forms are stripped and the prestressing strands are released after adequate strength is added to the casting bed. As a result, the concrete and strands shorten under the load. Elastic shortening losses are highly dependent on the modulus elasticity of the strand, the modulus of elasticity of the concrete at release, and the stress applied to concrete beam. (Myers and Block, 2010).

7.2.2. Measurements and Discussion

Concrete strains and temperatures, recorded at the level of the centroid of prestressing strands using VWSGs were used to measure elastic shortening losses. Elastic shortening measurements were determined by comparing strain readings immediately after release to baseline strain measurement recorded just before release (Figure 7.1 and Figure 7.2). Measurements were taken at 5-min intervals during prestress transfer. Readings were recorded by data –acquisition system (DAS).

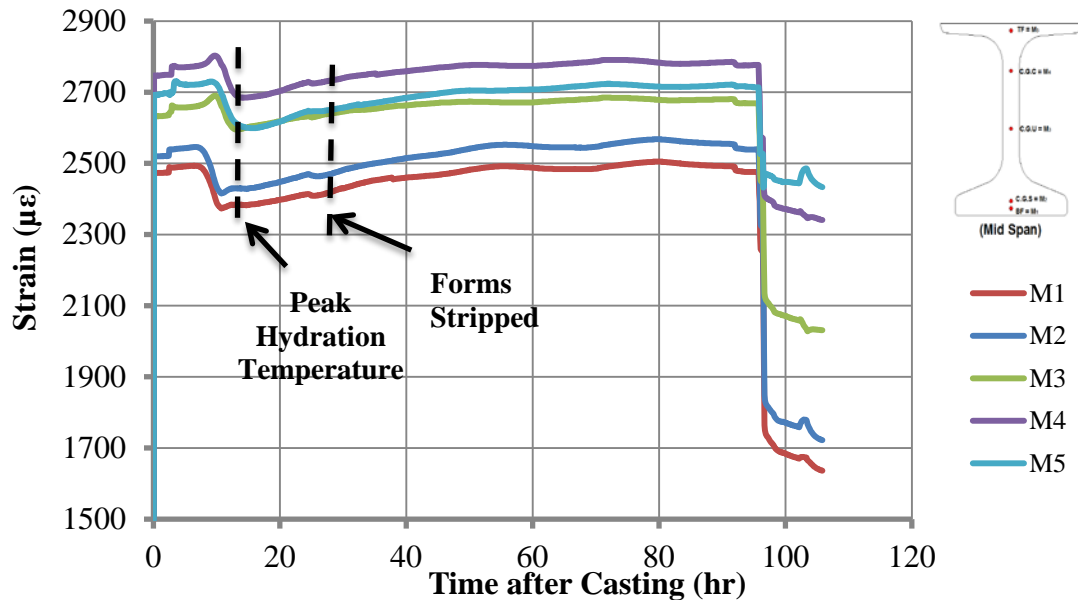


Figure 7.1 Strains at Release

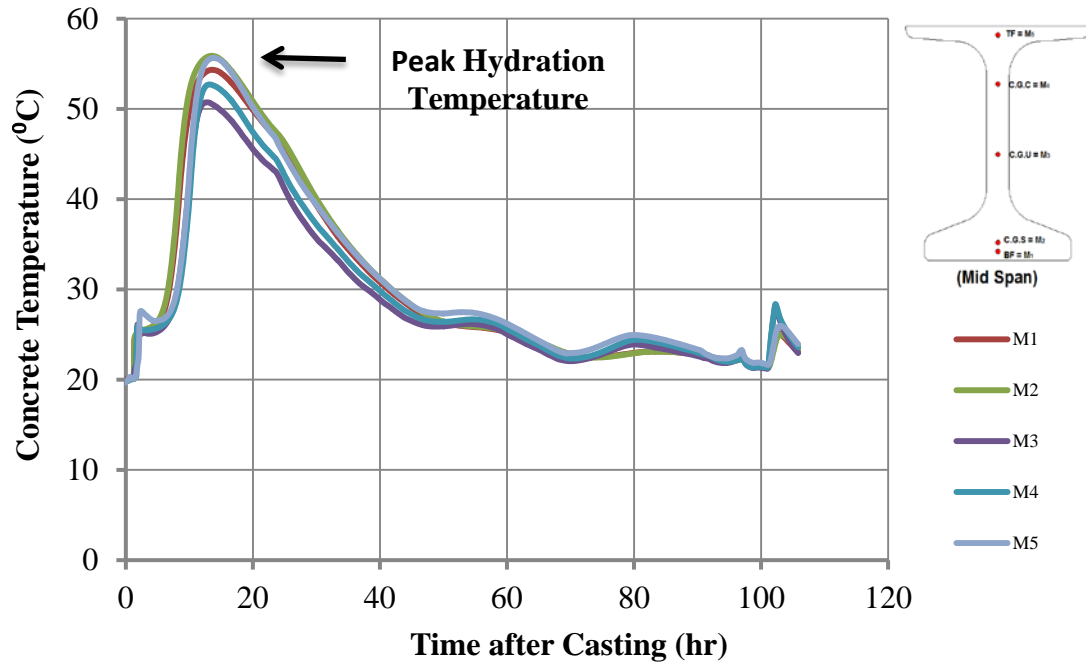


Figure 7.2 Hydration Temperature Before and After Release

Measurements were successfully recorded on five girders, including two HSC girders, two NS-SCC girders, and one HS-SCC girder. One measurement on HS-SCC girder was not successfully recorded because of missing baseline readings before release. The elastic shortening was calculated using Equation (7.5) from the measured strain reading.

The measured elastic shortening values were compared to predicted values specified in AASHTO LRFD (2012) and the PCI Design Handbook (2010) with actual modulus of elasticity measured on companion specimens and approximate modulus of the elasticity determined with Equations (6.1), (6.3) and (6.4). Table 7.1 displays a summary of the code equations used in the prediction of total prestress losses by components. These methods are commonly used by designers to predict prestress losses.

Table 7.1 Summary of the code equations used in the prediction of total prestress losses by components (Pretensioned Member)

Source of Losses	AASHTO LRFD – 2012 (ksi)	PCI – 2010 (ksi)
Elastic Shortening (Δf_{ES})	$\frac{E_p}{E_{ct}} f_{cgp}$	$K_{es} \frac{E_{ps}}{E_{ci}} f_{cir}$
Creep (Δf_{CR})	$\frac{E_{ps}}{E_{ci}} f_{cgp} \psi_b(t_d, t_i) K_{id}$ (Before deck placement) $\frac{E_{ps}}{E_{ci}} f_{cgp} [\psi_b(t_f, t_i) - \psi_b(t_d, t_i)] K_{df}$ $+ \frac{E_{ps}}{E_c} \Delta f_{cd} \psi_b(t_f, t_d) K_{df}$ (After deck placement)	$K_{cr} \left(\frac{E_{ps}}{E_c} \right) (f_{cir} - f_{cds})$
Shrinkage (Δf_{SH})	$\varepsilon_{bid} E_p K_{id}$ (Before deck placement) $\varepsilon_{bdf} E_p K_{df}$ (After deck placement)	$(8.2 \times 10^{-6}) K_{sh} E_{ps} \left(1 - 0.06 \frac{V}{S} \right) (100 - RH)$
Relaxation (Δf_{RE})	$\frac{f_{pt}}{K_L} \left(\frac{f_{pt}}{f_{py}} - 0.55 \right)$	$[K_{re} - J(SH + CR_{ES})C]$
Conversions: 1 ksi = 6.895 MPa, 1 in = 25.4 mm f_{cgp} = stress in concrete at c.g. of Pretensioned strands at release (due to Prestress and self-weight); f_{cir} = net compressive stress in concrete at c.g.c at release; f_{cds} = stress in concrete at c.g. of prestressing force due to all superimposed, permanent dead loads that are applied to the member after it has been prestressed; $E_p = E_{ps}$ = modulus of elasticity of prestressing steel, $E_{ct} = E_{ci}$ = modulus of elasticity of concrete at release; E_c = modulus of elasticity of concrete at 28 days; $\psi_b(t_d, t_i)$ = girder creep coefficient at time of deck placement due to loading introduced at transfer; $\psi_b(t_f, t_i)$ = girder creep coefficient at final time due to loading introduced at transfer; $\psi_b(t_f, t_d)$ = girder creep coefficient at final time due to loading at deck placement.		

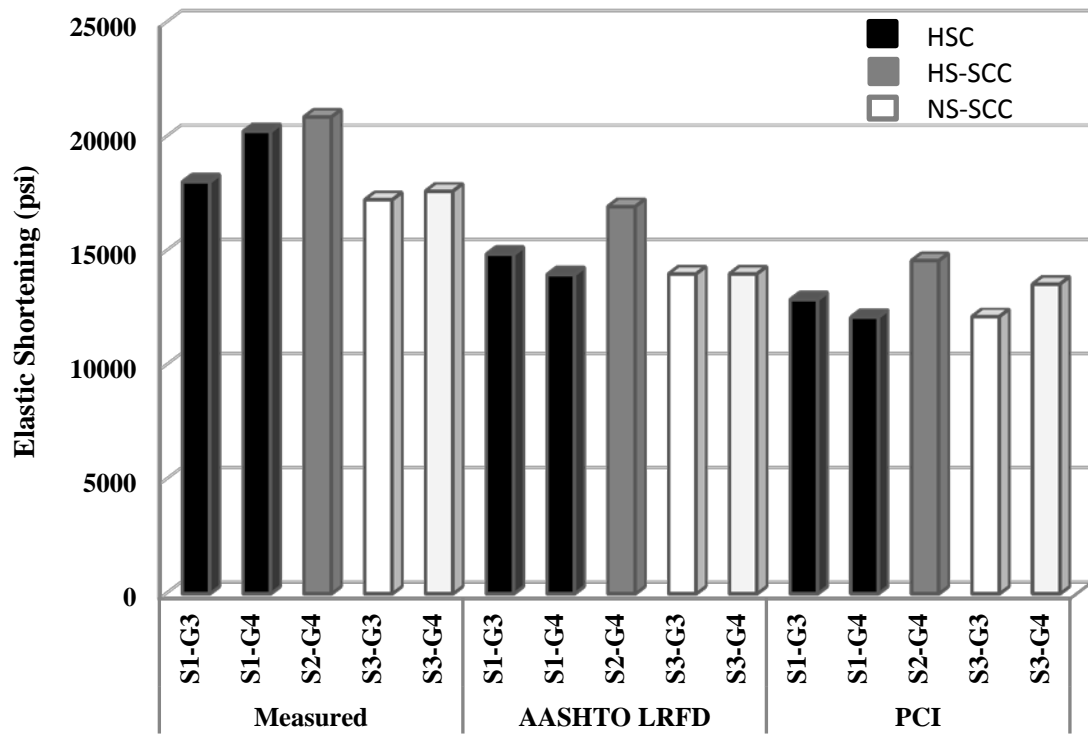
Table 7.2 illustrates the measured elastic shortening losses, in term of both change in strain, stress, and percentage loss, relative to a nominal jacking stress of 1371 MPa (199 ksi) and also to predicted elastic shortening specified by AASHTO and PCI methods.

Table 7.2. Measured vs. Predicted Elastic Shortening Losses

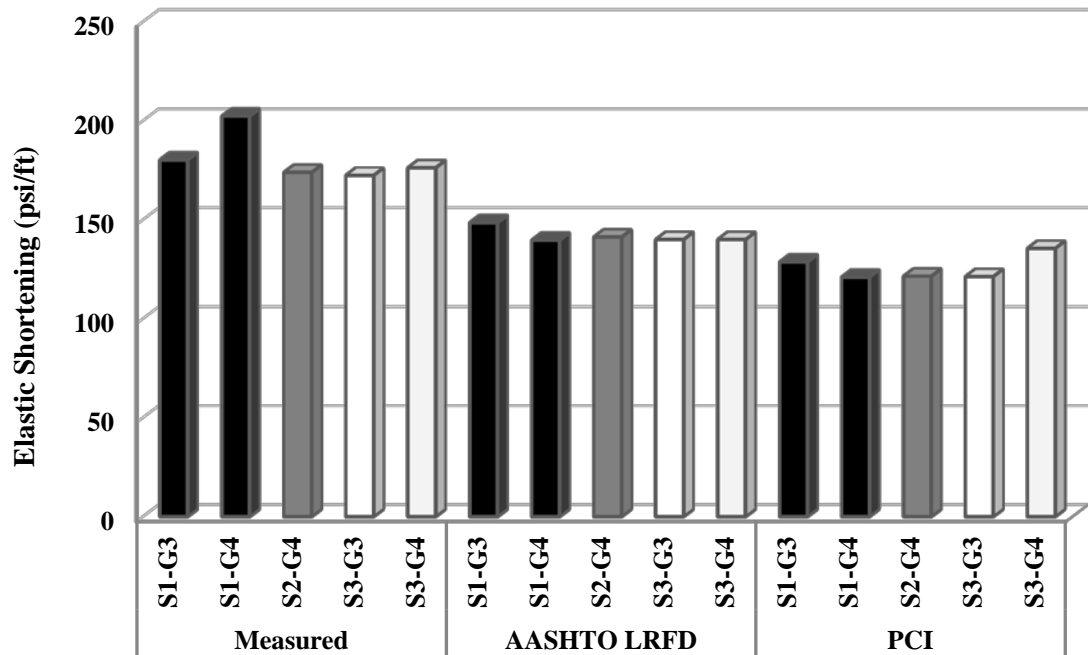
HSC								
Result Method	S1-G3				S1-G4			
	Strain ($\mu\epsilon$)	Stress (psi)	% Jacking	M/P Ratio	Strain ($\mu\epsilon$)	Stress (psi)	% Jacking	M/P Ratio
Measured	632	18024	9.1	1.00	710	20235	10.2	1.00
AASHTO*	521	14855	7.5	1.21	490	13968	7.0	1.45
AASHTO**	483	13769.5	6.9	1.31	459	13086	6.6	1.55
PCI*	452	12869.4	6.5	1.40	425	12100.6	6.1	1.67
PCI**	476	13580	6.8	1.33	461	13127	6.6	1.54
PCI***	463	13206.8	6.6	1.36	446	12697	6.4	1.59
HS-SCC								
Result Method	S2-G3				S2-G4			
	Strain ($\mu\epsilon$)	Stress (psi)	% Jacking	M/P Ratio	Strain ($\mu\epsilon$)	Stress (psi)	% Jacking	M/P Ratio
Measured					732	20866	10.5	1.00
AASHTO*	524	14940	7.5		524	14940	7.5	1.40
AASHTO**	525	14971.3	7.5		537	15312	7.7	1.36
PCI*	452	12876	6.5		511	14572.5	7.3	1.43
PCI**	533	15179.8	7.6		541	15409.3	7.7	1.35
PCI***	512	14590.5	7.3		521	14850.6	7.5	1.41
NS-SCC								
Result Method	S3-G3				S3-G4			
	Strain ($\mu\epsilon$)	Stress (psi)	% Jacking	M/P Ratio	Strain ($\mu\epsilon$)	Stress (psi)	% Jacking	M/P Ratio
Measured	605	17240	8.7	1.00	618	17621	8.9	1.00
AASHTO*	491	13998	7.0	1.23	491	13998	7.0	1.26
AASHTO**	482	13741.6	6.9	1.25	500	14255	7.2	1.24
PCI*	425	12126.5	6.1	1.42	500	14255.3	7.2	1.24
PCI**	476	13561	6.8	1.27	488	13897.7	7.0	1.27
PCI***	463	13186.3	6.6	1.31	476	13562	6.8	1.30

* Measured MOE. ** MOE estimated using Equation (6.1) for AASHTO and Equation (6.4) for PCI approaches. *** MOE estimated using Equation (6.3) for PCI method

Measured elastic shortening losses were highest in HS-SCC girders, with measured loss of 20.8 ksi. NS-SCC girders exhibited less elastic shortening losses than the HS-SCC and the HSC with differences of 16.5% and 9%, respectively. Figure 7.3 displays a comparison of measured losses to prediction for elastic shortening losses and normalized stress losses for girder length. It can be highlighted that the measured values of elastic shortening were greater than those predicted by both AASHTO and PCI methods. The AASHTO equations were more accurate when the predicted MOE of concrete [Equation (6.1)] was used in the equation for HS-SCC and NS-SCC. However, the AASHTO equations were more accurate for HSC when measured MOE was employed in the model. The PCI method was more accurate when the predicted MOE [Equation (6.4)] was used in the model for HSC, HS-SCC, and NS-SCC. In general, the measured elastic shortening losses were substantially higher than predicted losses computed by AASHTO and PCI methods. Using these methods, average ratio of measured to predicted losses were between 1.21 and 1.67 for HSC. Ratios were between 1.35 and 1.43 for HS-SCC. For the NS-SCC, the ratios of measured to predicted losses were between 1.23 and 1.42. The differences between the measured and predicted elastic shortening losses can be attributed to the difference between the actual MOE and the value obtained from tests on companion specimens. Other reason may be related to the use of the empirical Equations (6.1), (6.3) and (6.4) to estimate the MOE values (Gross, 1999). When the normalized elastic shortening losses were compared between HSC, HS-SCC, and NS-SCC, it is apparent that the normalized losses are greater for HSC by approximately 10% than HS-SCC and NS-SCC. It can be inferred that the variation in the mix designs for each type of concrete (HSC and SCC) affected the MOE of the mixture at release. Therefore, it can be expected larger elastic shortening losses if the MOE is not sufficiently high for any of the concrete mixtures.



(a) Elastic Shortening



(b) Elastic shortening Normalized for Girder Length

Figure 7.3 Measured and Predicted Elastic Shortening Losses

7.3. TOTAL LOSSES

7.3.1. Background

In concrete bridge design, the total prestress losses consist of losses before release, elastic shortening losses (ES), shrinkage of concrete (SH), creep of concrete (CR), and relaxation of strand (RE), which are considered for serviceability cases. These losses do not affect the ultimate strength of a girder, but they may lead to poor predication of service camber and deflection. With regard to stresses, an underestimation of the total losses may result in cracking under service loads. Several different methods have been adopted by different current specifications. These methods exhibit varying levels of complexity and ease of use. Empirical models provided by AASHTO LRFD and PCI were utilized in this research to determine the total prestress losses. The magnitude of the loss due to each source is estimated separately and the total loss is taken as the sum of the individual components. The summary of the code equations used in the prediction of total prestress losses by components is displayed in Table 7.1.

7.3.2. Measurements and Discussion

The strain readings at c.g.s from VWSGs were utilized to measure the total prestress loss in the concrete. Long- term prestress losses were measured using the same procedure as presented in Section 7.2.2 and were corrected for temperature changes. To determine the total amount of creep and shrinkage losses, the elastic shortening and relaxation losses were subtracted from the total measured loss. Measured long-term losses are summarized in Table 7.3 for all instrumented girders. Elastic- shortening losses (ES) were presented in Section 7.2. The relaxation losses (RE) were estimated analytically. Time-dependent creep losses (CR) and shrinkage losses (SH) were measured for about a one year after release. The measured total prestress loss was compared to predicted total losses presented by AASHTO LRFD and PCI using measured elastic modulus of HSC, HS-SCC, and NS-SCC.

Table 7.3 Measured and Predicted Total Prestress Losses for Instrumented Girders

	Girder ID	Prestress Losses				Total Losses		Comparison	
		ES (psi)	SH (psi)	CR (psi)	RE (psi)	Stress (psi)	% Jacking	M/P Ratio	Diff. (+,-)
Measured	S1-G3	18024	13802		4630	36457	18.33	1.000	NA
	S1-G4	20235	15984		4640	40854	20.54	1.000	NA
	S2-G4	20866	23369		4620	48855	24.56	1.000	NA
	S3-G3	17240	19932		4620	41794	21.01	1.000	NA
	S3-G4	17621	22437		4630	44686	22.46	1.000	NA
AASHTO LRFD	S1-G3	14856	10299	9355	1144	35655	17.92	1.023	-
	S1-G4	13968	9730	8707	1144	33549	16.86	1.218	-
	S2-G4	16948	9435	11740	1144	39267	19.74	1.244	-
	S3-G3	13998	10139	9633	1144	34914	17.55	1.197	-
	S3-G4	13998	10733	10753	1144	36628	18.41	1.220	-
PCI	S1-G3	12869	5713	15819	2139	36540	18.37	0.998	+
	S1-G4	12100	5713	14206	2194	34214	17.20	1.194	-
	S2-G4	14573	5713	15241	2111	37638	18.92	1.298	-
	S3-G3	12126	5713	15693	2158	35691	17.94	1.171	-
	S3-G4	13549	5713	15244	2135	36642	18.42	1.220	-

Total measured losses of HSC girders averaged 38.6 ksi, or 19.4% of the nominal jacking stress of 199 ksi. However, total measured losses of SCC girders (both HS-SCC and NS-SCC) averaged 45.1 ksi, or 22.6 % of the nominal jacking stress. Elastic shortening losses represented in general 44.4 % of total loss. However, time-dependent loss due to creep and shrinkage was less than the elastic shortening for measured values in all monitored girders.

Predicted total prestress loss values using AASHTO LRFD and PCI underestimated the measured total strain. Surprisingly, the AASHTO and the PCI methods showed good agreement with measured losses for HSC girders. Losses computed using the PCI method with measured parameters resulted in under-predictions of total prestress losses. However, the calculated losses using this method are closer in magnitude to the measured losses than the losses calculated using the AASHTO LRFD method with measured parameters as can be seen in Figure 7.4.

Based on analysis above, for prestress precast HSC, HS-SCC, and NS-SCC, PCI Handbook method and AASHTO LRFD are recommended for prestress losses estimation in the design stage. The average difference of these methods was less than 20% from measured values.

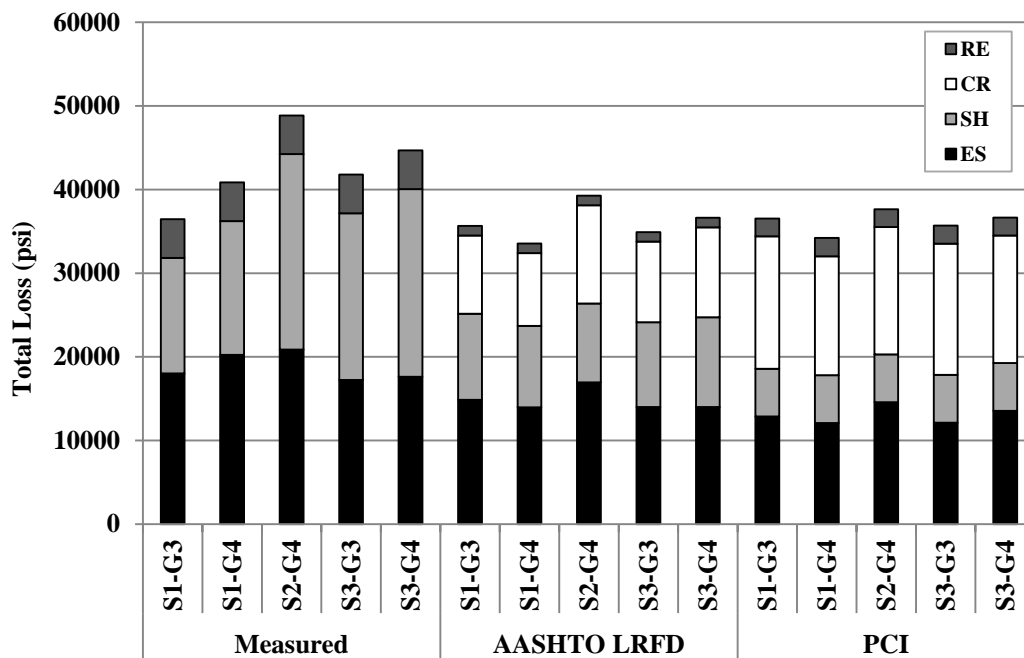


Figure 7.4 Measured and Predicted total Prestress Losses for all Instrumented Beams.

Table 7.4 displays the total measured prestress losses for HSC, HS-SCC, and NS-SCC. In overall, the HS-SCC girders had high total prestress loss. However, the data is not normalized to take into account the differences in lengths between girders. The normalized values indicated that the total loss over a unit length is less for HS-SCC than NS-SCC by about 6%. Furthermore, as can be anticipated, HSC showed lower magnitude values of total prestress losses than HS-SCC and NS-SCC.

Table 7.4. Total Prestress Losses for HSC, HS-SCC, and NS-SCC PC/PS Girders

Material	Length (ft.)	Average Total Loss (psi)	Avg. Total Loss/Length (psi/ft.)
HSC	100	38655	387
HS-SCC	120	48855	407
NS-SCC	100	43240	432

Conversion: 1 ft. = 0.3048 m, 1 ksi= 6.895 MPa

7.4. SUMMARY AND CONCLUSIONS

The following conclusions were reached from the HSC, HS-SCC, and NS-SCC mixes:

- The measured elastic shortening losses for the HSC, HS-SCC, and NS-SCC averaged 19.13 ksi, 20.866 ksi, and 17.43 ksi, respectively. For all the girders, the measured elastic shortening losses were higher than predicted using gross section and measured or predicted MOE.
- The average ratios of measured to predicted prestress losses by these methods were between 1.21 and 1.67 for HSC. Ratios were between 1.35 and 1.43 for HS-SCC. For the NS-SCC, the ratios of measured to predicted losses were between 1.23 and 1.42. The reasons of the difference between measured and predicted elastic shortening losses might be due to restraint against shortening of the girders prior to the release and this caused losses to appear artificially high. The other reason was that the differences between the actual MOE and the values determined from companion specimen tests.

- The total prestress losses averaged 38.65 ksi, 48.85 ksi, and 43.24 ksi for the HSC, HS-SCC, and NS-SCC girders, respectively.
- For all the girders, elastic shortening losses accounted for the largest component of the total measured loss.
- For most girders, the measured total prestress losses were greater than predicted using the AASHTO LRFD and the PCI Handbook methods. Unconservative results were obtained for the NS-SCC and HS-SCC. Reasons might be attributed to the higher paste volume and difference in the mixes content compare to the HSC.

APPENDIX A - DESIGN DRAWINGS

APPENDIX B - INSTRUMENTATION PLAN

Instrumentation Plan for BRIDGE A7957
Route 50
Osage County, Missouri

In Conjunction with
Research Investigation Number TRyy1236

Center for Infrastructure Engineering Studies
Department of Civil, Architectural and Environmental Engineering
Missouri University of Science and Technology
and
The Missouri Department of Transportation

Jan 25, 2013

Prepared by:

Dr. John J. Myers, P.E. (PI)
Dr. Jeffery S. Volz, P.E. (Co-PI)
Benjamin Gliha
Eli Hernandez

Department of Civil Engineering
1401 North Pine Street
325 Butler Carlton Hall
Missouri University of Science and Technology
Rolla, MO 65409-0710

Research Sponsored by:
The Missouri Department of Transportation and
The National University Transportation Center at
Missouri University of Science and Technology

Introduction:

For Bridge A7957 over the Maries River, Missouri University of Science and Technology (Missouri S&T), in conjunction with the Missouri Department of Transportation (MoDOT), will be performing research during the construction of the 3-span, NU-girder bridge. This research will include instrumentation during and after construction of the selected NU girders, Bent No. 3, Bent No. 4, and portion of the slab deck. This document outlines the instrumentation plan including locations and types of sensors as well as timing for the activities.

Goals:

The primary goals of the instrumentation plan are summarized as follows:

1. Monitor deflections from transfer through service life;
2. Compare predicted and measured deflections;
3. Monitor stresses along spans at c.g.s due to prestressing, applied loads, and thermal effects;
4. Develop stress blocks (strain blocks) along depth of members at support and midspan;
5. Monitor thermal gradients at similar cross-sections, for both interior and exterior spans;
6. Evaluate distribution of loading between adjacent interior and exterior sections of the same span through a live load test after construction has been completed;
7. Determine transfer length for 0.6-in diameter strands in the actual high-strength beams used in the structure;
8. Determine level of continuity (both M- and M+) provided at the intermediate bents.

Objectives:

The primary objectives of the instrumentation program are as follows:

1. Monitor components of the bridge superstructure during early-age and later-ages;
2. Identify trends in measured and observed behavior;
3. Examine applicability of current design procedures and assumptions for high performance concrete designs with 0.6-in. diameter prestressing strands. Provide recommendations for design of future Self Consolidating Concrete (SCC) and High

Volume Fly Ash Concrete (HVFAC) bridges in Missouri with 0.6-in. diameter prestressing strands as warranted.

Instrumentation:

The type of sensors used in (and on) the girders and deck will include:

1. Vibrating wire strain gauges, VWSG (see Fig. 1);
2. DEMEC points (see Fig. 2);
3. Taut-wire deflection gauges (see Figs. 3 and 4);
4. Load cell (see Fig. 5);
5. Thermocouples

The research team will coordinate their activities with MoDOT engineers and MoDOT's Research Group, Construction and Materials and with personnel from the precast concrete plant and jobsite such that early-age monitoring of temperature and strain histories is possible for the girders and deck.

Three independent systems will be used to monitor concrete strains. Vibrating wire strain gauges (VWSG) will be embedded in the concrete for selected girders. To assure proper orientation after concrete placement and adequate protection during casting, the research team will attach the VWSG as illustrated in Fig. 1.



Fig. 1. Instrumented Vibrating Wire Strain Gauge (VWSG) on Prestressing Strand

DEMEC points will be located on the side of the girder by the research team according to the image in Fig. 2.

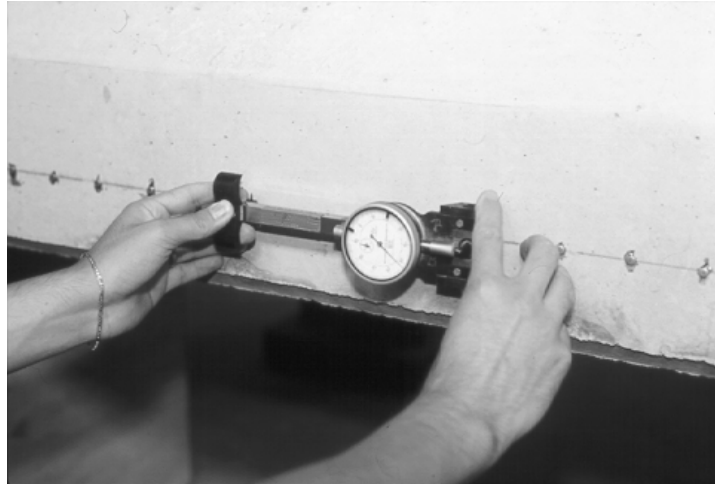


Fig. 2. Illustration of DEMEC Points and DEMEC Gauge

Estimating and comparing experimental camber/deflections to measured values is often very critical for new materials particularly those where the modulus of elasticity may vary. In order to measure camber at release, a tension wire system may be used as illustrated in Figs. 3 and 4. This requires the use of a dead weight, piano wire, and two expansion bolts that are attached to the girder after the forms are removed, but prior to de-tensioning of the prestressing force. This will be undertaken on a representative HS-SCC girder.

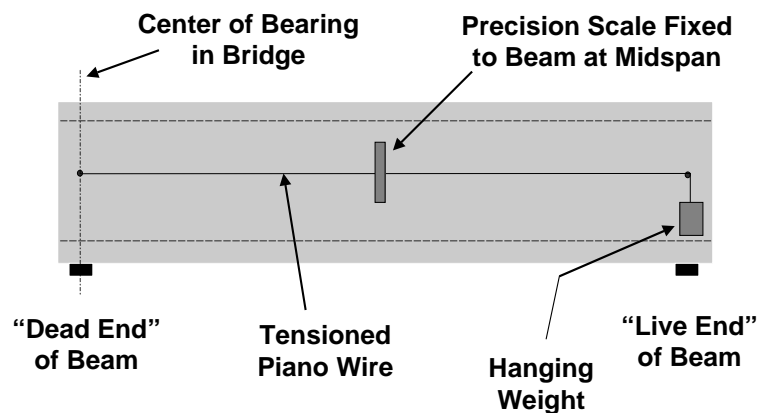


Fig. 3. Schematic of Tensioned Wire System



Fig. 4. Dead Weight for Tension-Wire System

In order to examine the associated prestress losses with the 0.6-in. diameter seven wire strands, a load cell and DAS will be required at the dead end of the member during fabrication. The set-up for this procedure is illustrated in Fig. 5. A thermocouple will also be attached to the strand to monitor the temperature of the strand by the researchers.

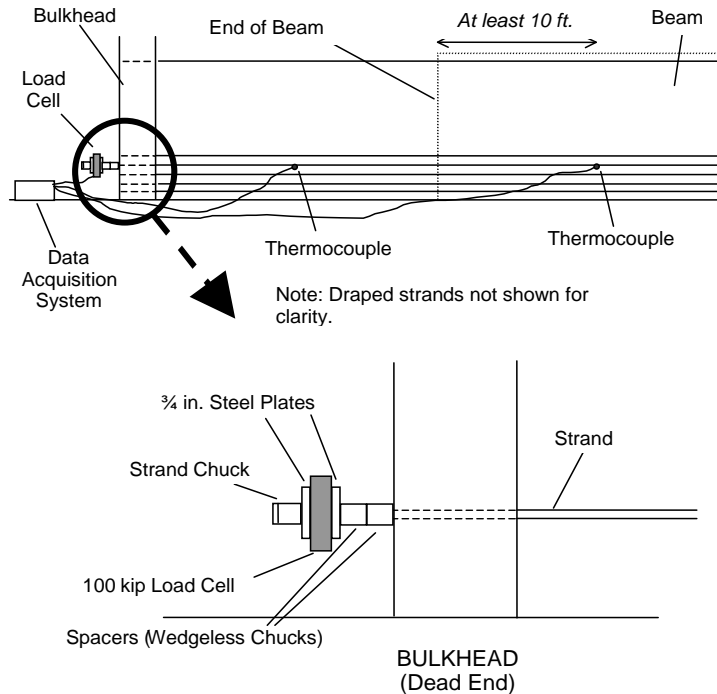


Fig. 5. Set-Up for Measurement of Strand Stresses and Temperature Before Release

A single exit point for all of the instruments' cables (VWSG and thermocouples) will be provided so as to facilitate the use of a data acquisition system (DAS) which will record data from the various instruments (see their locations in Fig. 6). The data will be acquired at regular intervals during the first few days after the casting. Thereafter, data will be acquired during placement of the girders and superstructure construction as described in subsequent sections of this instrumentation plan. The cost of furnishing and placing the instrumentation systems in and on the girders and any other incidental work items shall be considered as completely covered in the contract between Missouri S&T and MoDOT.

Location of Instrumentation:

The location of the instrumentation described above will consist of several "cluster" locations for Span (1-2), Span (2-3), and Span (3-4). These "cluster" locations occur in the prestressed / precast girders and cast-in-place deck directly above the girder instrumentation. Two data acquisition system boxes will be located and mounted along interior bents No. 2 and No. 3 as illustrated in Fig. 6.

Girders:

The research team will instrument a maximum of six out of twelve girders prior to casting by the fabricator as illustrated in Fig. 6. These will comprise one exterior and one interior girder for Span (1-2), Span (2-3), and Span (3-4). Within each girder of Span (1-2) and Span (3-4), the instrumentation "clusters" will be located at two cross-sections, one at midspan and one in a close proximity to the support at Bent 2 and Bent 3 respectively. For the girders of Span (2-3), the instrumentation "clusters" will be located at three cross-sections, one at midspan and one in a close proximity to each of the supports (Bents 2 and 3). Figs. 7 and 8 illustrate the instrumentation required at the girder cluster locations. In addition to the cluster locations described herein, a VWSG (and thermocouple) will be located at the quarter point (within the member) along the centroid of the prestressing strands for the instrumented girders on beam lines 3 and 4.

Cast-In-Place Deck:

The research team will instrument Span (2-3) at the same “cluster” location described for the girders at midspan in Fig. 6, but within the depth of the deck above the girders and along the transverse direction (see Fig. 7). There will be a total of four VWSG (two at each location according to the detail in Fig. 7).

NU Girder Instrumentation for Destructive Testing:

The research team will instrument two lab test girders with strain gauges prior to casting by the fabricator. The strain gauges will be installed at midspan according to the instrument configuration shown in Fig. 9.

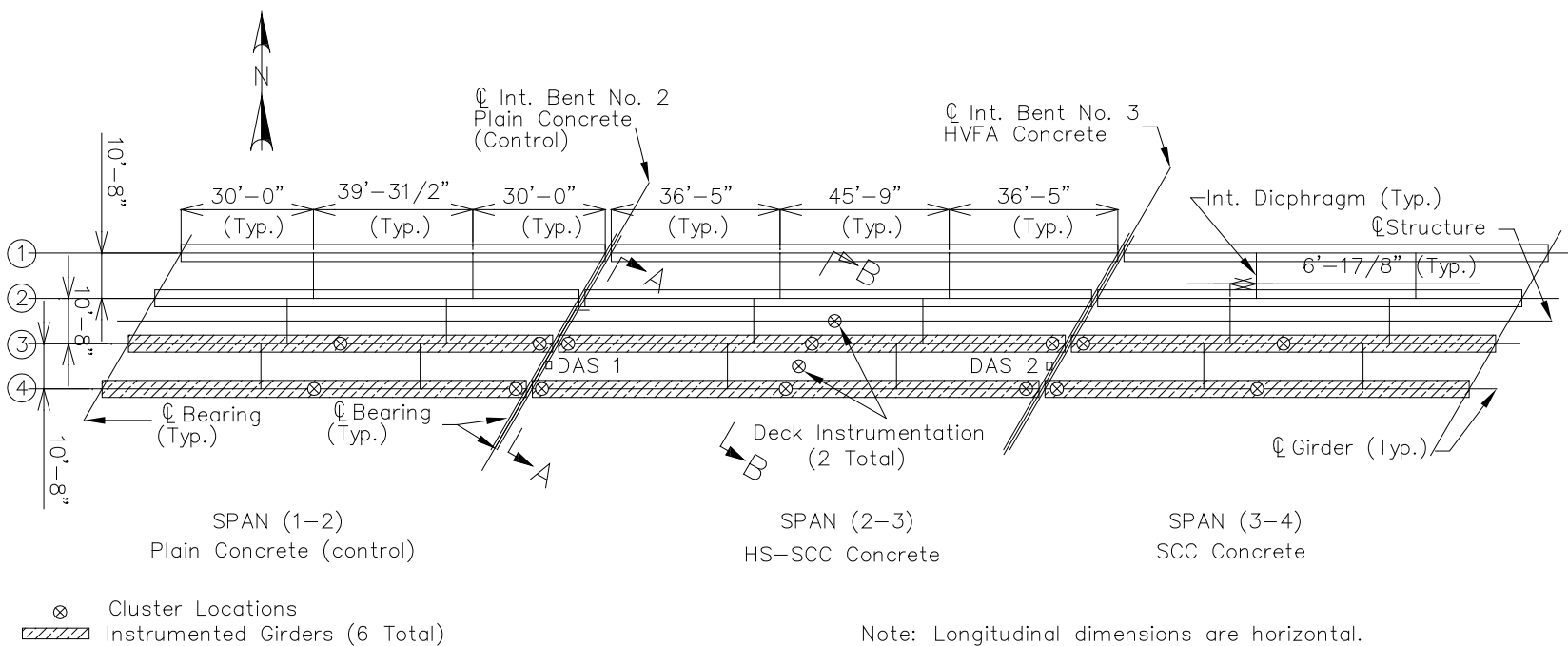


Fig. 6. Plan Illustrating Girders to be Instrumented and "Cluster" Locations

Location of VWSG at Girder Line 3 and 4 “Cluster” Locations (Midspan):

TD: Top Deck (2 in. Below Top Fiber of Deck)

BD: Bottom Deck (2 in. Above Bottom Fiber of Deck)

TF: Top Flange (2 in. Below Top Fiber)

CGC: Center of Gravity of Composite Beam Section (Midspan Only)

CGU/CGI: Center of Gravity of Non-Composite Beam Section (Midspan Only)

CGS: Center of Gravity of Pretensioning Strands

BF: Bottom Flange (2 in. Above Bottom Fiber)

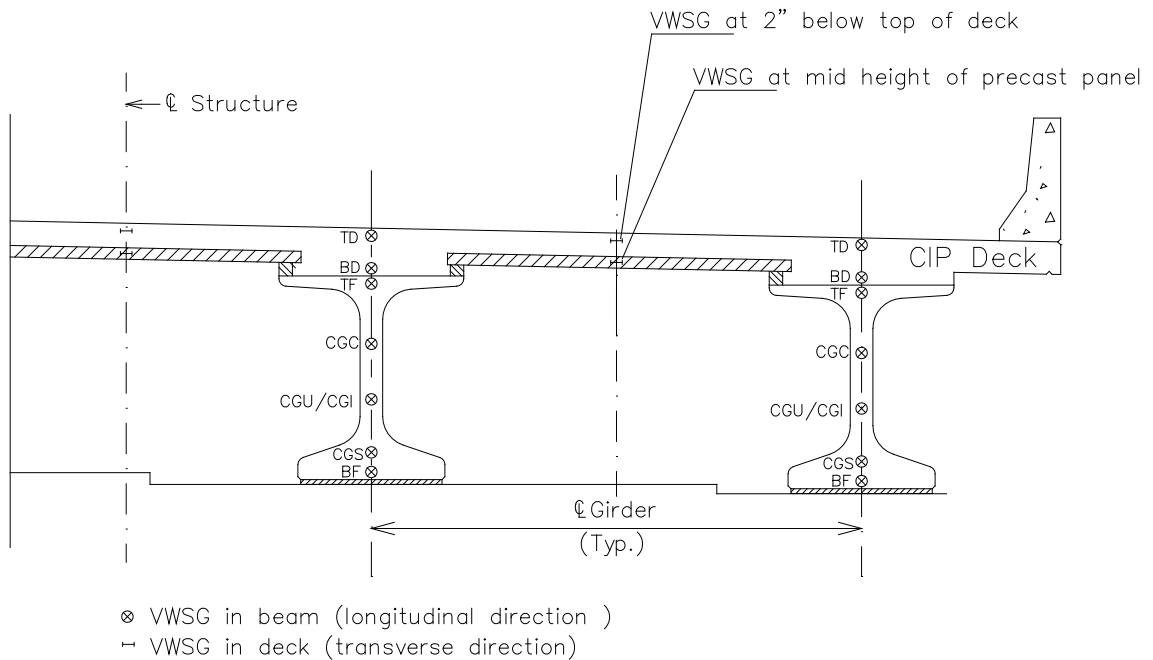


Fig. 7. Cross-Section of NU Girders Illustrating Instrumentation at Midspan

Location of VWSG at Girder Line 3 and 4 “Cluster” Locations (Near Supports)

TD: Top Deck (2 in. Below Top Fiber of Deck)

TF: Top Flange (2 in. Below Top Fiber)

CGC: Center of Gravity of Composite Beam Section

CGS: Center of Gravity of Pretensioning Strands

BF: Bottom Flange (2 in. Above Bottom Fiber)

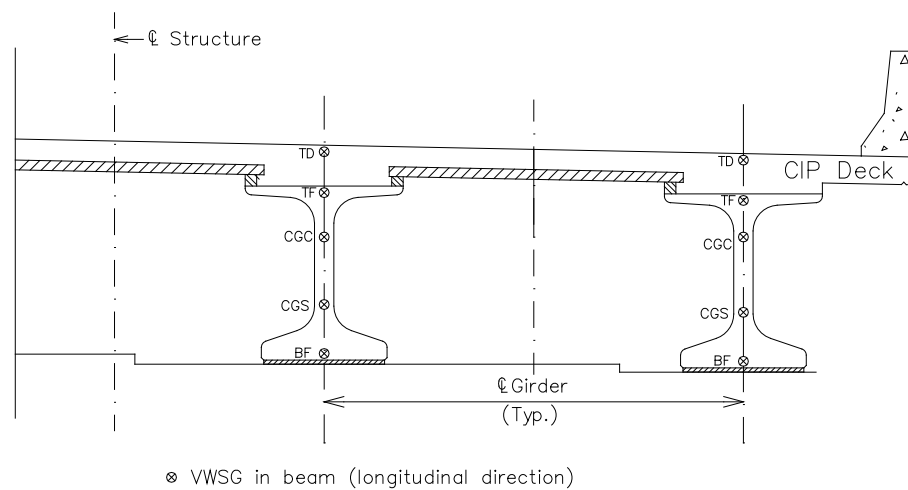


Fig. 8. Cross-Section of NU Girders Illustrating Instrumentation Near Supports

Location of Gauges at NU Lab Test Girder (Midspan)

TF: Top Flange (2 in. Below Top Fiber of Girder)

CGS: Center of Gravity of Pretensioning Strands

BF: Bottom Flange (2 in. Above Bottom Fiber of Girder)

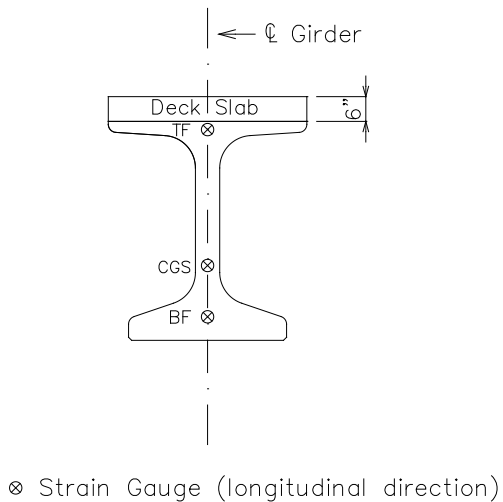
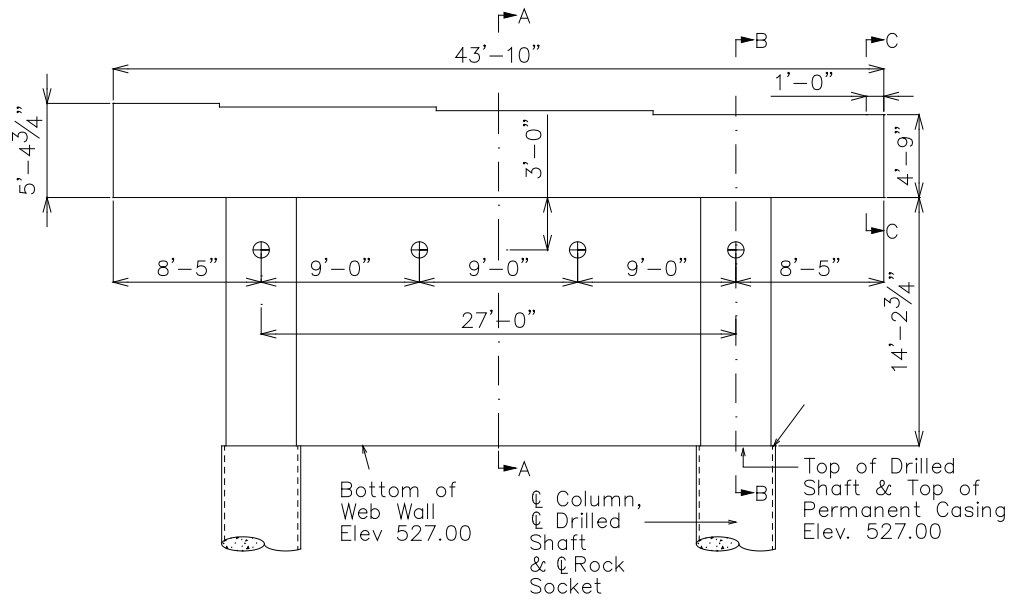


Fig. 9. Cross-Section of NU Girders Illustrating Instrumentation at Midspan for Lab Destructive Testing

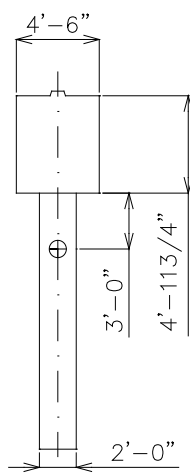
Bent Instrumentation:

The research team will instrument Bent Nos. 2 and 3 (see Fig. 6) according to the thermocouple arrangement shown in Fig. 10. For each bent, two thermocouples will be placed 3 ft from the top edge and at the center of the Web Wall [Fig. 10 (a) and Fig. 10(b)]. A second set of thermocouples will be installed on the bent columns, separated 3 ft. from the top of the pier [Fig. 10(a) and Fig. 10(c)]. The beam cap will be instrumented with three interior thermocouples and one exterior thermocouple according to the detail shown in Fig. 10(d).

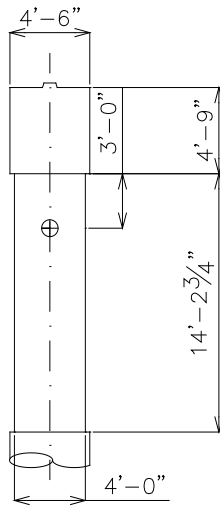


⊕ Thermocouple Location (TC)

(a) East Elevation

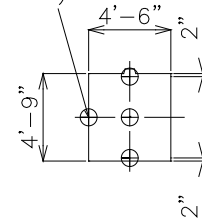


(b) Section A-A



(c) Section B-B

Exterior Thermocouple
(To measure ambient
air temperature)



(d) Section C-C

Fig. 10. Cross-Section of Bents Illustrating Thermocouple Locations

Additional Instrumentation:

A chloride detection sensor may be added to the instrumentation plan if available.

Staging of Instrumentation:

The anticipated staging of the instrumentation is as follows:

Plain Concrete / HVFA Bent – the instrumentation / research activity is in *italics*.

1. Operation – Bent forms are set by the contractor.
2. Operation – Reinforcement is placed by the contractor.
3. *The researchers will install thermocouple sensors in the locations shown in Fig. 10 prior to casting of the web walls and columns of the bents. It is desirable that the sensors be placed as close to the casting of the web walls and columns as possible. This is to avoid potential damage to these sensors. The contractor shall allow time for this activity as part of the construction process.*
4. Operation – Concrete is placed by the fabricator.
5. *Test Specimens for the researchers are cast when the concrete is placed.*
6. Operation – Concrete attains required strength, the fabricator removes forms.
7. *The researchers will inspect the bents and record thermocouple readings before and after the forms are removed. The fabricator may note that the Data Acquisition System (DAS) will “scan” readings periodically after concrete is cast. A “cherry picker” or equivalent will be required by the researchers to acquire readings and/or data by the researchers. During construction, this access is to be provided by the contractor. After construction, MoDOT will assist with this activity.*

Prestressed / Precast Girders – the instrumentation / research activity is in *italics*.

8. Operation – Prestressing strands are stressed by the fabricator.
9. *A load cell will be installed at the dead end prior to prestressing of the tendons during the stressing operation to monitor prestress losses during stressing and release of the strands (Fig. 5). This load cell and DAS will be removed when the strands are released after the member has attained the required concrete release strength.*

10. *After the strands have been stressed, but before the forms have been set, the researchers will install the girder sensors in the cluster locations described herein. The fabricator shall allow time for this activity as part of the fabrication process.*
11. Operation – Precast Forms are set by the fabricator.
12. Operation – Concrete is placed by the fabricator.
13. *Test Specimens for the researchers are cast including match cured cylinders when the concrete is placed. The fabricator shall provide a covered area (preferably temperature controlled) for the casting and curing of match cured specimens by the researchers. The fabricator shall have a calibrated compression-testing machine on site capable of testing the concrete cylinders at release.*
14. Operation – Concrete attains required release strength, the fabricator removes forms.
15. *DEMEC points are placed by the researchers near the ends of the members on each side of the lower flange with epoxy. After installation, the research team shall take baseline DEMEC readings. The fabricator shall allow time for this activity as part of the fabrication process.*
16. *Tension wire system installed by the researchers (Fig. 3). The fabricator shall allow time for this activity as part of the fabrication process.*
17. Operation – Pretensioning strands are released by the fabricator.
18. *The load cell is removed by the researchers in conjunction with release of the pretensioning strands.*
19. *The researchers will inspect the member, record DEMEC readings, and deflection readings (while the member is still on the bed). The fabricator may note that the Data Acquisition System (DAS) will “scan” readings periodically throughout the fabrication process.*
20. Operation – Place the member in storage at the precasting yard. (The support points for the members in storage should be similar to the final centerline of bearing after the member is erected.)
21. *Additional readings will be taken by the researchers periodically, but of note to the fabricator and contractor is that readings will be taken prior to shipment, at 28 days, at 56-days (optional to the researchers), after erection (before the formwork is set),*

after erection (before the slab is placed), after the slab is placed, during a live load test, and at later-ages (i.e. six months, 1 year, etc.).

Cast-In-Place (CIP) Deck – the instrumentation / research activity is in *italics*.

1. Operation – Girders are erected and braced by the contractor.
2. Operation – CIP deck forms are set by the contractor.
3. Operation – Reinforcement is placed by the contractor.
4. *The researchers will install the CIP sensors in the cluster locations prior to casting that section of the deck. It is desirable that the sensors be placed as close to the casting of the deck as possible. This is to avoid potential damage to sensors. The contractor shall allow time for this activity as part of the construction process. In addition, the contractor may note that a “PVC” type or equivalent sleeve will be installed through the deck by the researchers near Bent No. 2. This will be of adequate size for the bundle of instrumentation wiring that will feed into the data acquisition system / data logging box. The researchers will coordinate the location of this sleeve with the contractor before the instrumentation is installed.*
5. Operation – Concrete is placed by the contractor.
6. *Test Specimens for the researchers are cast when the concrete is placed.*
7. *Additional readings will be taken by the researchers periodically, but of note to the contractor is that readings will be taken after erection of the girders (before and after the formwork is set), after the slab is placed, during a live load test, and at later-ages (i.e. six months, 1 year, etc.). A “cherry picker” or equivalent will be required by the researchers to acquire readings and/or data by the researchers. During construction, this access is to be provided by the contractor. After construction, MoDOT will assist with this activity.*

Damage to Instrumentation:

Many of the sensors that will be installed in the girders, bents, and CIP deck are sensitive to the construction process. Jobsite and plant workers must be aware of the location of the instrumentation to avoid damage. Equipment in particular that may cause damage to sensors or wiring includes hand held vibrators, foot traffic, and construction

equipment. During any handling, transportation and erection of the prestressed girders, the contractor shall make provisions to prevent damage to the instrumentation installed during the fabrication of the prestressed / precast girders. The contractor shall also make provisions to prevent damage to the instrumentation placed in the bents and deck during fabrication / casting of the cast-in-place elements.

Any damage sustained to the instrumentation installed in or on the prestressed / precast girders, bents, or CIP deck as a result of the contractor's operations shall be the responsibility of the contractor. All costs of repair and/or replacement shall be as determined by the researchers.

Representative Test Specimens:

Additional specimens for the purpose of research testing will be collected by the researchers during fabrication of the prestressed girders, casting of the HVFAC web walls and bents, and casting of the deck. Fabrication of research specimens and the associated testing will require a maximum of 0.50 cubic yard of additional concrete to be provided per casting date where concrete is sampled. The researchers will be required to cast test specimens to monitor the mechanical and material performance of the in-place concrete. Fig. 11 illustrates representative quality control test specimens that may be required by the researchers.

The contractor shall notify both the researchers [Dr. John Myers and Dr. Jeffery Volz] and the MoDOT Research Group, Construction and Materials, Division [Ms. Jennifer Harper and Mr. William Stone] with written notice four weeks prior to the commencement of fabrication of the prestressed girders, bents, and CIP deck. It is most desirable that the tentative fabrication / production schedule be sent to the researchers as soon as feasible since the preparation of instrumentation can be very time consuming. If possible, it is recommended that the instrumented beams be fabricated last to allow the greatest lead-time.



Fig. 11. Representative QC/QA Test Specimens

During fabrication / casting of the girders, bents, and CIP deck, the contractor's fabricator and site crew shall be required to allow access to the work as required by the researchers. Specimen collection activities including use of equipment provided by research personnel will be accomplished with the minimum disturbance to the fabricator's and contractor's operations.

APPENDIX C - INSTRUMENTATION LABELING

Date: 7/29/2013
 Span: 1-2
 Member: Girder 4 (S1-G4)
 Stage: **Fabrication**

Location	S/N	Begin #	End #	Chanel #	DAS	MODULE
S1-G4-M1	114013049	9244	9269	17	1	2
S1-G4-M2	114013040	9920	9945	18	1	2
S1-G4-M3	114013039	9893	9918	19	1	2
S1-G4-M4	114013034	10325	10351	20	1	2
S1-G4-M5	114013068	9784	9810	21	1	2
S1-G4-M6	114013033	10352	10377	N/A	N/A	N/A
S1-G4-M7	114013056	10109	10135	N/A	N/A	N/A
S1-G4-E1	114013080	7243	7251	23	1	2
S1-G4-E2	114013110	7595	7603	24	1	2
S1-G4-E3	114013111	7386	7394	25	1	2
S1-G4-E4	114013112	7585	7594	26	1	2
S1-G4-E5	114013114	7319	7327	N/A	N/A	N/A

Date: 8/1/2013
 Span: 1-2
 Member: Girder 3 (S1-G3)
 Stage: **Fabrication**

Location	S/N	Begin #	End #	Chanel #	DAS	MODULE
S1-G3-M1	114013037	10244	10270	60	2	2
S1-G3-M2	114013036	10271	10297	61	2	2
S1-G3-M3	114013053	9162	9188	62	2	2
S1-G3-M4	114013055	9514	9540	63	2	2
S1-G3-M5	114013035	10298	10324	64	2	2
S1-G3-M6	114013067	9757	9783	N/A	N/A	N/A
S1-G3-M7	114013042	10190	10216	N/A	N/A	N/A
S1-G3-E1	114013116	7329	7337	70	2	2
S1-G3-E2	114013117	7348	7356	71	2	2
S1-G3-E3	114013118	7338	7346	72	2	2
S1-G3-E4	114013115	7405	7412	73	2	2
S1-G3-E5	114013081	7252	7260	N/A	N/A	N/A

Date: 8/3/2013
 Span: 3-4
 Member: Girder 4 (S3-G4)
 Stage: **Fabrication**

Location	S/N	Begin #	End #	Chanel #	DAS	MODULE
S3-G4-W1	114013091	7452	7460	72	2	2
S3-G4-W2	114013092	7300	7308	73	2	2
S3-G4-W3	114013086	7290	7297	74	2	2
S3-G4-W4	114013093	7433	7441	75	2	2
S3-G4-W5	114013103	7548	7556	N/A	N/A	N/A
S3-G4-M1	114013050	7604	7630	60	2	2
S3-G4-M2	114013041	10217	10243	61	2	2
S3-G4-M3	114013065	9703	9729	62	2	2
S3-G4-M4	114013045	9270	9296	63	2	2
S3-G4-M5	114013062	9460	9485	64	2	2
S3-G4-M6	114013063	9487	9512	N/A	N/A	N/A
S3-G4-M7	114013061	9433	9458	N/A	N/A	N/A

Date: 8/5/2013
 Span: 3-4
 Member: Girder 3 (S3-G3)
 Stage: **Fabrication**

Location	S/N	Begin #	End #	Chanel #	DAS	MODULE
S3-G3-W1	114013083	7262	7267	66	2	2
S3-G3-W2	114013098	7519	7527	67	2	2
S3-G3-W3	114013084	7271	7279	68	2	2
S3-G3-W4	114013085	7281	7289	69	2	2
S3-G3-W5	114013082	7415	7423	N/A	N/A	N/A
S3-G3-M1	114013078	9568	9593	60	2	2
S3-G3-M2	114013074	9838	9864	61	2	2
S3-G3-M3	114013059	10055	10081	62	2	2
S3-G3-M4	114013070	10020	10052	63	2	2
S3-G3-M5	114013058	9542	9567	64	2	2
S3-G3-M6	114013073	9947	9972	N/A	N/A	N/A
S3-G3-M7	114013060	9407	9431	N/A	N/A	N/A

Date: 8/8/2013
Span: 2-3
Member: Girder 4 (S2-G4)
Stage: **Fabrication**

Location	S/N	Begin #	End #	Chanel #	DAS	MODULE
S2-G4-W1	114013102	7557	7565	60	2	2
S2-G4-W2	114013094	7443	7450	61	2	2
S2-G4-W3	114013107	7576	7584	62	2	2
S2-G4-W4	114013105	7538	7545	63	2	2
S2-G4-W5	114013104	7367	7375	N/A	N/A	N/A
S2-G4-M1	114013077	9595	9621	1	1	1
S2-G4-M2	114013044	9297	9323	2	1	1
S2-G4-M3	114013066	9730	9755	3	1	1
S2-G4-M4	114013076	9622	9648	4	1	1
S2-G4-M5	114013075	9676	9702	5	1	1
S2-G4-M6	114013043	9352	9377	N/A	N/A	N/A
S2-G4-M7	114013047	10136	10162	N/A	N/A	N/A
S2-G4-E1	114013095	7424	7432	11	1	1
S2-G4-E2	1140130101	7500	7508	12	1	1
S2-G4-E3	114013100	7510	7518	13	1	1
S2-G4-E4	114013097	7529	7537	14	1	1
S2-G4-E5	114013099	7309	7317	N/A	N/A	N/A

Date: 8/13/2013

Span: 2-3

Member: Girder 3 (S2-G3)

Stage: **Fabrication**

Location	S/N	Begin #	End #	Chanel #	DAS	MODULE
S2-G3-W1	114013113	7395	7404	72	2	2
S2-G3-W2	114013088	7491	7499	73	2	2
S2-G3-W3	114013087	7481	7489	74	2	2
S2-G3-W4	114013079	7234	7242	75	2	2
S2-G3-W5	114013109	7376	7385	N/A	N/A	N/A
S2-G3-M1	114013057	10083	10108	60	2	2
S2-G3-M2	114013048	9326	9350	61	2	2
S2-G3-M3	114013052	9189	9215	62	2	2
S2-G3-M4	114013046	10163	10189	63	2	2
S2-G3-M5	114013054	9379	9404	64	2	2
S2-G3-M6	114013051	9217	9242	N/A	N/A	N/A
S2-G3-M7	114013069	9811	9837	N/A	N/A	N/A
S2-G3-E1	114013090	7462	7470	11	1	1
S2-G3-E2	114013106	7568	7573	12	1	1
S2-G3-E3	114013096	7357	7365	13	1	1
S2-G3-E4	114013108	9153	9161	14	1	1
S2-G3-E5	114013089	7471	7479	N/A	N/A	N/A

Date: 8/21/2013

Panels (Mid-span 2-3 between girders 2 and 3, Mid-span 2-3 between girders 3 and 4)

Stage: **Fabrication**

Location	S/N	Begin #	End #	Chanel #	DAS	MODULE
S2-D23-M1	114013064	9651	9675	10, 10	1	1
S2-D23-M2	114013071	10001	10027	N/A	N/A	N/A
S2-D34-M1	114013072	9975	10200	7, 50	2	1
S2-D34-M2	114013038	9865	9891	N/A	N/A	N/A

Date: 9/24/2013

Span: 2-3

Member: Girder 4 (S2-G4)

Stage: **Erection**

Location	S/N	Begin #	End #	Chanel #	DAS	MODULE
S2-G4-W1	114013102	7557	7565	N/A	N/A	N/A
S2-G4-W2	114013094	7443	7450	N/A	N/A	N/A
S2-G4-W3	114013107	7576	7584	N/A	N/A	N/A
S2-G4-W4	114013105	7538	7545	N/A	N/A	N/A
S2-G4-W5	114013104	7367	7375	N/A	N/A	N/A
S2-G4-M1	114013077	9595	9621	1, 17	1	2
S2-G4-M2	114013044	9297	9323	2, 18	1	2
S2-G4-M3	114013066	9730	9755	3, 19	1	2
S2-G4-M4	114013076	9622	9648	4, 20	1	2
S2-G4-M5	114013075	9676	9702	5, 21	1	2
S2-G4-M6	114013043	9352	9377	N/A	N/A	N/A
S2-G4-M7	114013047	10136	10162	N/A	N/A	N/A
S2-G4-E1	114013095	7424	7432	1, 33	1	3
S2-G4-E2	1140130101	7500	7508	2, 34	1	3
S2-G4-E3	114013100	7510	7518	3, 35	1	3
S2-G4-E4	114013097	7529	7537	4, 36	1	3
S2-G4-E5	114013099	7309	7317	N/A	N/A	N/A

Date: 9/25/2013

Span: 3-4

Member: Girder 4 (S3-G4)

Stage: **Erection**

Location	S/N	Begin #	End #	Chanel #	DAS	MODULE
S3-G4-W1	114013091	7452	7460	33	1	3
S3-G4-W2	114013092	7300	7308	34	1	3
S3-G4-W3	114013086	7290	7297	35	1	3
S3-G4-W4	114013093	7433	7441	36	1	3
S3-G4-W5	114013103	7548	7556	N/A	N/A	N/A
S3-G4-M1	114013050	7604	7630	17	1	2
S3-G4-M2	114013041	10217	10243	18	1	2
S3-G4-M3	114013065	9703	9729	19	1	2
S3-G4-M4	114013045	9270	9296	20	1	2
S3-G4-M5	114013062	9460	9485	21	1	2
S3-G4-M6	114013063	9487	9512	N/A	N/A	N/A
S3-G4-M7	114013061	9433	9458	N/A	N/A	N/A

Date: 10/15/2013 (Connected to CR800 DAS)

Span: 1-2

Member: Girder 3 (S1-G3)

Stage: **Deck Placement**

Location	S/N	Begin #	End #	Chanel #	DAS	MODULE
S1-G3-M1	114013037	10244	10270	1	1	1
S1-G3-M2	114013036	10271	10297	2	1	1
S1-G3-M3	114013053	9162	9188	3	1	1
S1-G3-M4	114013055	9514	9540	4	1	1
S1-G3-M5	114013035	10298	10324	5	1	1
S1-G3-M6	114013067	9757	9783	6	1	1
S1-G3-M7	114013042	10190	10216	7	1	1
S1-G3-E1	114013116	7329	7337	8	1	1
S1-G3-E2	114013117	7348	7356	9	1	1
S1-G3-E3	114013118	7338	7346	10	1	1
S1-G3-E4	114013115	7405	7412	11	1	1
S1-G3-E5	114013081	7252	7260	12	1	1

Date: 10/15/2013 (Connected to CR800 DAS)

Span: 1-2

Member: Girder 4 (S1-G4)

Stage: **Deck Placement**

Location	S/N	Begin #	End #	Chanel #	DAS	MODULE
S1-G4-M1	114013049	9244	9269	13	1	1
S1-G4-M2	114013040	9920	9945	14	1	1
S1-G4-M3	114013039	9893	9918	15	1	1
S1-G4-M4*	114013034	10325	10351	16	1	1
S1-G4-M5	114013068	9784	9810	17	1	2
S1-G4-M6	114013033	10352	10377	18	1	2
S1-G4-M7	114013056	10109	10135	19	1	2
S1-G4-E1	114013080	7243	7251	20	1	2
S1-G4-E2	114013110	7595	7603	21	1	2
S1-G4-E3	114013111	7386	7394	22	1	2
S1-G4-E4	114013112	7585	7594	23	1	2
S1-G4-E5	114013114	7319	7327	24	1	2

*: VWSG did not work properly

Date: 10/15/2013 (Connected to CR800 DAS)

Span: 2-3

Member: Girder 3 (S2-G3)

Stage: **Deck Placement**

Location	S/N	Begin #	End #	Chanel #	DAS	MODULE
S2-G3-W1	114013113	7395	7404	25	1	2
S2-G3-W2	114013088	7491	7499	26	1	2
S2-G3-W3	114013087	7481	7489	27	1	2
S2-G3-W4	114013079	7234	7242	28	1	2
S2-G3-W5	114013109	7376	7385	29	1	2
S2-G3-M1	114013057	10083	10108	35	1	2
S2-G3-M2	114013048	9326	9350	36	1	3
S2-G3-M3	114013052	9189	9215	37	1	3
S2-G3-M4	114013046	10163	10189	38	1	3
S2-G3-M5*	114013054	9379	9404	39	1	3
S2-G3-M6	114013051	9217	9242	40	1	3
S2-G3-M7	114013069	9811	9837	41	1	3
S2-G3-E1	114013090	7462	7470	51	2	1
S2-G3-E2	114013106	7568	7573	52	2	1
S2-G3-E3	114013096	7357	7365	53	2	1
S2-G3-E4	114013108	9153	9161	54	2	1
S2-G3-E5	114013089	7471	7479	55	2	1

*: VWSG did not work properly

Date: 10/15/2013 (Connected to CR800 DAS)

Span: 2-3

Member: Girder 4 (S2-G4)

Stage: **Deck Placement**

Location	S/N	Begin #	End #	Chanel #	DAS	MODULE
S2-G4-W1	114013102	7557	7565	30	1	2
S2-G4-W2	114013094	7443	7450	31	1	2
S2-G4-W3	114013107	7576	7584	32	1	2
S2-G4-W4	114013105	7538	7545	33	1	3
S2-G4-W5	114013104	7367	7375	34	1	3
S2-G4-M1	114013077	9595	9621	44	2	1
S2-G4-M2	114013044	9297	9323	45	2	1
S2-G4-M3	114013066	9730	9755	46	2	1
S2-G4-M4	114013076	9622	9648	47	2	1
S2-G4-M5	114013075	9676	9702	48	2	1
S2-G4-M6	114013043	9352	9377	49	2	1
S2-G4-M7	114013047	10136	10162	50	2	1
S2-G4-E1	114013095	7424	7432	56	2	1
S2-G4-E2	1140130101	7500	7508	57	2	1
S2-G4-E3	114013100	7510	7518	58	2	1
S2-G4-E4	114013097	7529	7537	59	2	1
S2-G4-E5	114013099	7309	7317	60	2	2

Date: 10/15/2013 (Connected to CR800 DAS)

Span: 3-4

Member: Girder 3 (S3-G3)

Stage: **Deck Placement**

Location	S/N	Begin #	End #	Chanel #	DAS	MODULE
S3-G3-W1	114013083	7262	7267	61	2	2
S3-G3-W2	114013098	7519	7527	62	2	2
S3-G3-W3	114013084	7271	7279	63	2	2
S3-G3-W4	114013085	7281	7289	64	2	2
S3-G3-W5	114013082	7415	7423	65	2	2
S3-G3-M1	114013078	9568	9593	66	2	2
S3-G3-M2	114013074	9838	9864	67	2	2
S3-G3-M3	114013059	10055	10081	68	2	2
S3-G3-M4	114013070	10020	10052	69	2	2
S3-G3-M5	114013058	9542	9567	70	2	2
S3-G3-M6	114013073	9947	9972	71	2	2
S3-G3-M7	114013060	9407	9431	72	2	2

Date: 10/15/2013 (Connected to CR800 DAS)

Span: 3-4

Member: Girder 4 (S3-G4)

Stage: **Deck Placement**

Location	S/N	Begin #	End #	Chanel #	DAS	MODULE
S3-G4-W1	114013091	7452	7460	73	2	2
S3-G4-W2	114013092	7300	7308	74	2	2
S3-G4-W3	114013086	7290	7297	75	2	2
S3-G4-W4	114013093	7433	7441	76	2	3
S3-G4-W5	114013103	7548	7556	77	2	3
S3-G4-M1	114013050	7604	7630	78	2	3
S3-G4-M2	114013041	10217	10243	79	2	3
S3-G4-M3	114013065	9703	9729	80	2	3
S3-G4-M4	114013045	9270	9296	81	2	3
S3-G4-M5	114013062	9460	9485	82	2	3
S3-G4-M6	114013063	9487	9512	83	2	3
S3-G4-M7	114013061	9433	9458	84	2	3

REFERENCES

- AASHTO M 31 (2007). "Standard Specification for Deformed and Plain Carbon-Steel Bars for Concrete Reinforcement." *American Association of State Highway and Transportation Officials (AASHTO)*. Washington, D.C.
- AASHTO M 203 (2012). "Standard Specification for Steel Strand, Uncoated Seven-Wire for Concrete Reinforcement." *American Association of State Highway and Transportation Officials (AASHTO)*. Washington, D.C.
- AASHTO M 221 (2009). "Standard Specification for Steel Welded Wire Reinforcement, Deformed, for Concrete." *American Association of State Highway and Transportation Officials (AASHTO)*. Washington, D.C.
- ACI Committee 224 (2001). "Control of Cracking in Concrete Structures." *American Concrete Institute*, Farmington Hills, Michigan.
- ACI Committee 237 (2007). "Self-Consolidating Concrete." *American Concrete Institute*, Farmington Hills, Michigan.
- ACI Committee 318 (2011). "Building Code Requirements for Structural Concrete and Commentary." *American Concrete Institute*, Farmington Hills, Michigan.
- ACI Committee 363 (2010). "State of the Art Report on High Strength Concrete." *American Concrete Institute*, Farmington Hills, Michigan.
- ACI-ASCE Committee 326 (1962). "Shear and Diagonal Tension." *American Concrete Institute*, Farmington Hills, Michigan.
- ACI-ASCE Committee 426 (1973). Shear strength of reinforced concrete members. *Journal of the Structural Division, ASCE*, 99(ST6), 1091-1187.
- ACI-ASCE Committee 445 (1999). "Recent Approaches to Shear Design of Structural Concrete." *American Concrete Institute*, Farmington Hills, Michigan.
- Alejandro, R., Avendano, V., and Bayrak, O. (2008). *Shear Strength and Behavior of Prestressed Concrete Beams* (Report IAC-88-5DD1A003-3). University of Texas at Austin, Austin, Texas.
- American Association of State Highway and Transportation Officials (2012). "AASHTO LRFD Bridge Design Specifications, 6th Edition." *American Association of State Highway and Transportation Officials*, Washington, D.C.
- ASTM A 416 (2012a). "Standard Specification for Steel Strand, Uncoated Seven-Wire for Prestressed Concrete." *American Society for Testing and Materials (ASTM) International*, West Conshohocken, Pennsylvania.

- ASTM A 615 (2012). “Standard Specification for Deformed and Plain Carbon-Steel Bars for Concrete Reinforcement.” *American Society for Testing and Materials (ASTM) International*, West Conshohocken, Pennsylvania.
- ASTM A 1064 (2012). “Standard Specification for Carbon-Steel Wire and Welded Wire Reinforcement, Plain and Deformed, for Concrete.” *American Society for Testing and Materials (ASTM) International*, West Conshohocken, Pennsylvania.
- ASTM C 31 (2012). “Standard Practice for Making and Curing Concrete Test Specimens in the Field.” *American Society for Testing and Materials (ASTM) International*, West Conshohocken, Pennsylvania.
- ASTM C 39 (2012). “Standard Test Method for Compressive Strength of Cylindrical Concrete Specimens.” *American Society for Testing and Materials (ASTM) International*, West Conshohocken, Pennsylvania.
- ASTM C 78 (2010). “Standard Test Method for Flexural Strength of Concrete.” *American Society for Testing and Materials (ASTM) International*, West Conshohocken, Pennsylvania.
- ASTM C 143 (2012). “Standard Test Method for Slump of Hydraulic-Cement Concrete.” *American Society for Testing and Materials (ASTM) International*, West Conshohocken, Pennsylvania.
- ASTM C 231 (2010). “Standard Test Method for Air Content of Freshly Mixed Concrete by the Pressure Method.” *American Society for Testing and Materials (ASTM) International*, West Conshohocken, Pennsylvania.
- ASTM C 469 (2010). “Standard Test Method for Static Modulus of Elasticity and Poisson’s Ratio of Concrete in Compression.” *American Society for Testing and Materials (ASTM) International*, West Conshohocken, Pennsylvania.
- ASTM C 496 (2011). “Standard Test Method for Splitting Tensile Strength of Cylindrical Concrete Specimens.” *American Society for Testing and Materials (ASTM) International*, West Conshohocken, Pennsylvania.
- ASTM C 1610 (2010). “Standard Test Method for Static Segregation of Self-Consolidating Concrete using Column Technique.” *American Society for Testing and Materials (ASTM) International*, West Conshohocken, Pennsylvania.
- ASTM C 1611 (2009). “Standard Test Method for Slump Flow of Self-Consolidating Concrete.” *American Society for Testing and Materials (ASTM) International*, West Conshohocken, Pennsylvania.

- ASTM C 1621 (2009). "Standard Test Method for Passing Ability of Self-Consolidating Concrete by J-Ring." *American Society for Testing and Materials (ASTM) International*, West Conshohocken, Pennsylvania.
- Baali, L. (2009). "Self-Consolidating Concrete for Precast, Prestressed Concrete Bridge Elements." Master's Thesis, McGill University, Montreal, Quebec.
- Bentz, E. (2000). "Sectional Analysis of Reinforced Concrete Members." Doctoral Dissertation, University of Toronto, Toronto, Ontario.
- Bentz, E. and Collins, M. (2000). Response 2000 [Software]. Available from: www.ecf.utoronto.ca/~bentz/r2k.htm.
- Bhide, S. and Collins, M. (1989). Influence of axial tension on the shear capacity of reinforced concrete members. *ACI Structural Journal*, 86(5), 570-581.
- Brewe, J. and Myers, J. (2010). High strength self-consolidating concrete girders subjected to elevated compressive fiber stresses; part 1: Prestress loss and camber behavior. *PCI Journal*, 55(4), 59-77.
- Cervenka Consulting (2013). ATENA Engineering 3-D (v. 5.0.3) [Software]. Prague, Czech Republic. www.cervenka.cz.
- Collins, M., Mitchell, P., Adebar, P., and Vecchio, F. (1996). A general shear design method. *ACI Structural Journal*, 93(1), 36-45.
- De Silva, S., Mutsuyoshi, H., and Witchukreangkrai, E. (2008). Evaluation of shear crack width in I-shaped prestressed reinforced concrete beams. *Journal of Advanced Concrete Technology* 6(3), 443-458.
- Domone, P. (2007). A review of hardened mechanical properties of self-compacting concrete. *Cement and Concrete Composites*, 29(1), 1-12.
- EFNARC (2005). "The European Guidelines for Self-Compacting Concrete." Retrieved from <http://www.efnarc.org> (Feb. 4. 2014).
- Elzanaty, A., Nilson, A., and Slate, F., (1987). Shear capacity of prestressed concrete beams using high-strength concrete. *ACI Structural Journal*, 83(2), 359-368.
- Elzanaty, A., Nilson, A. and Slate, F. (1985). *Shear-Critical High-Strength Concrete Beams* (Report 85-1). Cornell University, Ithaca, New York.
- EN206-1 (2000). "Concrete – Part 1: Specification, Performance, Production, and Conformity." *European Committee for Standardization*, Brussels, Belgium.

- Frosch, R. and Wolf, T. (2003). *Simplified Shear Design of Prestressed Concrete Members* (Report FHWA/IN/JTRP-2003/5). Purdue University, West Lafayette, Indiana.
- Garber, D., Gallardo, J., Deschenes, D., Dunkman, D., and Bayrack, O. (2013). *Effect of New Prestress Loss Estimates on Pretensioned Concrete Bridge Girder Design*, (Report FHWA/TX-12/0-6347-2). University of Texas at Austin, Austin, Texas.
- Gross, S.P. (1999); "Field Performance of Prestressed High Performance Concrete Highway Bridges in Texas;" Dissertation; University of Texas at Austin.
- Haines, R. (2005). "Shear Testing of Prestressed High Performance Concrete Bridge Girders." Master's Thesis, Civil Engineering, Georgia Institute of Technology, Atlanta, Georgia.
- Hanna, K., Morcou, G., and Tadros, M. (2010). *Design Aids of NU I-Girders Bridges*, (Report SPR-P1(09) P322). University of Nebraska-Lincoln, Lincoln, Nebraska.
- Hartman, D., Breen, J., and Kreger, M. (1988). *Shear Capacity of High Strength Prestressed Concrete Girders* (Report FHWA/TX-88+381-2). University of Texas at Austin, Austin, Texas.
- Hassan, A., Hossain, K., and Lachemi, M. (2010). Strength, cracking and deflection performance of large-scale self-consolidating concrete beams subjected to shear failure. *Engineering Structures*, 32, 1262-1271.
- Hawkins, N., Kuchma, D., Mast, R., Marsh, M., and Reineck, K. (2005). *Simplified Shear Design of Structural Concrete Members* (NCHRP 549). Transportation Research Board, Washington, D.C.
- Hawkins, N. and Kuchma, D. (2007). *Application of LRFD Bridge Design Specifications to High-Strength Structural Concrete: Shear Provisions* (NCHRP 579). Transportation Research Board, Washington, D.C.
- Heckman, C. and Bayrak, O. (2008). *Effects of Increasing the Allowable Compressive stress at Release on the Shear Strength of Prestressed Concrete Girders* (Report FHWA/TX-09/0-5197-3). University of Texas at Austin, Austin, Texas.
- Hedegaard, B., French, C., and Shield, C.K. (2013). Investigation of Thermal Gradients Effects in the I-35W St. Anthony Falls Bridge. *ASCE Journal of Bridge Engineering*. 18(9), 890-900.
- Imbsen, R.A., Vandershof, D.E, Schamber, R.A., and Nutt, R.V. (1985). *Thermal Effects in Concrete Bridge Superstructures* (NCHRP 276). Transportation Research Board, Washington, DC.

- Kani, G. (1967). How safe are our large reinforced concrete beams? *ACI Journal*, 64 (3), 128-141.
- Khayat, K., and Mitchell, D. (2009). *Self-Consolidating Concrete for Precast, Prestressed Concrete Bridge Elements* (NCHRP 628). Transportation Research Board, Washington, D.C.
- Kim, Y., Hueste, M., Trejo, D. and Cline, D. (2010). Shear characteristics and design for high-strength self-consolidating concrete. *ASCE Journal of Structural Engineering*, 136 (8), 989-1000.
- Kim, Y. H. (2008). "Characterization of Self-Consolidating Concrete for the Design of Precast, Pretensioned Bridge Superstructure Elements." Doctoral Dissertation, Texas A&M University, College Station, Texas.
- Labib, E., Dhonde, H., Howser, R., Mo, Y., Hsu, T., and Ayoub, A. (2013). *Shear in High Strength Concrete Bridge Girders: Technical Report* (Report FHWA/TX-13/0-6152-2). University of Houston, Houston, Texas.
- Labonte, T. (2004). "Construction and Testing of AASHTO Type II Girders Using Self-Consolidating Concrete." Master's Thesis, Civil Engineering, University of Florida, Gainesville, Florida.
- Lachemi, M., Hossain, K., and Lambros, V. (2005). Shear resistance of self-consolidating concrete beams – experimental investigations. *Canadian Journal of Civil Engineering*, 32(6), 1103-1113.
- Lin, C. and Chen, J. (2012). Shear behavior of self-consolidating concrete beams. *ACI Structural Journal*, 109(3), 307-315.
- Long, W. and Khayat, K. (2011). Creep of prestressed self-consolidating concrete. *ACI Materials Journal*, 108(5), 476-484.
- Long, W., Khayat, K., and Hwang, S (2013). Mechanical properties of prestressed self-consolidating concrete. *Materials and Structures*, 46, 1473-1487.
- Martinez, S., Nilson, A. and Slate, F. (1984). *Spirally-Reinforced High-Strength Concrete Columns* (Report 82-10). Cornell University, Ithaca, New York.
- McSaveney, L., Khrapko, M., and Papworth, F. Self-Compacting Concrete Enhances Tauranga's New Harbour Link. Retrieved from <http://www.goldenbay.co.nz/mainmenu35/page163/Recent+Projects.html> (3 June 2014).
- McSaveney, L., Papworth, F., and Khrapko, M. (2011). Self-compacting concrete for superior marine durability and sustainability. *Concrete in Australia*, 37(2), 59-64.

- Missouri Department of Transportation (MoDOT) (2011). "Engineering Policy Guide, Category 751 LRFD Bridge Design Guidelines." MoDOT, Jefferson City, Missouri.
- Myers, J. and Bloch, K. (2011) Accelerated Construction for Pedestrian Bridges: A Comparison between High Strength Concrete (HSC) and High-Strength Self-Consolidating Concrete (HS-SCC). *Design, Construction, Rehabilitation, and Maintenance of Bridges*: 129-136. doi: 10.1061/47630(409)17.
- Myers, J., and Carrasquillo, R. (1998). *Production and Quality Control of High Performance Concrete in Texas Bridge Structures* (Report 9-580/589-1). University of Texas at Austin, Austin, Texas.
- Myers, J., Volz, J., Sells, E., Porterfield, K., Looney, T., Tucker, B., & Holman, K. (2012). *Self-Consolidating Concrete (SCC) for Infrastructure Elements*, (Report cmr 13-003). Missouri University of Science and Technology, Rolla, Missouri.
- Myers, J.J.; Yang, Yumin (2005); "High Performance Concrete for Bridge A6130-Route 412 Pemiscot County, MO;" UTC R39.
- Nagle, T. and Kuchma, D. (2007). *Nontraditional Limitations on the Shear Capacity of Prestressed Concrete Girders* (Report NSEL-003). University of Illinois, Urbana-Champaign, Illinois.
- Nakamura, E., Avendano, A., and Bayrak, O. (2013). Shear database for prestressed concrete members. *ACI Structural Journal*, 100(6), 909-918.
- Nawy, E. (2009). *Prestressed Concrete: A Fundamental Approach*. Upper Saddle River, New Jersey: Pearson Education, Inc.
- Nilson, A. (1987). *Design of Prestressed Concrete*. Ithaca, New York: John Wiley and Sons.
- Okamura, H. and Ouchi, M. (2003). Self-compacting concrete. *Journal of Advanced Concrete Technology*, 1(1), 5-15.
- Ouchi, M., Nakamura, S., Osterberg, T., Hallberg, S., and Lwin, M. (2003). "Applications of Self-Compacting Concrete in Japan, Europe, and the United States." Federal Highway Administration. ISHPC.
- Pauw, A. (1960). Static modulus of elasticity of concrete as affected by density. *Journal of the American Concrete Institute*, 32(6), 769-687.
- Price, W. (1951). Factors influencing concrete strength. *Journal of the American Concrete Institute*, 22(6), 417-432.

- Reineck, K., Kuchma, D., Kim, K., and Marx, S. (2003). Shear database for reinforced concrete members without shear reinforcement. *ACI Structural Journal*, 100(2), 240-249.
- Runzell, B., Shield, C., and French C., (2007). *Shear Capacity of Prestressed Concrete Beams* (Report MN/RC 2007-47). University of Minnesota, Minneapolis, Minnesota.
- Schindler, A., Barnes, R., Roberts, J., and Rodriguez, S. (2007). Properties of self-consolidating concrete for prestressed members. *ACI Materials Journal*, 104(1), 53-61.
- Sells, E. (2012). "Self-Consolidating Concrete for Infrastructure Elements Shear Characterization." Master's Thesis, Civil Engineering, Missouri University of Science and Technology, Rolla, Missouri.
- Shahawy, M. A., and Batchelor, B. (1996). Shear behavior of full-scale prestressed concrete girders: comparison between AASHTO specifications and LRFD Code. *PCI Journal*, 41(3), 48-62.
- Sozen, M.A., Zwoyer, E.M., and Siess, C.P. (1959). *Strength in Shear of Beams without Web Reinforcement* (Bulletin 452). University of Illinois, Urbana-Champaign, Illinois.
- Takagi, Y., Umetsu, K., Taira, Y., and Mizuno, K. (2000). Shear resisting behavior of prestressed concrete beams with inner and external cables. *Transactions of the Japan Concrete Institute*, 22(3), 685-690.
- Teng, S., Kong, F. K., and Poh, S. P. (1998b). Shear strength of reinforced and prestressed concrete deep beams. *Proceedings of the Institution of Civil Engineers, Structures and Buildings*, 128(2), 112-143.
- Trejo, D., Hueste, M., Kim, Y., and Atahan, H. *Characterization of Self-Consolidating Concrete for Design of Precast Prestressed Bridge Girders* (Report 0-5134-2). Texas A&M University, College Station, Texas.
- Vecchio, F. and Collins, M. (1986). The modified compression-field theory for reinforced concrete elements subjected to shear. *ACI Journal*, 83(2), 219-231.
- Wang, H., Qi, C., Farzam, H., & Turici, J. (2006). Interaction of materials used in concrete. *Concrete International*, 28(4), 47-52.
- Wight, K. and MacGregor, J. (6th ed.). (2009). *Reinforced Concrete Mechanics and Design*. Upper Saddle River, New Jersey: Pearson Education, Inc.